Synthesis and Validation of a Trifunctional Trimethoprim-based Probe for Use with Degradation Domain System

By

Adam Mason Metts

Thesis

Submitted to the Faculty of the

Graduate School of Vanderbilt University

in partial fulfillment of the requirements

for the degree of

MASTER OF SCIENCE

in

Chemistry

May 10, 2019

Nashville, Tennessee

Approved:

Lars Plate, Ph.D.

Brian O. Bachmann, Ph.D.

Carmelo J. Rizzo, Ph.D.

TABLE OF CONTENTS

Page

LIST OF TABLES

LIST OF FIGURES

LIST OF SCHEMES

CHAPTER I

INTRODUCTION

Genetic and Pharmacologic Tools to Probe Protein Function

The cell is regulated by a vast network of dynamic protein interactions that facilitate various sub-cellular functions and help maintain homeostasis. Pathways in signaling, protein folding, and trafficking are largely facilitated by protein-protein interactions (PPIs), and to understand how these systems operate requires an understanding of how these proteins function and interact with other cellular players on diverse time scale. Historically, some of the most powerful tools available for studying protein function have been genetic tools that alter protein expression. RNAi or CRISPR knockdown methods enable studies to determine how different cell pathways are affected when the protein expression is diminished by comparing the knock-down phenotype to that of the wild-type[1,2]. Alternatively, one can up-regulate the expression of a particular protein by gene overexpression,[3] inducible promoter systems,[4] or CRISPR activation[2] to study the effects of an excess of the protein in question. While these technologies have proven useful, they have several drawbacks. First, each of these methods operate at the transcriptional or pre-translational level, creating long experimental delays between the gene knock-down and the measurable change in protein expression. This prohibits the study of systems that operate on time scales faster than protein translation using these methods. Additionally, these methods are not easily reversible, and thus mainly enable studies of static protein states of being fully inhibited or fully present.

Another tool frequently used to control protein activity in cells is through pharmacologic inhibition using small molecules.[5] Compared to targeting the protein at the transcriptional level, post-translational targeting of proteins using small molecules avoids experimental delays, is reversible, affords greater temporal control, and avoids problems with cell permeability. However, many interesting cellular targets remain undruggable due to their lack of a deep ligand binding pocket. [6,7,8] Inhibition of protein-protein interaction using small molecules that specially targets the protein interfaces also remains challenging. [9,10,11] For the cellular targets that are druggable, significant challenges remain in finding ligands that bind specifically to the target and avoid issues of absorption, metabolism, and distribution.[12] Finally, any successful small

molecule that is developed to up- or down-regulate a protein of interest will be specific for its protein target, thus making small molecule development as a general solution for regulating protein activity very time- and resource-consuming.

PROTACs as Chemical Genetic Tools to Post-translationally Induce Protein Degradation

In the past two decades, new technologies have emerged that control protein levels by selectively degrading proteins of interest, thus avoiding the experimental delays that hamper the aforementioned techniques. These approaches take advantage of the existing proteasomal degradation machinery in cells to selectively induce the degradation of a protein of interest. The main mechanism by which proteins are targeted for degradation is through tagging with ubiquitin, a 76 amino acid protein that can be attached to lysine residues by an isopeptide bond.[13,14] Since ubiquitin itself contains lysine residues, proteins can accumulate poly-ubiquitin chains that serve to signal the protein for proteasomal degradation.[15] This ubiquitination process is carefully mediated by a suite of increasingly specific enzymes (E1, E2, and E3 ubiquitin ligases) that transfer the ubiquitin to the protein in question. After the E1 complex binds to free ubiquitin forming a thioester between the ubiquitin C-terminus and a Cys residue, the E2 complex transfers the resulting ubiquitin thioester from the E1 to itself by trans-thioesterification. The E3 ligase then takes the ubiquitin from the E2 complex and attaches it via an isopeptide bond to the protein substrate bound to it. While there is only one E1 complex, there are over 600 E3 ligases with high substrate specificity, and they can exist as a single protein or as a multiprotein complex.[16]

PROTAC (PROteolysis TArgeting Chimera) is a recently developed technique to artificially target protein substrates towards degradation by the ubiquitin-proteasome system (**Figure 1.1**).[17] PROTACs are heterobifunctional compounds that selectively bind to an E3 ubiquitin ligase and to a protein of interest, thus tethering the two proteins together. The induced proximity between the two proteins causes the E3 ligase to transfer its ubiquitin to the protein of interest as if it were bound as a substrate, which thereby targets it for degradation. Since the E3 ligase does not need to recognize the protein of interest as it would a bound substrate, the issue of substrate specificity is avoided, so long as both sides of the PROTAC bind specifically to their

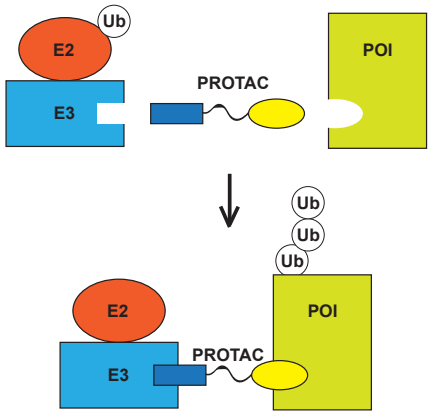

Figure 1.1. Mechanism of PROTAC-induced protein degradation.

respective binding partners.[18] Sakamoto et. al. first developed this methodology in 2001 by inducing the proteasomal degradation of methionine amino-peptidate inhibitor (MetAP-2).[19] This first tool compound, dubbed PROTAC-1, tethered a covalent MetAP-2 inhibitor, ovilicin, to a phospho-peptide fragment of IκBα known to bind a specific F-box protein as part of an E3 ubiquitin ligase complex, thereby targeting MetAP-2 for proteasomal degradation by proximity. The groups later applied this method to mammalian cells via microinjection of PROTAC in HEK293 cells and validated its mechanism of action by reversing the observed degradation using a proteasome inhibitor.[18]

While this approach established the method as a proof of concept, the use of a peptide recognition sequence caused the first PROTACs to have low cell permeability, micromolar potency, and phosphatase sensitivity.[20,21] Schneekloth et. al. addressed these problems by introducing the first all-small-molecule PROTACS, which employed a nutlin derivative that binds to an E3 ligase MDM2.[21] Using a PEG linker, the authors coupled the nutlin moiety to a selective ligand for an androgen receptor and induced its degradation in HeLa cells.[21] In addition to targeting other E3 ligases, such as VHL[22] and cereblon,[23] this technology has been utilized in a variety of therapeutically relevant cellular settings, including for Alzheimer's disease,[24] hepatitis B,[25] and acute myeloid leukemia.[26]

Though great improvements have been made to PROTAC technology since its design was first published, the technology as a whole still presents drawbacks that are intrinsic to the system's design. Most notably, the PROTACs require constant incubation with the PROTAC probe in order for the protein of interest to be degraded, requiring large quantities of probe to run

each experiment. Furthermore, since the PROTACs cannot be quickly removed from the cell once they have been introduced, PROTAC systems can only provide new information in situations where rapid depletion of a protein is required. While PROTACs have distinct advantages over past technologies by acting post-translationally, they lack the ability to detail what happens in the cell once the protein is re-introduced.

Degradation Domains as Chemical Genetic Tools to Post-translationally Induce Protein Accumulation

In contrast to PROTACs, which post-translationally degrade a protein of interest, other small molecule approaches have been developed that post-translationally up-regulate a protein of interest. Degradation domains (DD) enable researchers to post-translationally control protein expression and study the effects of protein accumulation in the cell (**Figure 1.2**).[27] DDs work by creating a genetic fusion of an intrinsically unstable protein (or, the degron) and a protein of interest (POI) that is then transcribed and translated into a fusion protein. Instability of the DDs and partial unfolding results in constitutive ubiquitination and targeting for the proteasome in the absence of a stabilizing ligand.[28] This is in contrast to PROTACs, which require constant presence of the ligand to induce degradation. Upon addition of a ligand that selectively binds to the degron and renders it stable, the entire complex will be rescued from proteasomal degradation, thus allowing the protein of interest to repopulate in the cell. The rapid kinetics of this ligand-dependent stabilization allow researchers to study the effects of protein accumulation on cell processes with much higher temporal resolution than past methods discussed above that act at the transcriptional level. Additionally, DDs take advantage of small molecules that are already known to bind specifically to their target while providing a generalizable method to accumulate proteins with few limitations on which POIs can be targeted.[29]

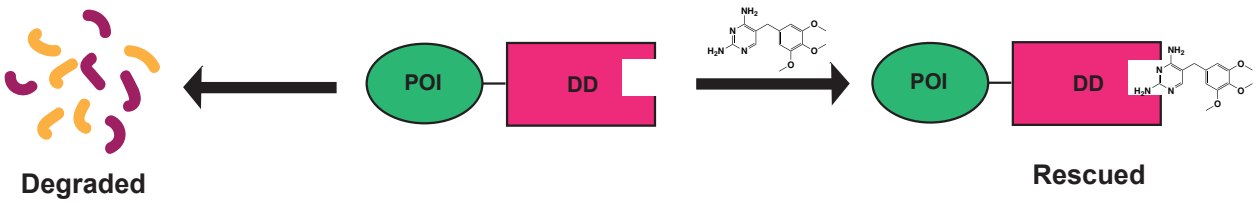

Figure 1.2. Mechanism of ligand-dependent protein stability in the degradation domain system

Early work toward the first degradation domain systems relied on the N-end rule to induce protein degradation.[30,31] N-terminal amino acids are recognized by E3 ubiquitin ligases, which then initiate the proteasomal degradation pathway, but Bachmair et. al. found that the rate at which a protein is degraded varies based on the identity of the N-terminal amino acid.[32] The N-end rule refers to the empirically determined rates of degradation that different amino acids confer onto a protein when they are located at the N-terminus. After this rule was discovered, researchers began to exploit this phenomenon by introducing amino acids such as lysine that were known to result in short half-lives to the N-end of proteins.[33] Other early studies conducted by Dohmen et. al. utilized thermal destabilization to induce protein degradation. The authors identified a variant of dihydrofolate reductase (DHFR) in yeast containing an N-terminal arginine that was stable at 23˚C, but at 37˚C would be ubiquitinated and targeted for proteasomal degradation.[31] However, the DHFR could be saved from degradation by adding methotrexate, a small molecule inhibitor that binds to the DHFR active site and adjusts its folding pattern to render it more stable. This system comprised of a destabilized protein complex that could be rescued by addition of a small molecule constituted the first small-molecule degradation domain.

In subsequent studies, Banaszynski et. al. developed the first DD system to utilize an intrinsically unstable degron that required no particular temperature or binding state to induce its degradation.[34,35] The authors utilized an FKBP12-YFP fusion protein for their system, with the YFP fluorescence indicating the stable expression of FKBP12. After creating a FKBP12-YFP DNA fusion, they used error-prone PCR to generate a library of FKBP12 mutants. Once the resulting DNA had been transduced into cells, they used three rounds of flow cytometry to sort the cells that displayed low protein expression in the absence of a selective ligand and rescue of protein expression upon treatment with the ligand.[34] The stabilizing ligand they chose, SHIELD-1, was a synthetic derivative of rapamycin that specifically binds to FKBP12 and shows improved drug-like properties compared to other similar derivatives. Sequence analysis of the isolated DNA from this final pool of cells revealed some mutations that appeared frequently across this population. The final system allows C- or N-terminal linkages of POIs to the DD system, and its mechanism of action was validated as being a polyubiquitination event that targets the whole fused protein for the proteasome.[28]

Iwamoto et. al. further improved upon this work by creating an intrinsically unstable DHFR DD system. [36] When directly compared to the SHIELD system, the DHFR DD proved to

be more effective at destabilizing proteins of interest, and the stabilizing trimethoprim (TMP) ligand they used is over 1000x more potent in inhibiting bacterial DHFR than human DHFR, rendering it "biologically silent in mammalian cells."[36,37] The system also offers the flexibility to fuse proteins at the N- or C-terminus, or even within the protein sequence of the DHFR.[36] This system has been shown to be robust with many different proteins and cell types, and it has been applied to study transcription factors, [38,39,40] GPCRs, [36] neurotrophic factors, [41] RNA binding proteins, [42] and other systems.

Introduction to Dynamic Interactomics

Most cellular proteins interact with other protein partners and function as part of larger protein complexes. To understand the function of proteins and the regulation of cellular processes, it is necessary to map these dynamic protein-protein interactions. Protein interactomics studies have made it their goal to systematically determine the network of protein-protein interactions in a cellular context. Landmark studies in this field have mapped out interaction networks of protein-protein interactions (PPIs) in yeast[43] and in humans,[44, 45,46] as well as interaction maps of protein complexes in *E. coli*[47] and in yeast.[48] Even so, many studies in this field are conducted under basal conditions, and fewer have focused on how these PPIs change in response to different stimuli. It is challenging to study the dynamics of interactome remodeling because changes in PPIs can occur on a rapid time scale, and the tools used to interrogate these changes must therefore have sufficient time resolution to identify them. Applications of the technology currently available to perturb protein function and expression have been largely limited to studying static systems, and these previously described methods lack the time resolution or broad applicability needed to study interactome remodeling. Thus, new tools are needed that can address the limitations of the prior methods and enable the study of these dynamic systems.

Research groups have begun to interrogate interactome dynamics using various methods. One example is the LUMIER (luminescence-based mammalian interactome mapping) system, which was developed by Barrios-Rodiles et. al. as a high-throughput system combining affinity purification and luminescence-based quantification to detect protein-protein interactions in the presence and absence of transforming growth factor b (TGFb).[49] A later example from Bisson et. al. added a temporal component by using a mass-spectrometry-based method, affinity

purification–selected reaction monitoring (AP-SRM), to generate quantitative data measuring changes in protein interactions of the adaptor protein GBR2 before and after growth factor stimulation.[50] Here, the time dependent interactome changes were induced using a small molecule ligand inducing a signal transduction process. Lobingier et. al. further developed this technology by combining engineered ascorbic acid peroxidase (APEX) proximity labeling and quantitative proteomics to study both the spatial and temporal dynamics of GPCR signaling and protein-protein interactions.[51] This APEX approach combined the rapid labeling kinetics of proximity-induced labeling with the sensitivity of affinity purification mass spectrometry (AP-MS) to identify the local signaling networks of beta-2 adrenergic receptor (B2AR), a well-studied G-protein-coupled receptor (GPCR). In their workflow, they inserted an APEX tag as a genetic fusion to B2AR. After stimulation of the receptor through addition of a small molecule agonist, APEX reaction was initiated at different time-points to biotinylate proteins proximal to the B2AR-APEX fusion. Subsequently, purification of the protein complex at certain time points using streptavidin beads created "snapshots" of the temporal protein interactions. A potential drawback of the APEX system is that its high labeling activity may label off-pathway proteins, which was addressed by using an APEX-labeled spatial reference to differentiate between PPIs that belonged to a particular signaling network and those that were uninvolved bystanders. Their workflow concluded with a two-step MS analysis that compared the relative abundances of pathway interactions to bystander interactions.[51,52]

While this method serves as an excellent proof of principle, its requirement of having advanced knowledge of the signaling pathways being examined in order to pick an appropriate spatial reference limits the applicability of the system. Furthermore, this method has yet to be tested for cytosolic proteins, where determining spatial localization of the protein would pose a far greater challenge. Finally, this approach relies on the presence of an endogenous ligand that controls the PPIs of the POI, and it thus cannot be extended to other proteins that do not have such an endogenous ligand. In order to further understand how the time-dependence of protein-protein interactions facilitates a given cellular signaling, folding, or trafficking pathway, new methodologies need to be developed that can interrogate the timing and sequence of protein-protein interaction events in diverse cellular processes.

Rationale for Developing a New Probe for Time-Resolved Interactomics

An approach that could address this need for temporal deconvolution would be to combine the rapid small molecule-dependent protein stabilization from the DD technology and the ability of the APEX method to provide spatial and temporal information for a set of PPIs. The POI fused to the DD system is only expressed at a basal level in the absence of a stabilizing ligand and is constitutively degraded by the proteasome. One could use the introduction of the stabilizing ligand as the "start" for studying the time-dependent changes in protein-protein interaction partners of the POI. If one could modify the system to be able to affinity purify the POI and its interacting partners at given time points, a MS-based method could be used to identify the different interacting partners associated with the POI at a given time points, as well as quantify differences in protein abundances within the context of a temporal sequence. This would allow researchers to elucidate the temporal dynamics of new signaling, folding, and trafficking pathways that have previously been unexamined.

A model for how a DD system could be appropriately modified comes from Jing et. al., who exploited the specific binding of trimethoprim to wild-type DHFR to develop a fluorescent probe for live-cell imaging.[53] The authors synthesized a trifunctional TMP analog probe that contained a TMP moiety, a fluorescent tag, and a quencher linked to the probe by an electrophilic leaving group (**Fig. 1.3A**). From there, they incorporated active site cysteine mutations into the DHFR using site-directed mutagenesis. Upon the TMP probe binding to the mutated DHFR, the active site cysteines displaced the quencher, rendering the probe fluorescent and also covalently linked to the DHFR.

While Jing et. al. used the wild-type, stable and folded DHFR, their incorporation of active site mutations to covalently bind a TMP-based probe can be adapted to use in a degradation domain context by incorporating both the destabilizing mutations and the active-site cysteine mutations into the DHFR primary sequence. This would ensure that, upon TMP binding and stabilizing the DHFR complex, the probe would react covalently with the protein complex instead of transiently occupying the active site. The goal of this project is to further adapt the trifunctional TMP probe to include a TMP moiety, an electrophilic leaving group, and a click handle. In the DHFR DD system including both the cysteine mutations and the destabilizing mutations, the addition of a click handle to the TMP probe would allow for the POI and its

interacting partners to be isolated by affinity purification and studied by mass spectrometry, thus enabling protein-specific, time-resolved interactomic profiling (**Fig. 1.3B**).

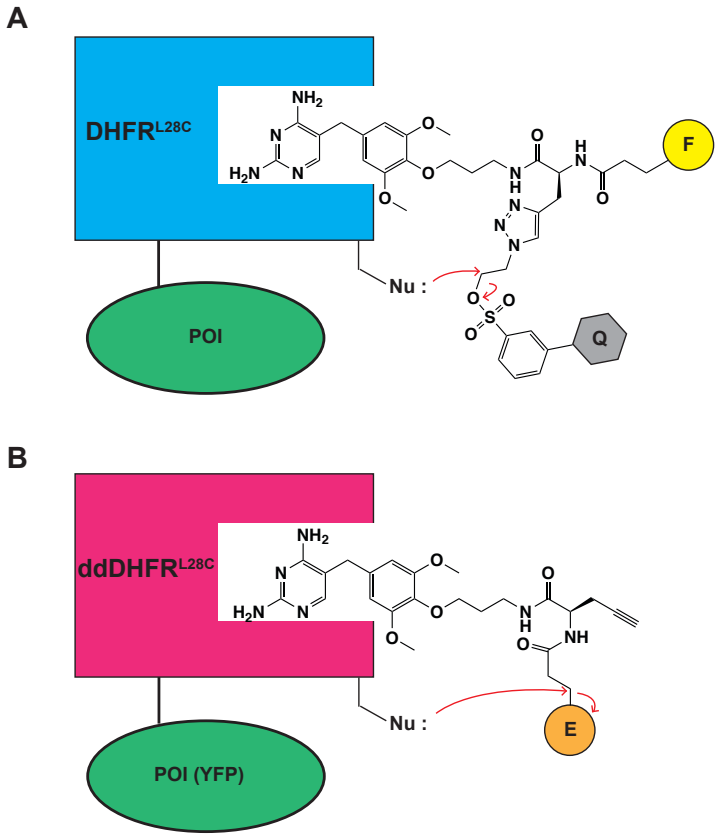

Figure 1.3. Comparison of the Jing et. al. TMP-based probe system with Cys-mutated DHFR and our proposed system.
A. Jing et. al. used stabilized DHFR with incorporated active-site Cys mutations in conjunction with a TMP-based probe including a fluorescent reporter (F) and a displaceable quencher (Q).
B. We propose to use the destabilized DHFR (ddDHFR) with incorporated active-site Cys mutations in conjunction with a TMP-based probe including a Cys-reactive electrophile (E) and an alkyne handle.

Chapter 2 of this thesis will describe the synthesis and characterization of the trifunctional TMP probe. This includes description of the considerations for probe selection, optimization of synthesis, and full description of reaction conditions, and spectral characterization of each synthesized intermediate. Chapter 3 will describe the site-directed mutagenesis (SDM) of the DHFR and the subsequent labeling studies with the probe in lysates and in cells to validate the desired activity of the probes stabilizing DHFR and covalently labeling the protein. This includes description of how the model system was selected; the experimental protocols for the SDM, cell culture, and Click-reaction imaging; the raw data generated from each of these experiments; and future directions for this project.

References

(1) Agrawal, N.; Dasaradhi, P. V. N.; Mohmmed, A.; Malhotra, P.; Bhatnagar, R. K.; Mukherjee, S. K. *Microbiol. Mol. Biol. Rev.* **2003**, *67* (4), 657–685.

(2) Doudna, J. A.; Charpentier, E. *Science* **2014**, *346* (6213), 1258096–1258096.

(3) Prelich, G. *Genetics* **2012**, *190* (3), 841–854.

(4) Andrianantoandro, E.; Basu, S.; Karig, D. K.; Weiss, R. *Mol Syst Biol* **2006**, *2* (1), 1866.

(5) Khera, N.; Rajput, S. *J. Cell. Biochem.* **2017**, *118* (5), 959–961.

(6) Backus, K. M.; Correia, B. E.; Lum, K. M.; Forli, S.; Horning, B. D.; González-Páez, G. E.; Chatterjee, S.; Lanning, B. R.; Teijaro, J. R.; Olson, A. J.; Wolan, D. W.; Cravatt, B. F. *Nature* **2016**, *534* (7608), 570–574.

(7) Edfeldt, F. N. B.; Folmer, R. H. A.; Breeze, A. L. *Drug Discovery Today* **2011**, *16* (7-8), 284–287.

(8) Hopkins, A. L.; Groom, C. R. *Nat Rev Drug Discov* **2002**, *1* (9), 727–730.

(9) Arkin, M. R.; Tang, Y.; Wells, J. A. *Chemistry & Biology* **2014**, *21* (9), 1102–1114.

(10) Ran, X.; Gestwicki, J. E. *Curr Opin Chem Biol* **2018**, *44*, 75–86.

(11) Fuller, J. C.; Burgoyne, N. J.; Jackson, R. M. *Drug Discovery Today* **2009**, *14* (3-4), 155–161.

(12) Balani, S.; Miwa, G.; Gan, L.-S.; Wu, J.-T.; Lee, F. *Curr Top Med Chem* **2005**, *5* (11), 1033–1038.

(13) McDowell, G. S.; Philpott, A. *The International Journal of Biochemistry & Cell Biology* **2013**, *45* (8), 1833–1842.

(14) Yau, R.; Rape, M. *Nat Cell Biol* **2016**, *18* (6), 579–586.

(15) Preston, G. M.; Brodsky, J. L. *Biochem. J.* **2017**, *474* (4), 445–469.

(16) Ardley, H. C.; Robinson, P. A. *Essays Biochem.* **2005**, *41*, 15–30.

(17) Burslem, G. M.; Crews, C. M. *Chemical reviews* **2017**, *117* (17), 11269–11301.

(18) Sakamoto, K. M.; Kim, K. B.; Verma, R.; Ransick, A.; Stein, B.; Crews, C. M.; Deshaies, R. J. *Mol. Cell Proteomics* **2003**, *2* (12), 1350–1358.

(19) Sakamoto, K. M.; Kim, K. B.; Kumagai, A.; Mercurio, F.; Crews, C. M.; Deshaies, R. J. *Proceedings of the National Academy of Sciences of the United States of America* **2001**, *98* (15), 8554–8559.

(20) Schneekloth, J. S.; Fonseca, F. N.; Koldobskiy, M.; Mandal, A.; Deshaies, R.; Sakamoto, K.; Crews, C. M. *J. Am. Chem. Soc.* **2004**, *126* (12), 3748–3754.

(21) Schneekloth, A. R.; Pucheault, M.; Tae, H. S.; Crews, C. M. *Bioorg. Med. Chem. Lett.* **2008**, *18* (22), 5904–5908.

(22) Ivan, M.; Kondo, K.; Yang, H.; Kim, W.; Valiando, J.; Ohh, M.; Salic, A.; Asara, J. M.; Lane, W. S.; Kaelin, W. G. *Science* **2001**, *292* (5516), 464–468.

(23) Lu, J.; Qian, Y.; Altieri, M.; Dong, H.; Wang, J.; Raina, K.; Hines, J.; Winkler, J. D.; Crew, A. P.; Coleman, K.; Crews, C. M. *Chem. Biol.* **2015**, *22* (6), 755–763.

(24) Chu, T.-T.; Gao, N.; Li, Q.-Q.; Chen, P.-G.; Yang, X.-F.; Chen, Y.-X.; Zhao, Y.-F.; Li, Y.-M. *Cell Chemical Biology* **2016**, *23* (4), 453–461.

(25) Montrose, K.; Krissansen, G. W. *Biochemical and Biophysical Research Communications* **2014**, *453* (4), 735–740.

(26) Winter, G. E.; Buckley, D. L.; Paulk, J.; Roberts, J. M.; Souza, A.; Dhe-Paganon, S.; Bradner, J. E. *Science* **2015**, *348* (6241), 1376–1381.

(27) Maynard-Smith, L. A.; Chen, L.-C.; Banaszynski, L. A.; Ooi, A. G. L.; Wandless, T. J. *J. Biol. Chem.* **2007**, *282* (34), 24866–24872.

(28) Egeler, E. L.; Urner, L. M.; Rakhit, R.; Liu, C. W.; Wandless, T. J. *J. Biol. Chem.* **2011**, *286* (36), 31328–31336.

(29) Rodriguez, S.; Wolfgang, M. J. *Chemistry & Biology* **2012**, *19* (3), 391–398.

(30) Park, E. C.; Finley, D.; Szostak, J. W. *Proceedings of the National Academy of Sciences of the United States of America* **1992**, *89* (4), 1249–1252.

(31) Dohmen, R. J.; Wu, P.; Varshavsky, A. *Science* **1994**, *263* (5151), 1273–1276.

(32) Bachmair, A.; Finley, D.; Varshavsky, A. *Science* **1986**, *234* (4773), 179–186.

(33) Bachmair, A.; Varshavsky, A. *Cell* **1989**, *56* (6), 1019–1032.

(34) Banaszynski, L. A.; Chen, L.-C.; Maynard-Smith, L. A.; Ooi, A. G. L.; Wandless, T. J. *Cell* **2006**, *126* (5), 995–1004.

(35) Edwards, S. R.; Wandless, T. J. *J. Biol. Chem.* **2007**, *282* (18), 13395–13401.

(36) Iwamoto, M.; Björklund, T.; Lundberg, C.; Kirik, D.; Wandless, T. J. *Chem. Biol.* **2010**, *17* (9), 981–988.

(37) Matthews, D. A.; Bolin, J. T.; Burridge, J. M.; Filman, D. J.; Volz, K. W.; Kraut, J. *J. Biol. Chem.* **1985**, *260* (1), 392–399.

(38) Harrison, H.; Pegg, H. J.; Thompson, J.; Bates, C.; Shore, P. *BMC Cancer* **2018**, *18* (1), R92.

(39) Shoulders, M. D.; Ryno, L. M.; Cooley, C. B.; Kelly, J. W.; Wiseman, R. L. *J. Am. Chem. Soc.* **2013**, *135* (22), 8129–8132.

(40) Moore, C. L.; Dewal, M. B.; Nekongo, E. E.; Santiago, S.; Lu, N. B.; Levine, S. S.; Shoulders, M. D. *ACS Chem. Biol.* **2015**, *11* (1), 200–210.

(41) Quintino, L.; Namislo, A.; Davidsson, M.; Breger, L. S.; Kavanagh, P.; Avallone, M.; Elgstrand-Wettergren, E.; Isaksson, C.; Lundberg, C. *Molecular Therapy - Methods & Clinical Development* **2018**, *11*, 29–39.

(42) Wagner, T. E.; Becraft, J. R.; Bodner, K.; Teague, B.; Zhang, X.; Woo, A.; Porter, E.; Alburquerque, B.; Dobosh, B.; Andries, O.; Sanders, N. N.; Beal, J.; Densmore, D.; Kitada, T.; Weiss, R. *Nat. Chem. Biol.* **2018**, *14* (11), 1043–1050.

(43) Tarassov, K.; Messier, V.; Landry, C. R.; Radinovic, S.; Molina, M. M. S.; Shames, I.; Malitskaya, Y.; Vogel, J.; Bussey, H.; Michnick, S. W. *Science* **2008**, *320* (5882), 1465–1470.

(44) Stelzl, U.; Worm, U.; Lalowski, M.; Haenig, C.; Brembeck, F. H.; Goehler, H.; Stroedicke, M.; Zenkner, M.; Schoenherr, A.; Koeppen, S.; Timm, J.; Mintzlaff, S.; Abraham, C.; Bock, N.; Kietzmann, S.; Goedde, A.; Toksöz, E.; Droege, A.; Krobitsch, S.; Korn, B.; Birchmeier, W.; Lehrach, H.; Wanker, E. E. *Cell* **2005**, *122* (6), 957–968.

(45) Huttlin, E. L.; Ting, L.; Bruckner, R. J.; Gebreab, F.; Gygi, M. P.; Szpyt, J.; Tam, S.; Zarraga, G.; Colby, G.; Baltier, K.; Dong, R.; Guarani, V.; Vaites, L. P.; Ordureau, A.; Rad, R.; Erickson, B. K.; Wühr, M.; Chick, J.; Zhai, B.; Kolippakkam, D.; Mintseris, J.; Obar, R. A.; Harris, T.; Artavanis-Tsakonas, S.; Sowa, M. E.; De Camilli, P.; Paulo, J. A.; Harper, J. W.; Gygi, S. P. *Cell* **2015**, *162* (2), 425–440.

(46) Hein, M. Y.; Hubner, N. C.; Poser, I.; Cox, J.; Nagaraj, N.; Toyoda, Y.; Gak, I. A.; Weisswange, I.; Mansfeld, J.; Buchholz, F.; Hyman, A. A.; Mann, M. *Cell* **2015**, *163* (3), 712–723.

(47) Butland, G.; Peregrín-Alvarez, J. M.; Li, J.; Yang, W.; Yang, X.; Canadien, V.; Starostine, A.; Richards, D.; Beattie, B.; Krogan, N.; Davey, M.; Parkinson, J.; Greenblatt, J.; Emili, A. *Nature* **2005**, *433* (7025), 531–537.

(48) Gavin, A.-C.; Aloy, P.; Grandi, P.; Krause, R.; Boesche, M.; Marzioch, M.; Rau, C.; Jensen, L. J.; Bastuck, S.; Dümpelfeld, B.; Edelmann, A.; Heurtier, M.-A.; Hoffman, V.; Hoefert, C.; Klein, K.; Hudak, M.; Michon, A.-M.; Schelder, M.; Schirle, M.; Remor, M.; Rudi, T.; Hooper, S.; Bauer, A.; Bouwmeester, T.; Casari, G.; Drewes, G.; Neubauer, G.; Rick, J. M.; Kuster, B.; Bork, P.; Russell, R. B.; Superti-Furga, G. *Nature* **2006**, *440* (7084), 631–636.

(49) Barrios-Rodiles, M. *Science* **2005**, *307* (5715), 1621–1625.

(50) Bisson, N.; James, D. A.; Ivosev, G.; Tate, S. A.; Bonner, R.; Taylor, L.; Pawson, T. *Nat Biotechnol* **2011**, *29* (7), 653–658.

(51) Lobingier, B. T.; Hüttenhain, R.; Eichel, K.; Miller, K. B.; Ting, A. Y.; Zastrow, von, M.; Krogan, N. J. *Cell* **2017**, *169* (2), 350–360.e12.

(52) Choi, H.; Larsen, B.; Lin, Z.-Y.; Breitkreutz, A.; Mellacheruvu, D.; Fermin, D.; Qin, Z. S.; Tyers, M.; Gingras, A.-C.; Nesvizhskii, A. I. *Nat Methods* **2010**, *8* (1), 70–73.

(53) Jing, C.; Cornish, V. W. *ACS Chem. Biol.* **2013**, *8* (8), 1704–1712.

CHAPTER II

SYNTHESIS OF TMP-BASED TRIFUNCTIONAL AFFINITY PROBES

Synthetic Strategy

The synthetic design of the probe was rationalized around a linear synthesis that would couple trimethoprim to a click handle and a cysteine-reactive electrophile (**Scheme 2.1**). Using amide linkages to couple each of these components together enabled a four-step linear sequence that was precedented in the literature until the last step of the sequence.[1] The maleimide was chosen as the electrophilic group for its ease of preparation and its known reactivity with cysteine residues.

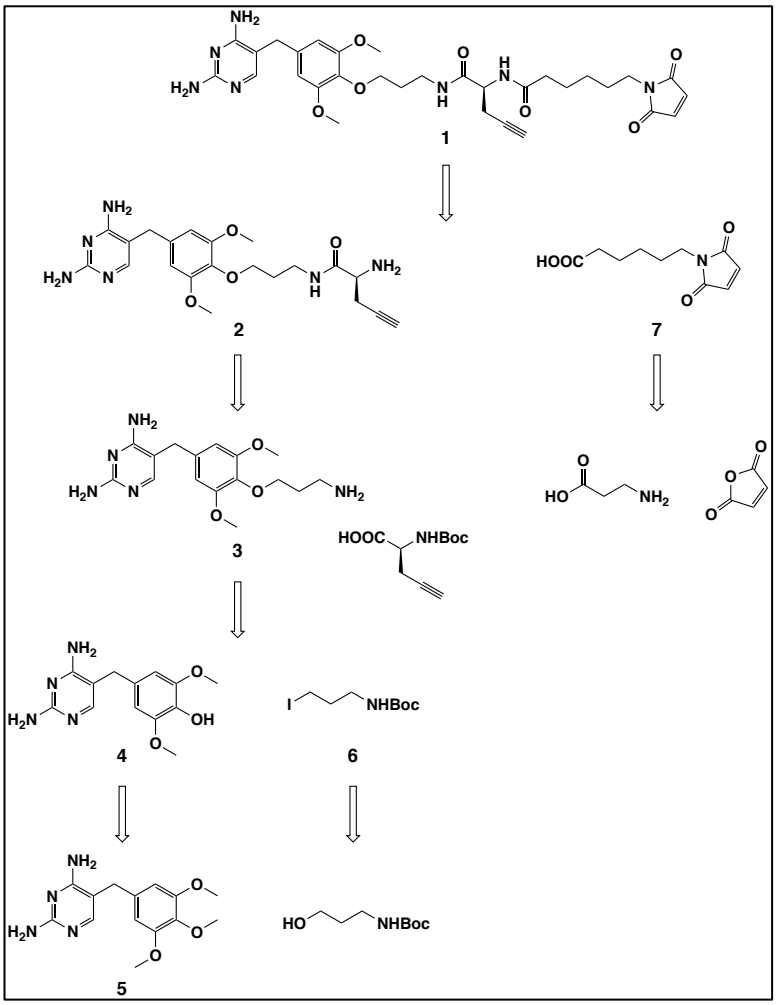

Scheme 2.1. Retro-synthetic Design of TMP Trifunctional Affinity Probe.

The forward synthesis (**Scheme 2.2**) would begin with the *para*-selective demethylation of trimethoprim **5**, which was commercially available, yielding **4** (TMP-OH). The linker to the

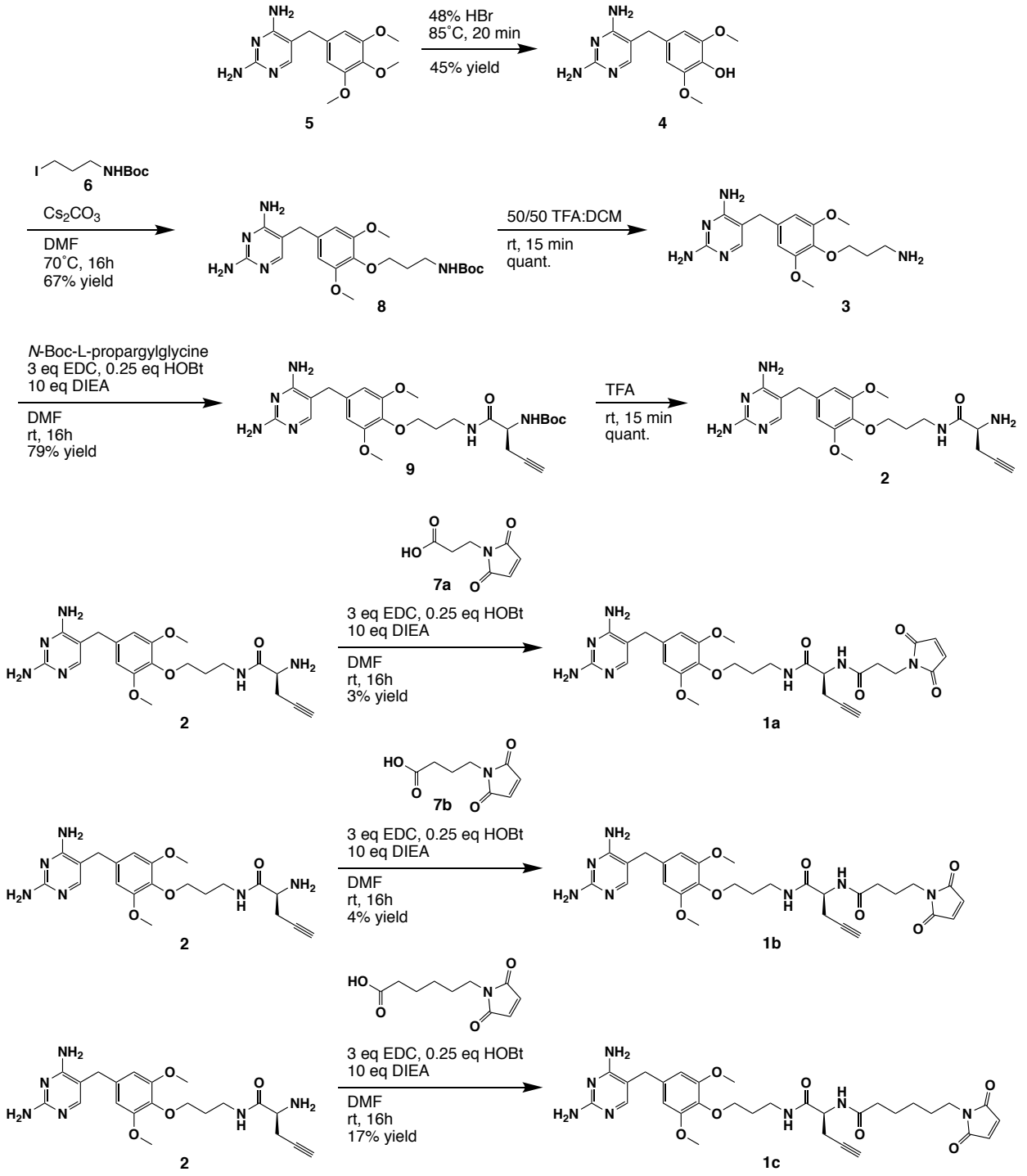

Scheme 2.2. Synthesis of TMP Probe.

Click handle would be installed via S_N2 reaction between **4** and tert-butyl-N-(3-iodopropyl)carbamate **6**, which could be prepared from the commercially available alcohol by an Appel reaction. The S_N2 product **8** (TMP-C3-NHBoc) was then subjected to Boc deprotection using trifluoroacetic acid (TFA) to yield **3** (TMP-C3-NH_2). An amide coupling would then be used to attach *N*-Boc-L-propargylglycine as the click handle to yield **9** (TMP-alkyne-NHBoc), and subsequent Boc deprotection would yield **2** (TMP-alkyne-NH_2). Here, the maleimide-n-alkyl carboxylic acids **7a-7b** would be prepared by condensation of maleic anhydride with β-alanine or the appropriately-sized amino-n-alkyl-carboxylic acid. A second amide coupling would then be used to attach **7a-7b** to **2**. This method of attaching the maleimide-n-alkyl carboxylic acid would allow modularity to be introduced into the probe at the last step of the sequence, as linkers of various lengths would be used to connect the propargyl glycine to the maleimide to yield the final probes **1a-1c**. This approach gave the additional benefit of eliminating a step from the linear sequence by avoiding the condensation reaction with maleic anhydride as the final linear step.

Results

The synthesis was embarked upon with optimization of the TMP demethylation. A literature search showed that many published examples of this reaction were performed at over 20g scale,[2,3] with the smallest published scale being with 5g of TMP.[3,4] In order to replicate these experimental conditions without potentially wasting large amounts of material during optimization, a 1g scale was chosen. Temperature and length of reaction were the first conditions to be optimized. Replicating the literature conditions of 100˚C for 30 minutes yielded over-reacted product, so a time-course experiment was performed. At a 1g scale, time point experiments shows that 20 minutes at 100˚C gave full conversion to **4** with minimal over-reacted product, while 5 and 10 minutes showed a mix of starting material and product by NMR (**Supplemental Figure 1**). Additional experiments showed that lowering the temperature from 100˚C to 85˚C and reacting for 15 minutes gave more consistent formation of **4** without over-oxidation. While published examples tracked the formation of product by TLC using 1:1 EtOAC: Hex, product formation could not be detected using this gradient in our hands.[5]

Further optimization focused on the reaction vessel and the nature of the heat bath. When using an aluminum pie block with a 40 mL vial, the hot plate used would give up to 5˚C

fluctuations in temperature throughout the course of the experiment. Therefore, the pie block was substituted for an oil bath, and the vial was substituted for a 50 mL round-bottom flask and a condenser. Additionally, since 48% aqueous HBr was used, it was determined that returning to the 100˚C temperature would give better control over temperature fluctuations, as the condenser would prevent the water from boiling away at oil bath temperatures over 100˚C. Under these conditions, it was found that a 14 min reaction time gave full conversion to **4** with minimal over-oxidation (**Table 2.1**).

	Vessel/ Heat source	**Temperature (˚C)**	**Reaction Time**	**Result/ Yield**
1	vial/ hot plate	100	30:00	overreacted
2	vial/ hot plate	100	20:00	clean by NMR (no yield taken)
3	vial/ hot plate	85	15:00	425 mg (45%)
4	50mL RB/ oil bath	100	15:00	overreacted
5	50mL RB/ oil bath	100	14:00	509 mg (55%)

Table 2.1. Reaction conditions for optimization of TMP demethylation.

From here, the tert-butyl (3-iodopropyl)carbamate was prepared from the alcohol by an Appel reaction. Following literature precedent, a 3 hour reaction under inert conditions followed by chromatographic separation using 30% ethyl acetate in hexanes gave the product **6** in 54% yield.[6] An S_N2 reaction was then performed using the demethylated trimethoprim **4** and freshly-prepared tert-butyl (3-iodopropyl)carbamate **6**. Reacting overnight with cesium carbonate in DMF at 70˚C was shown by NMR to yield the product, but finding optimal purification conditions proved challenging. Initial attempts started with 10% MeOH in DCM, which gave rapid elution of product **8** but lacked clean separation. After trying lower percentages of polar solvent and finding that the product stuck to the column, a 95:4.5:0.5 mixture of DCM:MeOH:NH_4OH was used which more efficiently eluted the product. However, LC/MS analysis of the TMP-C3-NHBoc product identified a 16% impurity corresponding to TMP that had been doubly demethylated and subsequently performed the S_N2 reaction at both phenolic oxygens. This product was carried forward with the impurity present, as it could not be separated by normal-phase chromatography.

From here, the TFA deprotection was optimized from taking place over twelve hours to running for only fifteen minutes, as full product formation was observed by TLC after 15min. It was also found that using a 50% TFA:DCM mixture led to increased solubility of the product **3** and led to faster and cleaner deprotection.

Next, the TMP-C3-NH_2 product **3** underwent amide coupling with *N*-Boc-L-propargyl glycine. The reaction was initially attempted using the HATU coupling reagent, but this reagent led to increased difficulty eluting the product from the column, resulting in low yields. Switching to the EDC coupling reagent led to higher yields of **9**, but challenges in the purification remained. To ensure that there was no residual TFA left over from the TMP-C3-NHBoc (**8**) deprotection that could deprotect the Boc group on the propargyl glycine, 10 equivalents of DIEA were stirred with the TMP-C3-amine (**3**) in DMF before any additional reagents were added to the reaction mixture. When it was discovered that DIEA was co-eluting from the column with the product but was not detectable by UV on a TLC plate, $KMnO_4$ stain was employed to monitor the chromatography column, which readily distinguished between the product **9** and DIEA at 9:1 DCM:MeOH. Using 7% of 9:1 MeOH:NH_4OH in DCM successfully eluted the product **9** in 79% yield with no signs of DIEA by NMR. LC/MS analysis identified a 25% impurity distinct from the desired product, but its identity has not been determined. The deprotection step was then performed in pure TFA for 15 minutes to form **2**, showing full deprotection by TLC and NMR.

The maleimide-n-alkyl carboxylic acids **7a-7b** were then prepared for the final amide coupling step. While the 6-maleimidohexanoic acid was commercially available, the 3- and 4-carbon versions had to be synthesized by condensing maleic anhydride with either β-alanine or 4-aminobutanoic acid in boiling acetic acid according to literature precedent.[7] Chromatographic separation in 1:6 EtOAc: Et_2O yielded the pure products **7a-7b** in 51-66% yields. The second amide coupling step between the maleimide-n-alkyl carboxylic acids and **2** was performed under the same conditions as the first amide coupling step, but the chromatography column required higher methanol concentrations to elute the product from the column. These reactions were low-yielding, but it is unclear whether this is due to the reaction conditions, the separation conditions, or to the relatively small scale of reaction (25 mg). Additionally, the ^1H NMR and the LC/MS data from these reactions showed significant impurities present that had been carried forward from past reactions. However, the product was deemed pure enough to carry forward for

preliminary biological testing based on the presence of the maleimide peak in the ^{1}H-NMR spectrum in the aromatic region for each synthesized probe and detection of product by LC/MS. Further optimization of this reactions step is warranted to improve the yield and the purity of the products.

In summary, three trifunctional TMP-based affinity probes were synthesized in sufficient quantities to bring forward for *in vivo* testing. However, significant optimization of the final amide coupling step is still required, and alternative purification conditions should be considered throughout the course of the synthesis. Future directions for the synthetic chemistry include synthesizing probes with different Cys-reactive groups, such as iodoacetamides, vinyl ketones, or tosylates. To synthesize these variants, the second amide coupling step would be performed with N-Boc-aminobutanoic acid rather than the maleimide-n-alkyl carboxylic acid. After Boc deprotection, the cysteine-reactive group would be coupled to the free amine to form the final product.

Methods

General Methods. Unless otherwise noted, all reagents and solvents were ordered from Sigma Aldrich and were used without further purification. Acetone, methanol, hexanes, ethyl ether, and ethyl acetate were purchased from Fisher. Chloroform-D was sourced from Cambridge Isotope Laboratories, Inc. 3-(Boc-amino)-1-propanol, 6-Maleimidocaproic acid, 4-Aminobutyric acid, 1-(3-Dimethylaminopropyl)-3-ethylcarbodiimide (EDC), Boc-L-propargylglycine, Boc-gamma-Abu-OH, Boc-6-aminohexanoic acid, HATU, and n-(3-iodopropyl)-,1,1-dimethyl ester were purchased from Combi-Blocks. Nuclear magnetic resonance (NMR) spectra were recorded on a Bruker 400 (400 MHz) Fourier Transform (FT) NMR spectrometer for ^{1}H-NMR experiments and on a Bruker 600 (600 MHz) FT NMR for ^{13}C NMR experiments at Vanderbilt University Department of Chemistry. ^{1}H NMR spectra are tabulated in the following order: multiplicity (s, singlet; d, doublet; t, triplet; q, quartet; p, pentet; m, multiplet; br, broad), number of protons. Liquid chromatography (LC) mass spectrometry (MS) data was obtained using either 1) an Agilent 1200 series HPLC paired with an Agilent 6100 series ESI single quadruopole mass spectrometer, or 2) a Thermo Fisher Scientific MSQ Plus ESI single quadrupole mass spectrometer.

Synthesis of 4-((2,4-diaminopyrimidin-5-yl)methyl)-2,6-dimethoxyphenol (TMP-OH, **4**). A 50 mL round bottom flask containing 48% hydrobromic acid (12 mL) was attached to a reflux condenser and placed in oil. The bath was heated to 100˚C before trimethoprim (1.00 g, 3.44 mmol) was added, and the solution was allowed to reflux for 14 minutes. The flask was removed from the oil bath, and the reaction was quenched by adding 50% (w/v) sodium hydroxide in water (6 mL). The reaction mixture was then allowed to cool to room temperature and was subsequently left to cool at 4˚C overnight. The resulting crystals were then filtered and rinsed with ice-cold water. The crystals were then dissolved in boiling water, and the solution was neutralized to pH 7 by adding NH_4OH drop-wise to the vial until the solution was judged as neutral using pH paper. The white-colored crystals crashed out of the solution, and the suspension was allowed to cool at 4˚C overnight. The crystals were then filtered, rinsed with cold water, and dried under vacuum to produce the desired product as tan crystals (522 mg, 55% yield). ^{1}H NMR (400 MHz, DMSO) δ ppm: 7.45 (s, 1H), 6.48 (s, 2H), 3.69 (s, 6H), 3.47 (s, 2H). ^{13}C NMR (600 MHz, DMSO) δ ppm: 163.88, 157.10, 148.43, 134.48, 128.49, 108.97, 106.83, 56.50, 32.67. Compound **8** m/z Calcd. for $C_{13}H_{16}N_4O_3$: 277.1. Found: 277.3. Full spectra shown in **Supplemental Figure 2-4.**

Synthesis of tert-butyl (3-iodopropyl)carbamate (**6**). To a stirring mixture of triphenylphosphine (748 mg, 1.0 Eq, 2.85 mmol) and 1H-imidazole (194 mg, 1.0 Eq, 2.85 mmol) under Ar in DCM (28 mL) was added diiodine (869 mg, 1.2 Eq, 3.42 mmol) at 0°C. Upon iodine addition, the solution went from clear to a bright yellow, and subsequently a dark red. The reaction mixture was stirred for 5 min before tert-butyl (3-hydroxypropyl)carbamate (500 mg, 1.0 Eq, 2.85 mmol) in DCM (6 mL) was added drop-wise. The reaction was allowed to warm to 25 °C and stir for 3.5 hour before the reaction mixture was washed successively with 30 mL of water, saturated sodium thiosulfate solution, and brine. The organic layer was then dried over $MgSO_4$, filtered, and concentrated *in vacuo*. The crude, yellow product was then subjected to column chromatography (30% EtOAc in Hex). Fractions containing product were isolated and concentrated to yield the desired product as a yellow oil (439 mg, 54.0 % yield)**.** R_f = 0.6 in 30% EtOAc in Hex. ^{1}H NMR (400 MHz, $CDCl_3$) δ ppm: 4.63 (br. s, 1H), 3.20 (m, 4 H), 2.01 (m, 2 H), 1.45 (s, 9 H). ^{13}C NMR (600 MHz, $CDCl_3$) δ ppm: 154.95, 78.32, 40.01, 32.42, 27.90, 2.20. Full spectra shown in **Supplemental Figure 5-7**.

Synthesis of TMP-C3-NH_2 (**3**). Into a 20 mL vial was placed TMP-OH **4** (425 mg, 1 Eq, 1.54 mmol) , tert-butyl (3-iodopropyl)carbamate **6** (439 mg, 1 Eq, 1.54 mmol) , and cesium carbonate (1000 mg, 2 Eq, 3.08 mmol). The mixture was dissolved in DMF (12 mL) and was allowed to stir at 70 °C for 12 hours. The solvent was then removed by adding toluene and subsequently using rotary evaporation, and the crude mixture was subjected to column chromatography (6-8% of 1:9 NH_4OH:MeOH in DCM, silica) to yield TMP-C3-NHBoc **8** as a light yellow solid. R_f = 0.3 in 1:9 MeOH: DCM. ^{1}H NMR (400 MHz, $CDCl_3$) δ ppm: 7.76 (s, 1H), 6.38 (s, 2H), 3.99 (t, *J* = 5.4 Hz, 2H), 3.80 (s, 6H), 3.64 (s, 2H), 3.39 (m, 2 H), 1.88 (m, 2 H), 1.44 (s, 9 H). ^{13}C NMR (600 MHz, $CDCl_3$) δ ppm: 162.81, 162.40, 156.47, 153.45, 135.38, 134.21, 105.99, 104.87, 78.60, 71.21, 55.92, 34.49, 29.30, 28.46. Compound **8** m/z Calcd. for $C_{21}H_{31}N_5O_5$: 434.2. Found: 434.5. Full spectra shown in **Supplemental Figure 8-10**

The product was then dissolved in 50% TFA in DCM (12 mL) and stirred for 15 minutes at room temperature before the solvent was evaporated *in vacuo* to afford 5-(4-(3-aminopropoxy)-3,5-dimethoxybenzyl)pyrimidine-2,4-diamine (**3,** TMP-C3-amine) as a white solid (362 mg, 71% yield over two steps). ^{1}H NMR (400 MHz, MeOD) δ ppm: 7.26 (s, 1H), 6.62 (s, 2H), 4.11 (t, *J* = 5.4 Hz, 2H), 3.85 (s, 6H), 3.69 (s, 2H), 3.26 (t, *J* = 6.2 Hz, 2 H), 2.06 (m, 2 H). ^{13}C NMR (600 MHz, MeOD) δ ppm: 166.11, 156.28, 154.48, 140.46, 136.39, 134.36, 110.69, 106.97, 73.44, 56.55, 40.32, 33.93, 28.28. Compound **3** m/z Calcd. for $C_{16}H_{23}N_5O_3$: 334.2. Found: 334.3. Full spectra shown in **Supplemental Figure 11-13.**

Synthesis of TMP-alkyne-NH_2 (**2**). A 40 mL vial was placed under vacuum and filled with Ar. To the vial was added 1 mL of DMF, which was de-gassed with Ar for 5 min. To the vial was then added TMP-C3-amine **3** (172.0 mg, 1.10 Eq, 515.9 µmol) and *N*-ethyl-N-isopropylpropan-2-amine (DIEA) (606.2 mg, 0.82 mL, 10 Eq, 4.690 mmol), which was allowed to stir for 5 min. Into a separate, inert 40 mL vial was added 1 mL of de-gassed DMF, 1H-benzo[d][1,2,3]triazol-1-ol hydrate (HOBt hydrate) (17.95 mg, .25 Eq, 117.2 µmol) , and (S)-2-((tert-butoxycarbonyl)amino)pent-4-ynoic acid (100.0 mg, 1.0 Eq, 469.0 µmol). The solution was allowed to stir for 5 min. The contents of the vial containing **3** and the DIEA were transferred via inert syringe to the vial containing the acid and HOBt, and the solution was allowed to stir for 15 min. To the vial was then added 3-(((ethylimino)methylene)amino)-N,N-dimethylpropan-1-

amine hydrochloride (EDC) (269.7 mg, 3 Eq, 1.407 mmol), and the solution was allowed to stir at 25 °C for 12 hours. The reaction was then analyzed by TLC and judged to be completed (1:9 MeOH:DCM, $R_f = 0.3$). The solvent was removed by adding toluene and subsequently using rotary evaporation. The crude product was purified by column chromatography. A column was run from 5-7% of (1:9 NH_4OH: MeOH) in DCM to yield TMP-alkyne-NHBoc **9** as a yellow solid. $R_f = 0.3$ in 1:9 MeOH:DCM. ^{1}H NMR (400 MHz, $CDCl_3$) δ ppm: 7.78 (s, 1 H), 6.40 (s, 2 H), 4.27 (br. s, 1 H), 4.03 (m, 2 H), 3.82 (s, 6 H), 3.66 (s, 2 H), 3.60 (m, 2 H), 2.75 (m, 1 H), 2.60 (m, 1 H), 1.99 (m, 1 H), 1.93 (m, 2 H), 1.38 (s, 9 H). Compound **9** m/z Calcd. for $C_{26}H_{36}N_6O_6$: 529.4. Found: 529.4. Full spectra shown in **Supplemental 14-15.**

The product was then dissolved in 50% TFA in DCM (2 mL) and was allowed to stir for 15 minutes at 25˚C before the solvent was evaporated *in vacuo*, yielding the product (S)-2-amino-N-(3-(4-((2,4-diaminopyrimidin-5-yl)methyl)-2,6-dimethoxyphenoxy)propyl)pent-4-ynamide (**2,** TMP-alkyne-NH_2) as a white solid (159 mg, 79% yield). ^{1}H NMR (400 MHz, $CDCl_3$) δ ppm: 7.25 (s, 1 H), 6.57 (s, 2 H), 3.99 (m, 3H), 3.82 (s, 6 H), 3.67 (s, 2 H), 3.54 (m, 1 H), 3.47 (m, 1 H) 2.82 (m, 2H), 2.59 (m, 1 H), 1.92 (m, 2 H). ^{13}C NMR (600 MHz, $CDCl_3$) δ ppm: 168.56, 166.09, 156.22, 154.88, 140.43, 136.78, 133.89, 110.74, 107.11, 77.32, 74.79, 72.14, 57.58, 52.89, 38.35, 33.88, 30.59, 22.32. Full spectra shown in **Supplemental 16-17.**

General procedure for preparation of maleimide-n-alkyl carboxylic acids (**7**). The appropriate amino acid (1.00 Eq, 1.00 mmol) and furan-2,5-dione (118 mg, 1.20 Eq, 1.20 mmol) in acetic acid (7 mL) were stirred at 120˚C for 6 hours. The reaction mixture was poured into water after cooling to room temperature and extracted with ethyl acetate (3 × 10 mL). The organic layers were combined, washed with brine, dried over anhydrous Mg_2SO_4, and evaporated under reduced pressure to give the crude product. Purification was performed by column chromatography in 1:6 ethyl acetate/petroleum ether (v/v).

3-maleimidopropanoic acid (7a) was prepared from β-alanine in 51% yield as a white solid according to the general protocol. ^{1}H NMR (400 MHz, $CDCl_3$) δ ppm: 6.72 (s, 2 H), 3.85 (t, J = 7.4, 2H), 2.71 (t, J = 7.4, 2 H). ^{13}C NMR (400 MHz, $CDCl_3$) δ ppm: 176.71, 170.47, 134.35, 33.33, 32.61. Full spectra shown in **Supplemental Figure 18-19.**

4-maleimidobutanoic acid (7b) was prepared from 4-aminobutyric acid in 66% yield as a white solid according to the general protocol. ^{1}H NMR (400 MHz, $CDCl_3$) δ ppm: 6.71 (s, 2 H), 3.60

(t, J = 6.9 Hz, 2 H), 2.38 (t, J = 7.4 Hz, 2 H), 1.93 (dd, J_1 = 7.0, J_2 = 7.2, 2 H). ^{13}C NMR (600 MHz, $CDCl_3$) δ ppm: 178.72, 170.90, 134.25, 37.05, 31.25, 23.60. Full spectra shown in **Supplemental Figure 20-21.**

General procedure for preparation of TMP-alkyne-mal (**1a-1c**). To a 40 mL vial under inert conditions was added 1 mL of DMF, which was de-gassed with Ar for 5 min. To the vial was then added DIEA (70.57 mg, 95 µL, 10.00 Eq, 546.0 µmol) and TMP-alkyne-NH_2 **2** (25.73 mg, 1.10 Eq, 60.06 µmol), which was allowed to stir for 5 min. Into a separate, inert 40 mL vial was added 1 mL of de-gassed DMF, HOBt hydrate (2.090 mg, .25 Eq, 13.65 µmol), and the maleimide-n-alkyl carboxylic acid (1.00 Eq, 54.60 µmol). This solution was allowed to stir for 5 min. The contents of the vial containing the amine and the DIEA were transferred to the vial containing the acid and HOBt, and the solution was allowed to stir for 15 min. To the vial was then added EDC (31.40 mg, 3.00 Eq, 163.8 µmol), and the solution was allowed to stir at 25˚C for 12 hours. The reaction was then analyzed by TLC and judged to be completed (R_f = 0.3 in 1:9 MeOH:DCM). The solvent was removed by adding toluene and subsequently using rotary evaporation. The crude product was purified by column chromatography. A column was run from 8-10% of (1:9 NH_4OH: MeOH) in DCM.

3CMal (1a) was prepared from 3-maleimidopropanoic acid **7a** in 3% yield according to the general protocol. Impure product was obtained; full spectra shown in **Supplemental Figure 22.**

4CMal (1b) was prepared from 4-maleimidobutanoic acid **7b** in 4% yield according to the general protocol. Impure product was obtained; full spectra shown in **Supplemental Figure 23.**

6CMal (1c) was prepared from 6-maleimidohexanoic acid in 17% yield according to the general protocol. ^{1}H NMR (400 MHz, $CDCl_3$) δ ppm: 7.76 (s, 1 H), 6.68 (s, 2 H), 6.41 (s, 2 H), 4.56 (m, 1 H), 4.04 (m, 2 H), 3.82 (s, 6 H), 3.67 (s, 2 H), 3.58 (t, J = 5.8 Hz, 2 H), 3.49 (t, J = 7.2 Hz, 2 H), 2.70 (m, 1 H), 2.64 (m, 1 H), 2.13 (t, J = 7.5 Hz, 2H), 2.01 (m, 1 H), 1.93 (m, 2 H), 1.56 (m, 2 H), 1.26 (m, 4 H). Compound **1c** m/z Calcd. for $C_{31}H_{39}N_7O_7$: 622.3. Found: 622.5. Full spectra shown in **Supplemental Figure 24-25**.

Acknowledgements

I would like to thank Dr. Lars Plate for his unyielding support on the project and for providing all laboratory materials. I give my thanks to Robert Mason Clark for his contributions toward the

optimization of reaction conditions for the TMP demethylation and for assistance with producing material. I also thank Dr. Steve Townsend for his guidance on the TMP demethylation and for access to his laboratory equipment, Dr. Don Stec for assistance with the NMR, and Dr. Plamen Christov for his assistance with the LC/MS.

References

(1) Jing, C.; Cornish, V. W. *ACS Chem. Biol.* **2013**, *8* (8), 1704–1712.

(2) Long, M. J. C.; Pan, Y.; Lin, H.-C.; Hedstrom, L.; Xu, B. *J. Am. Chem. Soc.* **2011**, *133* (26), 10006–10009.

(3) Liu, W.; Li, F.; Chen, X.; Hou, J.; Yi, L.; Wu, Y.-W. *J. Am. Chem. Soc.* **2014**, *136* (12), 4468–4471.

(4) Liu, P.; Calderon, A.; Konstantinidis, G.; Hou, J.; Voss, S.; Chen, X.; Li, F.; Banerjee, S.; Hoffmann, J.-E.; Theiss, C.; Dehmelt, L.; Wu, Y.-W. *Angew. Chem. Int. Ed.* **2014**, *53* (38), 10049–10055.

(5) Rashid, U.; Ahmad, W.; Hassan, S. F.; Qureshi, N. A.; Niaz, B.; Muhammad, B.; Imdad, S.; Sajid, M. *Bioorg. Med. Chem. Lett.* **2016**, *26* (23), 5749–5753.

(6) Ensch, C.; Hesse, M. *Helvetica Chimica Acta* **2002**, *85* (6), 1659–1673.

(7) Han, J.; Sun, L.; Chu, Y.; Li, Z.; Huang, D.; Zhu, X.; Qian, H.; Huang, W. *J. Med. Chem.* **2013**, *56* (24), 9955–9968.

CHAPTER III

VALIDATION OF THE TRIFUNCTIONAL TMP-BASED AFFINITY PROBES IN CELLULAR MODEL SYSTEMS

Introduction

As a first step toward determining the ability of these probes to operate in complex cellular environments, a proof-of-concept experiment was designed to validate the probe's design. Such an experiment should determine if the DNA construct coding for DHFR can be successfully transfected in cells; whether the TMP portion of the probe can successfully stabilize the expressed DHFR; and whether the probe can covalently attach to the DHFR.

Enhanced yellow fluorescence protein (YFP) was selected as the protein of interest (POI) to be fused to DHFR for its ability to readily demonstrate transfection success by monitoring fluorescence. (**Figure 3.1**) In experiments using the destabilized DHFR construct, YFP fluorescence can demonstrate successful stabilization of the construct by the TMP moiety of the probe, as fluorescence should only be observed after treatment with TMP. To determine whether the probe has been covalently linked to the DHFR, a Cy3 azide fluorophore can be attached to the alkyne on the probe via Cu-catalyzed Click reaction. Subsequent SDS-PAGE and Western blot analysis can show whether probe-dependent Cy3 fluorescence is visible at the molecular

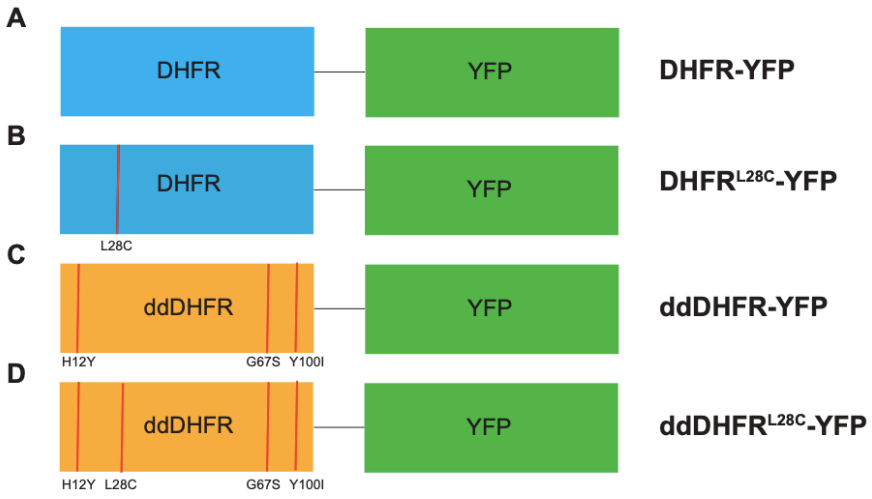

Figure 3.1. DHFR-YFP constructs tested. A. Stabilized DHFR-YFP with no active-site cysteine mutations. B. Stabilized DHFR-YFP with active-site cysteine introduced by SDM. L28C is shown, but other Cys mutations were also tested. C. De-stabilized DHFR with no active-site cysteine mutation. Location of the mutations for the destabilized domain are indicated. D. De-stabilized DHFR with active-site cysteine introduced by SDM. L28C is shown, but other Cys mutations were also tested.

weight corresponding to the DHFR, confirming covalent labeling under these denaturing conditions. The general workflow of this project was to a) use site-directed mutagenesis to take stabilized, wild-type DHFR and incorporate cysteine mutations near the TMP binding site based on a previous study from Jing et. al.;[1] b) once the probe was synthesized and the stabilized cysteine mutations were generated, add the TMP probe to the stabilized DHFR cysteine mutants and probe for GFP expression and Cy3 incorporation after a Click reaction; and c) once these experiments were validated, use the destabilized DHFR and incorporate cysteine mutations using site-directed mutagenesis and subsequently probe for GFP and Cy3 incorporation after a Click reaction.

Site-Directed Mutagenesis to Generate Cysteine-Mutated DHFR

The first step toward generating the necessary Cys-mutated DHFR constructs was to insert the ^{WT}DHFR-YFP DNA into a pDEST40 expression vector using an NEBuilder HiFi DNA Assembly kit. We started from a ddDHFR-YFP-pDEST40 construct from Shoulders et. al.,[2] in which we replaced the ddDHFR with ^{WT}DHFR that was PCR-amplified from *E. coli*. The DNA was then transformed in *E. coli,* plasmid DNA was isolated and purified by miniprep, and the correct DNA sequence was confirmed. Upon verifying that the plasmid assembly was successful, plasmid preparation was scaled up using midipreps.

From here, site-directed mutagenesis was used to incorporate the cysteine mutations into the active site. Past work from Jing et. al. was used to select the most efficient residues that were modified by a similar probe, and these positions were prioritized for mutagenesis.[1] The authors observed that a 12-atom spacer between the 4'-OH group of TMP and the β-carbon of the electrophile led to the best reactivity with the cysteine residues near the TMP binding site. To select the active-site residues to mutate to cysteines, the authors then examined residues that were within 12 Å (~9 C−C bonds) from the 4'-OH group of TMP and selected 16 of them based on their location on DHFR's surface, their orientation toward the active site, and their lack of interference with TMP binding or protein stability. Based on this work, we tested probes containing 13, 14, or 16 atoms between the *p*-methoxy on the trimethoprim and the double bond of the maleimide (i.e. probes containing a 3, 4, and 6-carbon maleimido-n-alkylamide). We then selected the five DHFR active site residues that Jing et. al. found to have the highest reactivity for their probe electrophile to mutate into cysteines and test with our synthesized probe system.

Work toward this aim began by designing primers that would include the cysteine mutations. Initially, the primers were designed for a QuikChange mutagenesis protocol using Pfu Ultra polymerase and were fully complementary and overlapping, with the mutation site in the middle of the primer. This method was successful for the L28C, K32C, and P55C mutations. After multiple failed attempts using this method to produce the N23C and P25C mutations, the Q5 mutagenesis system (NEB) was then used. In this approach, the primers were designed to point away from one another to ensure that the entire plasmid was being exponentially amplified creating blunt ends, and the mutation site was located in the middle of one primer. After optimizing the temperature conditions for the polymerization, the two mutations were successfully incorporated. Once each of these mutations had its DNA sequence verified, the miniprepped DNA samples were used to transform more bacterial cultures to prepare glycerol stocks and concentrated DNA stocks.

This same process was later used to develop cysteine mutants for the destabilized DHFR-YFP. Starting from a stock of the destabilized DHFR-YFP pDEST40 DNA, the same primers and polymerases were used to incorporate the cysteine mutations without any optimization or alteration of conditions.

Application of TMP Probes to Stabilized DHFR Cysteine Mutants

Once the Cys-containing DHFR-YFP constructs had been made, the system was validated in cell models. HEK293^{DAX} cells{Shoulders:2013ek} were first transformed with either the wild-type DHFR-YFP or one of the cysteine mutants. A day later, synthesized TMP probes were introduced to the cells, and the cells were harvested after 24 hours. After lysing the cells and normalizing the protein concentrations, a Cu-catalyzed Click reaction was performed to link a Cy3-picolyl azide fluorophore to the alkyne handle on the probe. The samples were then analyzed by SDS-PAGE and Western blot to test for the presence of YFP and Cy3 signal.

Initial experiments used TMP probes **1a-1c** (referred to as 3CMal for **1a**, 4CMal for **1b**, and 6CMal for **1c**) with various linker lengths between the maleimide electrophile and the amide bond connecting it to the propargyl glycine. Probes with linker lengths of 3, 4, and 6 carbons were applied directly to cells at 50 μM for 3 hours, and the resulting cell lysates were subjected to Click reaction conditions. While the Western blot showed mostly consistent GFP signal across samples, no Cy3 signal was observed (**Figure 3.2**).

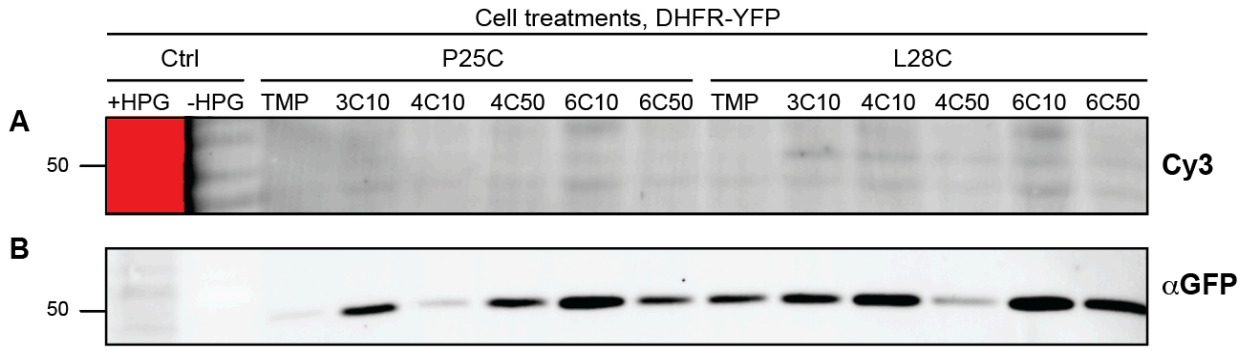

Figure 3.2. Western blot of DHFR^{P25C}-YFP and DHFR^{L28C}-YFP expressed in HEK293DAX cells that were reacted with 50 μM of TMP or with the indicated compound at the indicated concentration (3CMal at 10 μM, 4CMal at 10 μM, etc) for 3 hours. These were compared with control lanes of whole cell lysates with or without proteome-wide incorporation of homo-propargyl glycine (HPG). A. Blot imaged for Cy3 after Click reaction with probe labeled lysates with pycolyl-azide-Cy3 to visualize extent of covalent labeling. B. Western blot using anti-GFP antibody to visualize total expressed DHRF-YFP. Lanes showing red refer to over-exposed labeling.

To account for the possibility that the probe could not pass through the cell membrane, we applied the probe to the cell lysates rather than directly to cells and repeated the same set of experimental conditions to test different probe linker lengths and Cys positions on DHFR. New cell lysates were prepared that had been transformed with the stabilized DHFR-YFP (N23C, P25C, L28C, K32C, and P55C) but were not incubated with the probe. The cell lysates of these samples were then treated with the TMP probes for 4 hours at 50 μM and subjected to the Click reaction. The subsequent Western blots showed GFP and Cy3 signal at approximately the same molecular weight, confirming that the DNA construct was being successfully transformed in cells and that the probe was covalently linked to the DHFR active site. When the five DHFR mutants were each tested with the three synthesized probes (3CMal, 4CMal, 6CMal), it was found that the L28C mutant showed the highest Cy3 signal, and the 4CMal probe consistently showed higher Cy3 signal than the 3CMal or the 6CMal **(Figure 3.3)**.

With this preliminary data in hand, further probe labeling experiments were performed in lysates using the L28C mutant and the 4CMal probe (**1b**). Time-point experiments were conducted by incubating the lysates for 1h, 2h, 4h, and 24h with the TMP probe at 50 μM before performing the Click reaction and running SDS-PAGE. The Cy3 signal showed a time-dependent increase in signal, confirming that longer incubation times led to better probe labeling. (**Figure 3.4**).

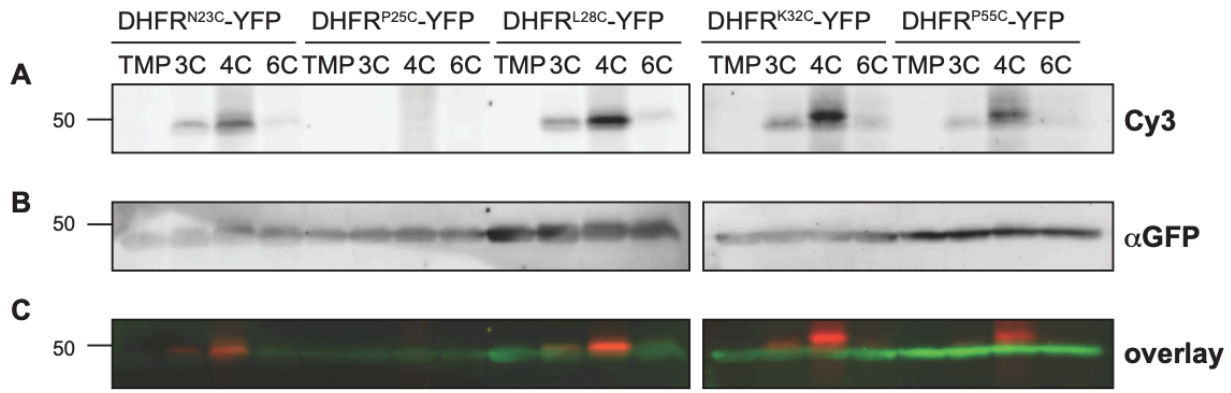

Figure 3.3. Western blot of DHFR-YFP cysteine mutant variants expressed in HEK293^{DAX} cells and cell lysates reacted with the indicated probe compounds (50µM) for 4h to test labeling efficiency for combination of Cys mutants and linker lengths (**1a**: 6-carbon, **1b**, 4-carbon, **1c**, 3-carbon, TMP control). A. Blot imaged for Cy3 after Click reaction with probe labeled lysates with pycolyl-azide-Cy3 to visualize extent of covalent labeling. B. Western blot using anti-GFP antibody to visualize total expressed DHRF-YFP. C. overlay of both image channels (green: anti-GFP, red: Cy3).

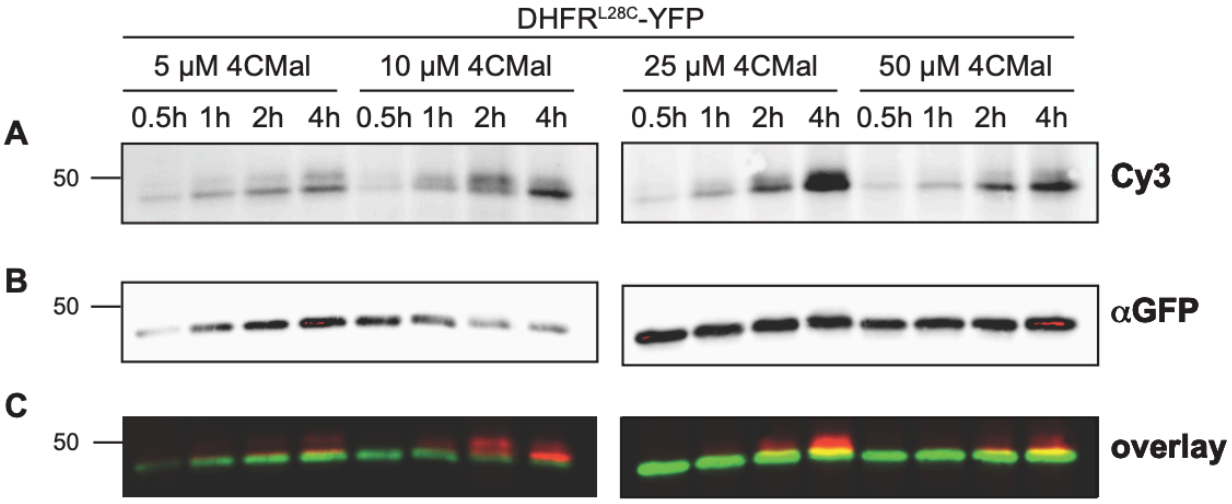

Figure 3.4. Western blot of DHFR^{L28C}-YFP cysteine mutant expressed in HEK293^{DAX} cells and cell lysates reacted with the 4CMal probe compound (**1b**) for 4 hours to test labeling efficiency at various concentrations using the probe and Cys-mutant combination showing the most efficient labeling. A. Blot imaged for Cy3 after Click reaction with probe labeled lysates with pycolyl-azide-Cy3 to visualize extent of covalent labeling. B. Western blot using anti-GFP antibody to visualize total expressed DHRF-YFP. C. overlay of both image channels (green: anti-GFP, red: Cy3).

Furthermore, the optimal concentration of the probe compounds was determined. For this purpose, the lysates were incubated with different concentrations of 4CMal. After 4 hour

incubation with 5, 10, 25, and 50 μM of probe and subsequent Click reactions, it was determined that there was little increase in signal above probe concentrations of 10 μM (**Figure 3.5**).

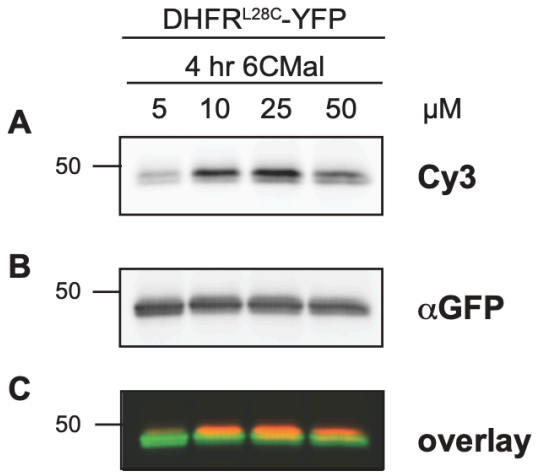

Figure 3.5. Western blot of DHFR^{L28C}-YFP cysteine mutant expressed in HEK293DAX cells and cell lysates reacted with the 4CMal probe compound (**1b**) to test labeling efficiency at various concentrations and time points using the probe and Cys-mutant combination showing the most efficient labeling. A. Blot imaged for Cy3 after Click reaction with probe labeled lysates with pycolyl-azide-Cy3 to visualize extent of covalent labeling. B. Western blot using anti-GFP antibody to visualize total expressed DHRF-YFP. C. overlay of both image channels (green: anti-GFP, red: Cy3).

Application of TMP Probes to Destabilized DHFR Cysteine Mutants

Given the success of the probe labeling experiments with the stabilized DHFR-YFP in cell lysates, we then wanted to see how the experiment would work with the ddDHFR. Unlike the stabilized DHFR-YFP system, where YFP fluorescence indicates a successful transfection, the YFP in the destabilized system does not fluoresce until the probe is added. Therefore, to confirm transfection success in the ddDHFR-YFP system, the probe would need to be added directly to cells before measuring YFP signal with a microscope. After the ddDHFR cysteine mutants were generated by SDM, the TMP probe was applied directly to cells expressing ddDHFR-YFP, and microscope images were captured of the cells after 24 hours of probe incubation. Compared to the DMSO negative control and the TMP positive control, the synthesized 6CMal (**1c**) probe showed comparable GFP signal to the TMP-treated cells, confirming that the probe was successfully permeating the cell membrane to enter the cell and stabilizing DHFR similarly to TMP. (**Figure 3.6**).

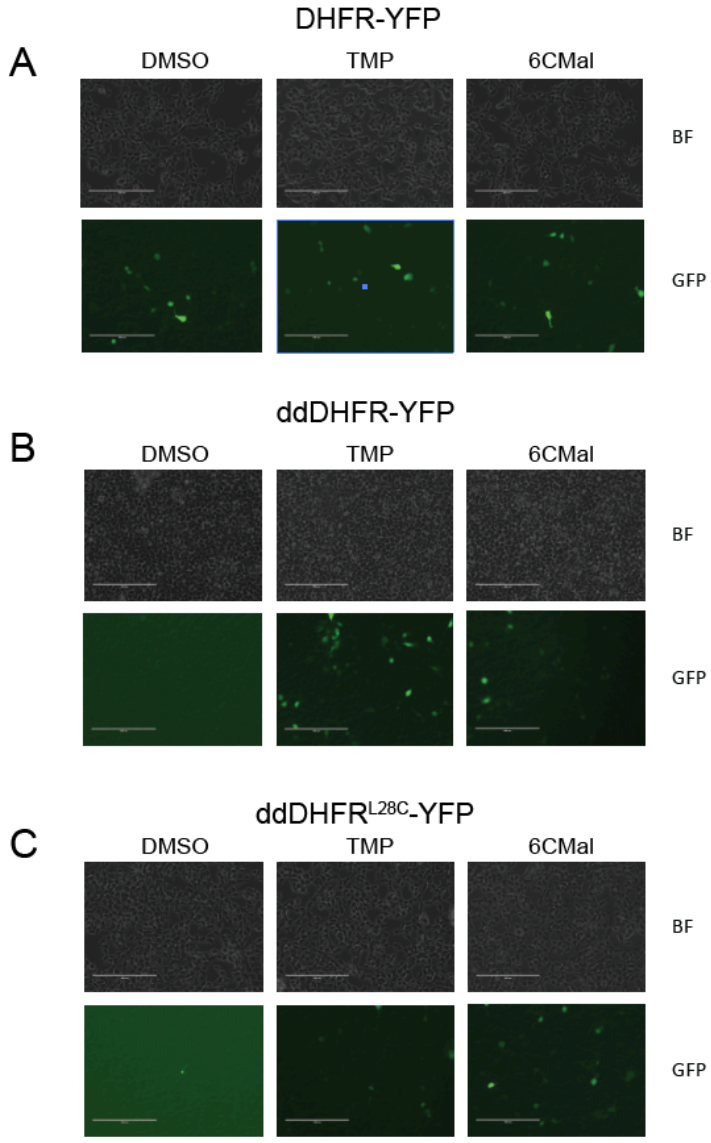

Figure 3.6. Microscope images of HEK293^{DAX} expressing a DHFR-YFP construct that were reacted with DMSO control, 50 μM of TMP, or 50 μM of 6CMal (**1c**) overnight. Images taken using Bright Field channel and GFP channel.
A. HEK293^{DAX} cells expressing DHFR-YFP
B. HEK293^{DAX} cells expressing ddDHFR-YFP
C. HEK293^{DAX} cells expressing ddDHFR^{L28C}-YFP

Time point experiments were then conducted by incubating the cells with the 6CMal probe for 30 min, 1h, 2h, 4h, and overnight before harvesting. The microscope images showed a time-dependent increase in YFP expression, with similar YFP levels in the TMP-treated cells and the probe-treated cells (**Figure 3.7**). Cells expressing ddDHFR-YFP that were treated overnight with TMP or the probe showed comparable YFP fluorescence to cells expressing the stabilized DHFR-YFP, while the 1-hour time point showed minimal fluorescence in cells expressing ddDHFR-YFP. This observation was further confirmed by Western blot monitoring GFP levels. (**Figure 3.8**).

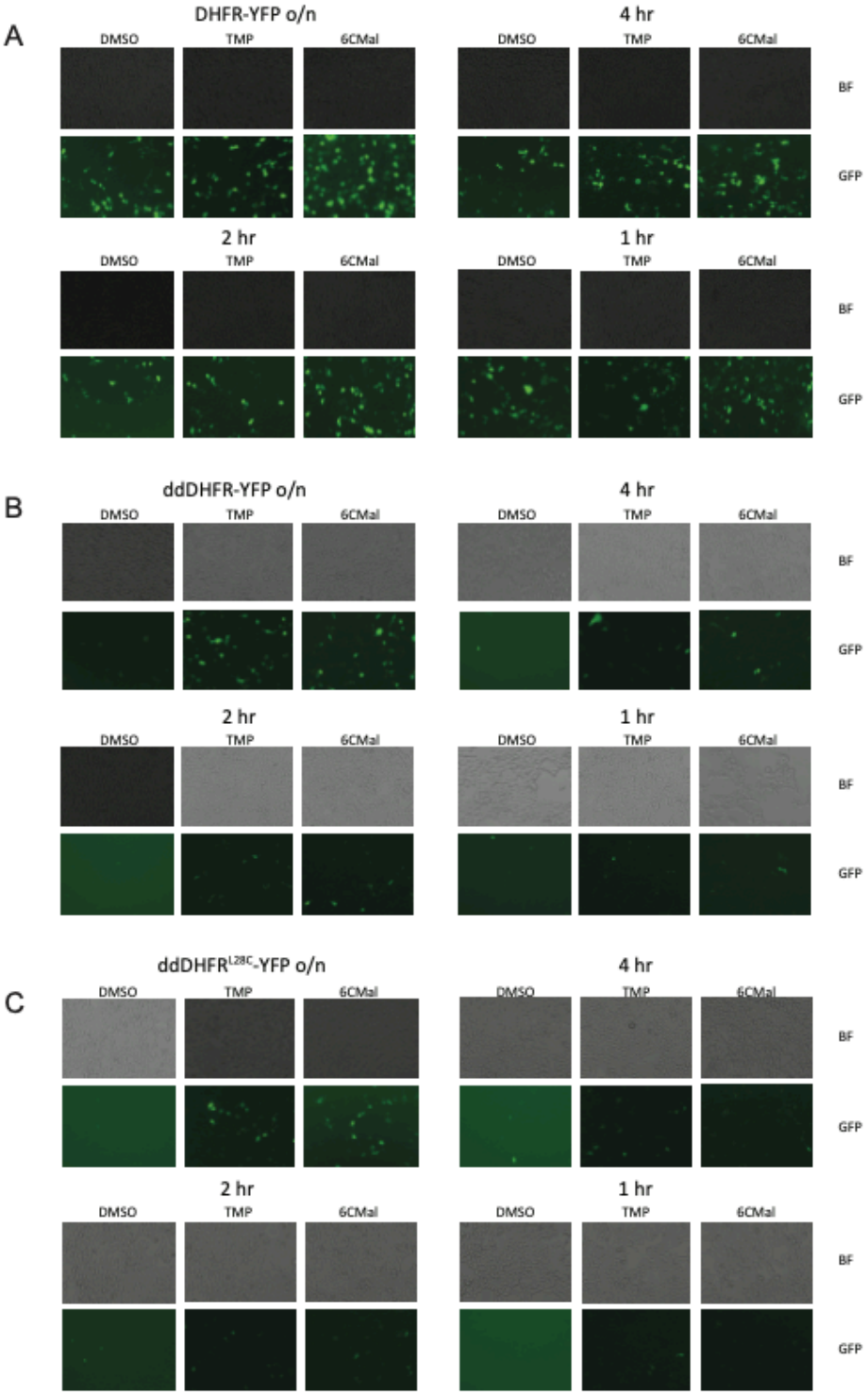

Figure 3.7. Microscope images of HEK293^{DAX} cells expressing a DHFR-YFP construct that were reacted with DMSO control, 50 μM of TMP, or 50 μM of 6CMal (**1c**) at various time points. Images taken using Bright Field channel and GFP channel.
A. HEK293^{DAX} cells expressing DHFR-YFP
B. HEK293^{DAX} cells expressing ddDHFR-YFP
C. HEK293^{DAX} cells expressing ddDHFR^{L28C}-YFP

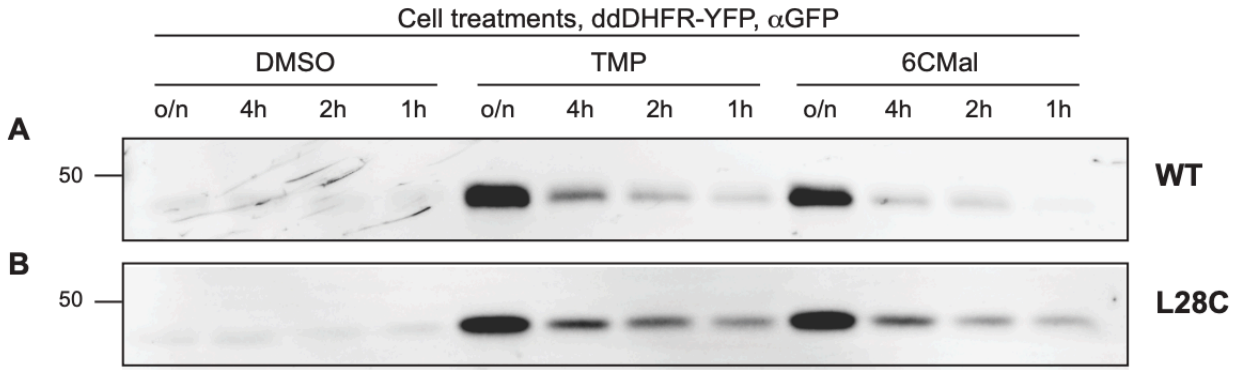

Figure 3.8. Western blot using anti-GFP antibody to visualize total expressed DHRF-YFP. A. Western blot of dd-DHFR-YFP expressed in HEK293^{DAX} cells that were reacted with DMSO control, 50 μM of TMP, or 50 μM of 6CMal (**1c**) at various time points. B. Western blot of dd-DHFR^{L28C}-YFP cysteine mutant expressed in HEK293DAX cells that were reacted with DMSO control, 50 μM of TMP, or 50 μM of 6CMal (**1c**) at various time points.

Future Directions

Thus far, we have successfully determined that the optimal probe for this system is the 4CMal, and the optimal cysteine mutant of the five tested is the L28C (**Figure 3.3**). Additionally, time course experiments of probe incubation times in cell lysates containing DHFR-YFP have shown a time-dependent increase in Cy3 signal, with appreciable signal being observed after 2 hours (**Figure 3.4**). Experiments in cell lysates containing DHFR-YFP where probe concentration was varied showed that no increase in Cy3 signal was observed above 10 μM of probe (**Figure 3.5**). However, some problems persist under these experimental conditions. In particular, when the 6CMal probe is applied directly to cells and then subjected to the click reaction and blotting, no Cy3 signal could be observed, regardless of whether the stabilized or destabilized DHFR was used (**Figure 3.9**).

While our imaging experiments demonstrate that the probe compound is able stabilize DHFR, indicating that it can successfully cross the cell membrane and bind to the ddDHFR, these results indicate that the probe molecule may not form a covalent adduct with the engineered Cys residue near the binding pocket. It may be the case that the maleimide is too reactive as an electrophile and it is binding non-specifically to other nucleophiles in the cell (e.g. glutathione), or that the cysteine in the active site of DHFR is binding nonspecifically to other electrophiles in the cell, effectively blocking it. Given the difficult nature of identifying which of

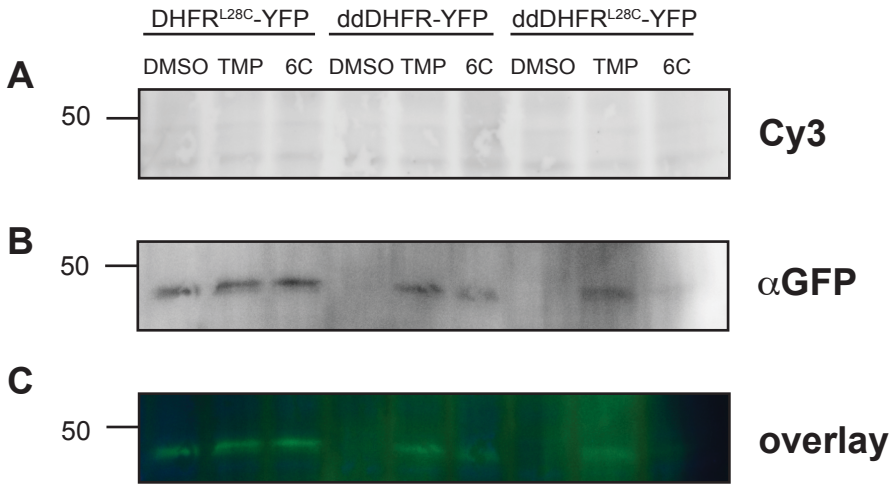

Figure 3.9. Western blot of DHFR^{L28C}-YFP, dd-DHFR-YFP, or ddDHFR^{L28C}-YFP expressed in HEK293^{DAX} cells that were reacted with DMSO control, 50 μM of TMP, or 50 μM of 6CMal (**1c**) overnight. A. Blot imaged for Cy3 after Click reaction with probe labeled lysates with pycolyl-azide-Cy3 to visualize extent of covalent labeling. B. Western blot using anti-GFP antibody to visualize total expressed DHRF-YFP. C. overlay of both image channels (green: anti-GFP, blue: Cy3).

these problems may be responsible for the lack of Cy3 signal, it was decided that the best plan moving forward would be to synthesize more probes with different electrophile groups attached that alter the reactivity. Other potential groups, such as iodoacetamides, vinyl ketones, or tosylates, could be coupled to the probe at the last step of the synthetic sequence. These probes could then be reacted with cells expressing one of the Cys-mutant variants of ddDHFR-YFP to judge whether the Cys-reactive group allows for better *in vivo* covalent labeling.

Additionally, the lysate labeling experiments showed that the Cy3-labeled band migrates slightly higher than the GFP bands when the blot images were overlapped, which is indicative of an increased molecular weight. While the Cy3 fluorophore alone has a molecular weight of 850 Da that could visibly shift the band corresponding to probe-labeled DHFR away from unlabeled protein, the probe was added at over 1000-fold excess and thus should occupy all of the DHFR present. Given that the majority of DHFR-YFP still migrates at the lower molecule weight, it may indicate that only a very small fraction of the overall protein pool is labeled by the probe, or that another protein of similar molecular weight binds non-specifically to the probe. One approach that could identify proteins that may be non-specifically labeled by the probe would be to click a biotin tag to the probe-labeled DHFR and pull down the protein complex using affinity purification with streptavidin beads. The identity of the protein could then be determined by

mass spectrometry. To determine the viability of this approach, a Click reaction was attempted with biotin azide and, after SDS-PAGE and transfer to a membrane, the blot was probed with streptavidin labeled with IR680 dye. However, no band showed up at the MW expected for the DHFR-YFP on the blot under the IR680 channel even when GFP expression was shown to be strong (**Figure 3.10**). Since the control lane containing an alkyne-labeled proteome did not show strong IR680 signal after the Click reaction, this is thought to be an issue with the biotin-streptavidin system rather than the Click reaction itself, and these conditions will be further optimized in the future.

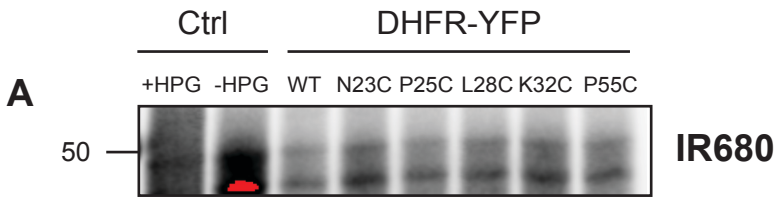

Figure 3.10. Western blot of DHFR-YFP cysteine mutant variants expressed in HEK293DAX cells that were reacted with 50 μM of 4CMal (**1b**) for 4 hours, with control lanes of whole cell lysates with or without proteome-wide incorporation of homo-propargyl glycine (HPG). A. Blot imaged for IR680 after Click reaction with probe labeled lysates with diazo-PEG-biotin azide and treated with streptavidin attached to an IR680 dye to visualize extent of covalent labeling.

Methods

Site-Directed Mutagenesis. The parent plasmid destabilized DHFR-YFP pDEST40 was obtained from Shoulders et al.[2] The destabilized DHFR sequence was replaced by *E. coli* wild-type DHFR using PCR and the NEBuilder HiFi DNA Assembly kit (Table S1). The forward and reverse primers for the NEBuilder reaction to generate the wtDHFR-YFP-pDEST40 construct are listed in **Table S1.** PCR products for DHFR were amplified from an *E. coli* DH5α colony and the pDEST40-YFP fragment was amplified from the parent dd-DHFR-YFP pDEST40 plasmid using Q5 polymerase (NEB). Fragments were then ligated according to standard instructions from the HiFi DNA Assembly kit. Five individual rounds of mutagenesis yielded 5 DHFR-YFP variants with additional Cys mutations: N23C, P25C, L28C, K32C, P55C, respectively. The forward and reverse primers for site-directed mutagenesis to generate 5 eDHFR:Cys mutants are listed in **Table S2**. PCR reactions were carried out with Pfu Turbo for

Table S1. Primer Sequences for NEBuilder HiFi DNA Assembly			
Overlaps	Oligo (Uppercase = gene-specific primer)	Anneals	F/R
WT-DHFR	GGTGGCGGATCCAGTCGA	pDEST40-YFP	Rev
pDEST-40-YFP	agtcgactggatccgccaccATGATCAGTCTGATTGCGGC	WT-DHFR	Fwd
pDEST-40-YFP	tcgcccttgctcacgcatgcTCGCCGCTCCAGAATCTC	WT-DHFR	Rev
WT-DHFR	GCATGCGTGAGCAAGGGC	pDEST40-YFP	Fwd

Table S2. Primer Sequences for Site-Directed Mutagenesis	
Mutation	**Forward Primer Sequence (5' → 3')**
DHFR-L28C-F	GGAACCTGCCTGCCGATTGCGCCTGGTTTAAACGCAAC
DHFR-L28C-R	GTTGCGTTTAAACCAGGCGCAATCGGCAGGCAGGTTCC
DHFR-P55C-F	CAATCGGTCGTCCGTTGTGTGGACGCAAAAATATTATCCTCAG
DHFR-P55C-R	CTGAGGATAATATTTTTGCGTCCACACAACGGACGACCGATTG
DHFR-K32C-F	CTGCCGATCTCGCCTGGTTTTGCCGCAACACCTTAAATAAACC
DHFR-K32C-R	GGTTTATTTAAGGTGTTGCGGCAAAACCAGGCGAGATCGGCAG
DHFR-P25C-F	GTGGAACCTGTGTGCCGATCTCGC
DHFR-P25C-R	GGCATGGCGTTTTCCATG
DHFR-N23C-F	CATGCCGTGGTGCCTGCCTGCC
DHFR-N23C-R	GCGTTTTCCATGCCGATAAC

the L28C, K32C, and P55C variants, and with Q5 polymerase (NEB) for the N23C and P25C variants. Melting temperatures were 60˚C for the Pfu Turbo and 65˚C for the Q5, and extension times were 8 minutes for the Pfu and 7 minutes for the Q5.

Products amplified with Pfu Turbo were digested with 1 uL of DpnI for 2hr and then ligated into DH5alpha. PCR products from the Q5 amplification were digested with 1 µL of DpnI for 2hr, phosphorylated with T4 phosphonucleotide kinase (PNK), ligated with T4 DNA ligase, and then transformed into DH5alpha.

Cell culture and transfection. DAX cells were cultured in Dulbecco's Modified Eagle Medium (DMEM) with 10% v/v fetal bovine serum (FBS), 1% v/v Pen/Strep, and 1% v/v Glutamine. All cells were maintained under 5% CO2 at 37 °C. Cells were plated in 10 cm dishes 24 h before transfected with expression plasmids for eDHFR fused target protein (5 μg DNA for one plate) using $Ca_3(PO_4)_2$. After 18 hours, the media was removed and replaced with 10 mL of fresh DMEM. When no probe labeling was performed, the plates were harvested the next day (described in following section).

For direct cell labeling experiments using the stabilized DHFR-YFP, plates were split an hour after exchange of the transfection media into 6-well chambered plates at 1.2e6 cells/ well. Starting four hours after transfection, cells were then incubated with compound at various time points by removing the media and replacing it with fresh DMEM that had been spiked with 50 μM of DMSO, TMP, or probe. The cells were immediately harvested at the designated time point (described in following section).

For direct cell labeling experiments using the ddDHFR-YFP, plates were split into 12-well chambered plates at 500K cells/ well. The cells were treated with DMSO, TMP, or probe as described above at various time points. After the designated time point, the cells were imaged and then immediately harvested (described in following section).

Live cell imaging. Images were obtained using an EVOS FL Imaging System inverted epifluorescence microscope. Images were collected using the bright field channel and the GFP channel with a 20x objective lens. Green channel was excited with a 488 nm laser and emission collected between 520 – 580 nm. Images were processed by EVOS FL software.

Cell Harvesting. For cell samples that were transfected with DHFR-YFP, cells were harvested as follows. Plates were placed on ice to stop the reaction, and each well was washed with ice-cold PBS (5 mL for a 10 cm dish, 1 mL for a 6-well dish). Cells were scraped in 1 mL of PBS + 1 mM EDTA (1 mL for a 10 cm dish, 300 μL for a 6-well dish) and transferred into cold 1.5-mL microcentrifuge tubes, pelleted, and the supernatant discarded. The cell pellets were then lysed using 2x the cell pellet volume of Radioimmunoprecipitation assay buffer (RIPA) + Complete protease inhibitor (Roche) and allowed to sit on ice for 30 minutes before being centrifuged at

14,000 rpm for 15 minutes. The supernatant was then separated from the pellet, and the protein concentrations were normalized to 0.5 mg/mL using a protein assay (BioRad).

For samples transfected with ddDHFR, cells were harvested as follows. The media was removed, the cells were washed with 200 uL of warm PBS + 1 mM EDTA, and the cells were treated with 100 uL of trypsin for 1 minute. To the cells was then added 400 uL of DMEM media to displace the cells from the plate, and the mixture was transferred to a 1.5 mL microcentrifuge tube and centrifuged at 400x g for 5 minutes. The supernatant was then removed before cells were washed a final time with PBS + 1 mM EDTA, and the cells were then placed on ice. The cell pellets were then lysed with 25 uL of RIPA + protease inhibitor and allowed to sit on ice for 30 minutes before being centrifuged at 14,000 rpm for 15 minutes. The supernatant was then separated from the pellet, and the protein concentrations were normalized to 0.5 mg/mL by BCA assay (Thermo Scientific).

Labeling of Samples with Cy3 Fluorophore for Click-blots. To an empty 1.5 mL microcentrifuge tube was added Cu^{2+} (0.8 mM, all concentration are final) and BTTAA (1.6 mM), which were mixed to form a Cu-BTTAA complex. To the mixture was then added Na ascorbate (5 mM) and Cy3-picolyl azide fluorophore (100 μM, ClickChemistryTools). A 3 μL aliquot of this mixture was then added to 20 μL of cell lysate diluted to 0.5 mg/mL of protein in RIPA buffer + Complete protease inhibitor (Roche). The samples were heated to 37˚C and allowed to shake at 700 rpm for 1 hour. The solution was then mixed with 6x SDS loading buffer (including 100 mM DTT) and heated to 95˚C for five minutes, followed by centrifugation at 13,000 rpm for 10 minutes. Proteomes were separated by 10% SDS-PAGE gels (Bio-Rad) for 20 minutes at 60 V and 80 minutes at 160 V. The BioRad Precision Plus AllBlue Standard was used to determine the protein molecular weights. The gels were transferred to PVDF (Millipore Immobilon) at 100 V for 80 minutes. The blots were then blocked with 5% milk in Tris-buffered saline, 0.05% Tween-20 (TBST) for 1 hour at 4˚C. After thorough rinsing with TBST, the blots were probed with mouse anti-GFP (Vanderbilt) primary at 4˚C for 2 hours and StarBright B700 anti-mouse secondary antibody (BioRad) at 4˚C for 1 hour. Blots were visualized on a BioRad ChemiDoc MP imaging system scanning at 602 nm emission for Cy3 (Green Epi Illumination) and 715 nm emission for StarBright B700 (Blue Epi Illumination).

Treatment of Samples for Click-blots with Streptavidin Fluorophore. To an empty 1.5 mL microcentrifuge tube was added Cu^{2+} (0.8 mM, all final concentrations) and BTTAA (1.6 mM), which were mixed to form a Cu-BTTAA complex. To the mixture was then added Na ascorbate (5 mM) and diazo-biotin fluorophore (100 μM, ClickChemistryTools). A 3 μL aliquot of this mixture was then added to 20 μL of cell lysate diluted to 0.5 mg/mL of protein in RIPA buffer + Complete protease inhibitor (Roche). The samples were heated to 37˚C and allowed to shake at 700 rpm for 1 hour. The solution was then mixed with 6x SDS loading buffer (including 100 mM DTT) and heated to 95˚C for five minutes, followed by centrifugation at 13,000 rpm for 10 minutes. Proteomes were separated by 10% SDS-PAGE gels (Bio-Rad) for 20 minutes at 60 V and 80 minutes at 160 V. The BioRad Precision Plus AllBlue Standard was used to determine the protein molecular weights. The gels were transferred to PVDF (Millipore Immobilon) at 100 V for 80 minutes. The blots were then blocked with 5% BSA at 4˚C for 1 hour. The solution was then spiked with 1 uL of Streptavidin IR680 fluorophore and allowed to rock at 4˚C for 1 hour. Blots were visualized on a BioRad ChemiDoc MP imaging system scanning at 715 nm emission for IR680 (Far Red Epi Illumination).

References

(1) Jing, C.; Cornish, V. W. *ACS Chem. Biol.* **2013**, *8* (8), 1704–1712.

(2) Shoulders, M. D.; Ryno, L. M.; Genereux, J. C.; Moresco, J. J.; Tu, P. G.; Wu, C.; Yates, J. R.; Su, A. I.; Kelly, J. W.; Wiseman, R. L. *Cell Rep* **2013**, *3* (4), 1279–1292.

Supplemental Figure 1. [1]H-NMR (400 MHz) in dDMSO of TMP demethylation time course experiment at 5, 10, and 20 minutes.

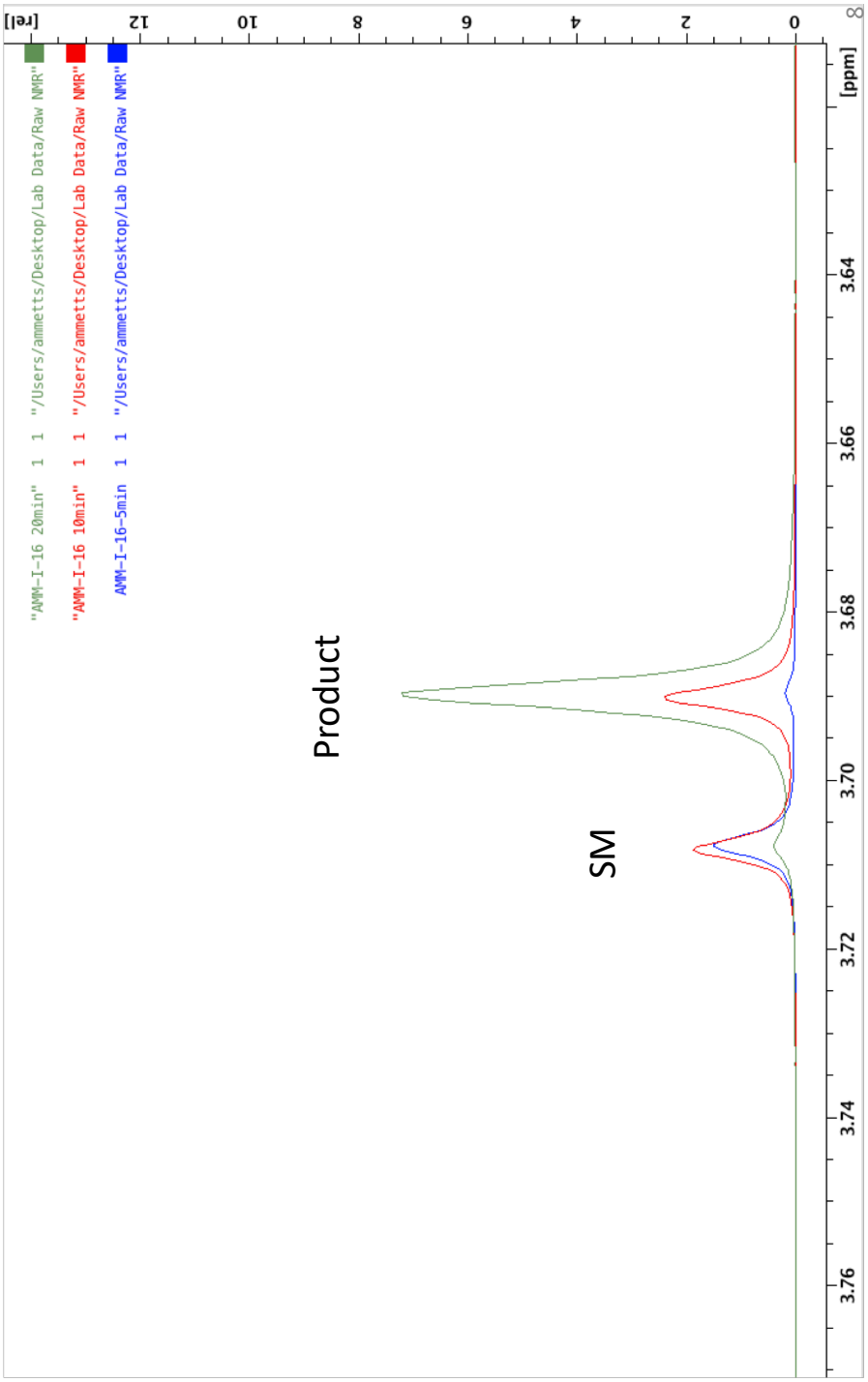

Supplemental Figure 2. ^{1}H-NMR (400 MHz) of TMP-OH **4** in $CDCl_3$.

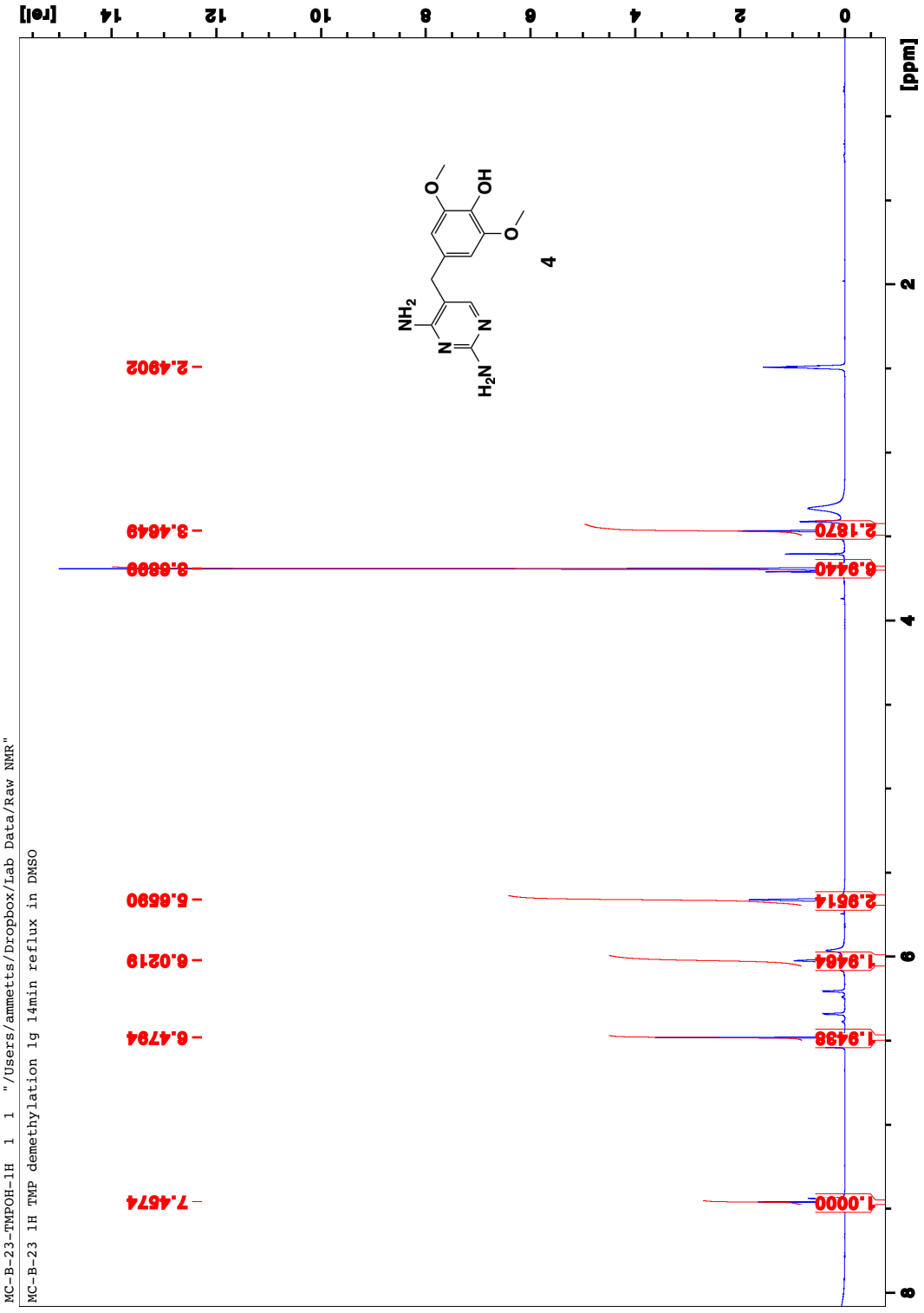

Supplemental Figure 3. ^{13}C-NMR (600 MHz) of TMP-OH **4** in dDMSO.

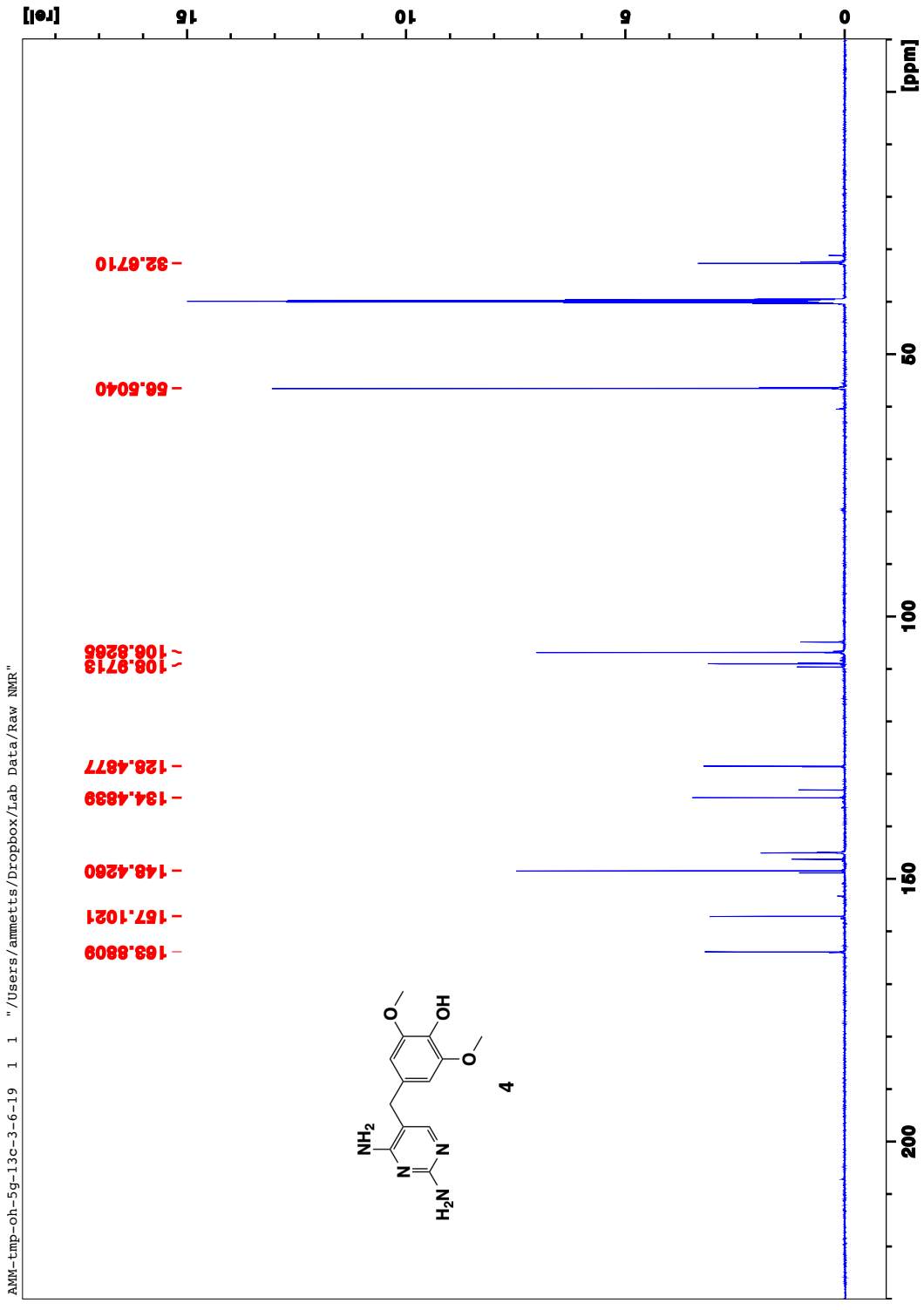

Supplemental Figure 4. LC/MS of TMP-OH **4**

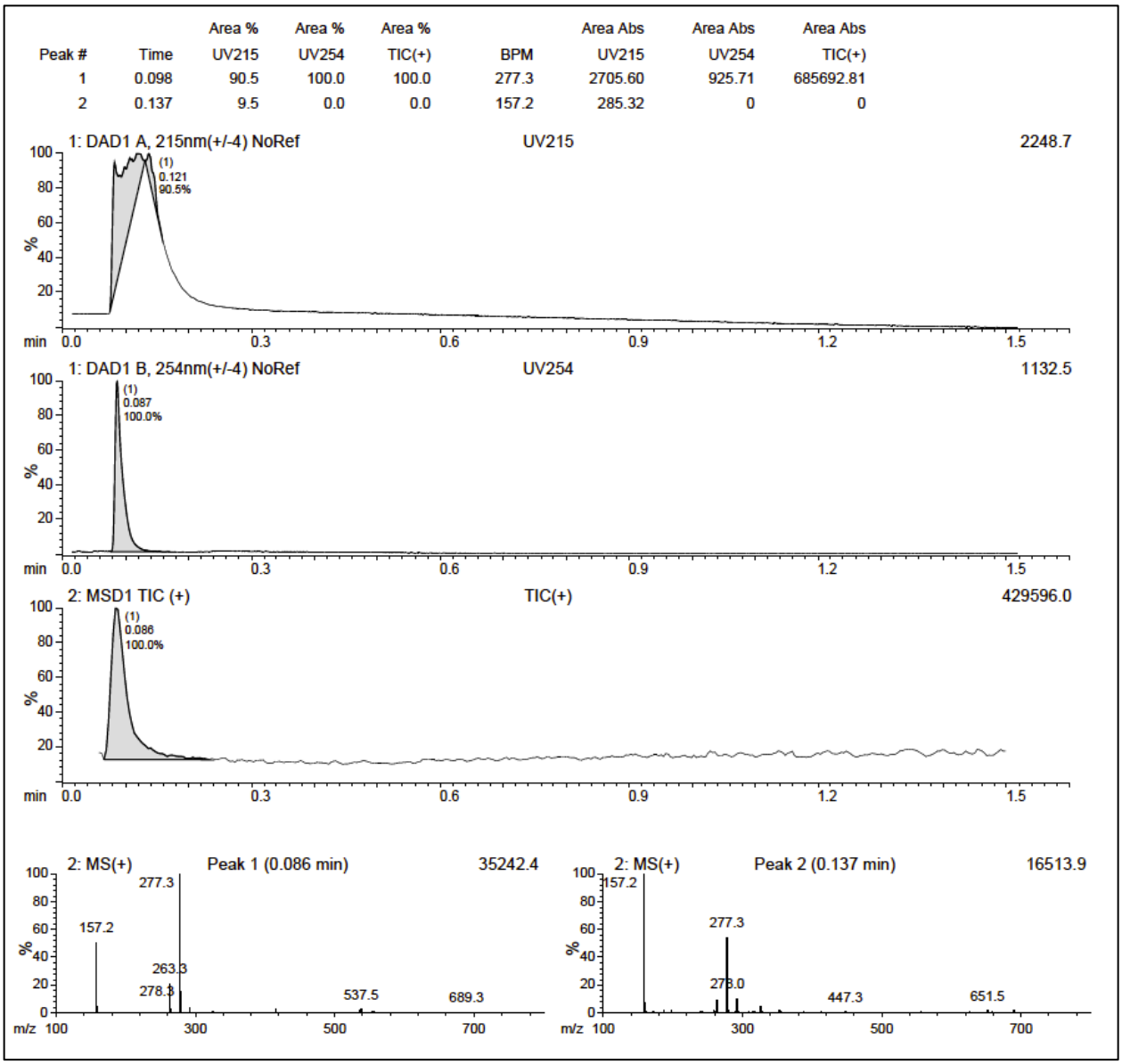

Supplemental Figure 5. ^{1}H-NMR (400 MHz) of tert-butyl(3-iodopropyl)carbamate **6** in $CDCl_3$.

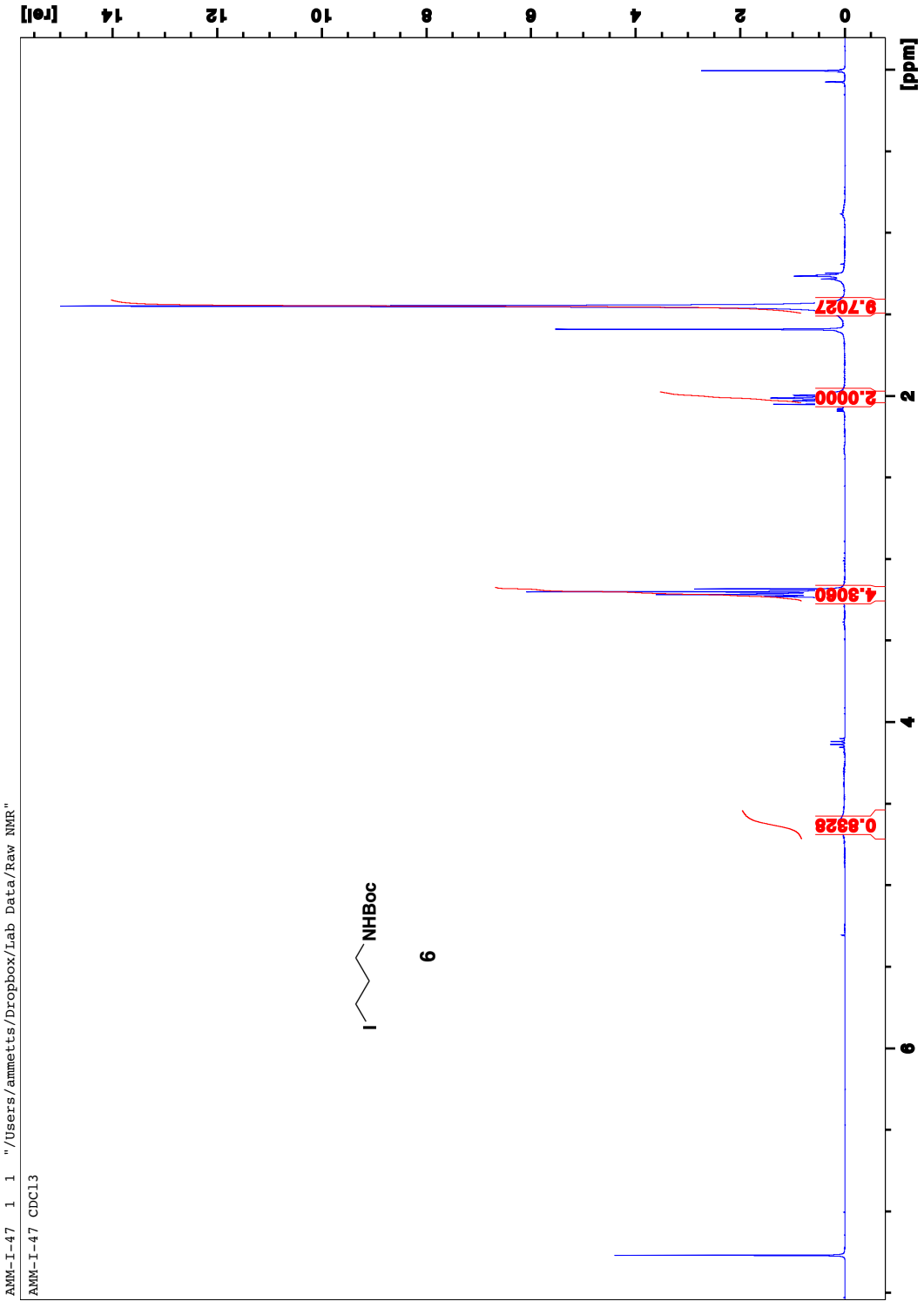

Supplemental Figure 6. ^{13}C-NMR (600 MHz) of tert-butyl(3-iodopropyl)carbamate **6** in $CDCl_3$.

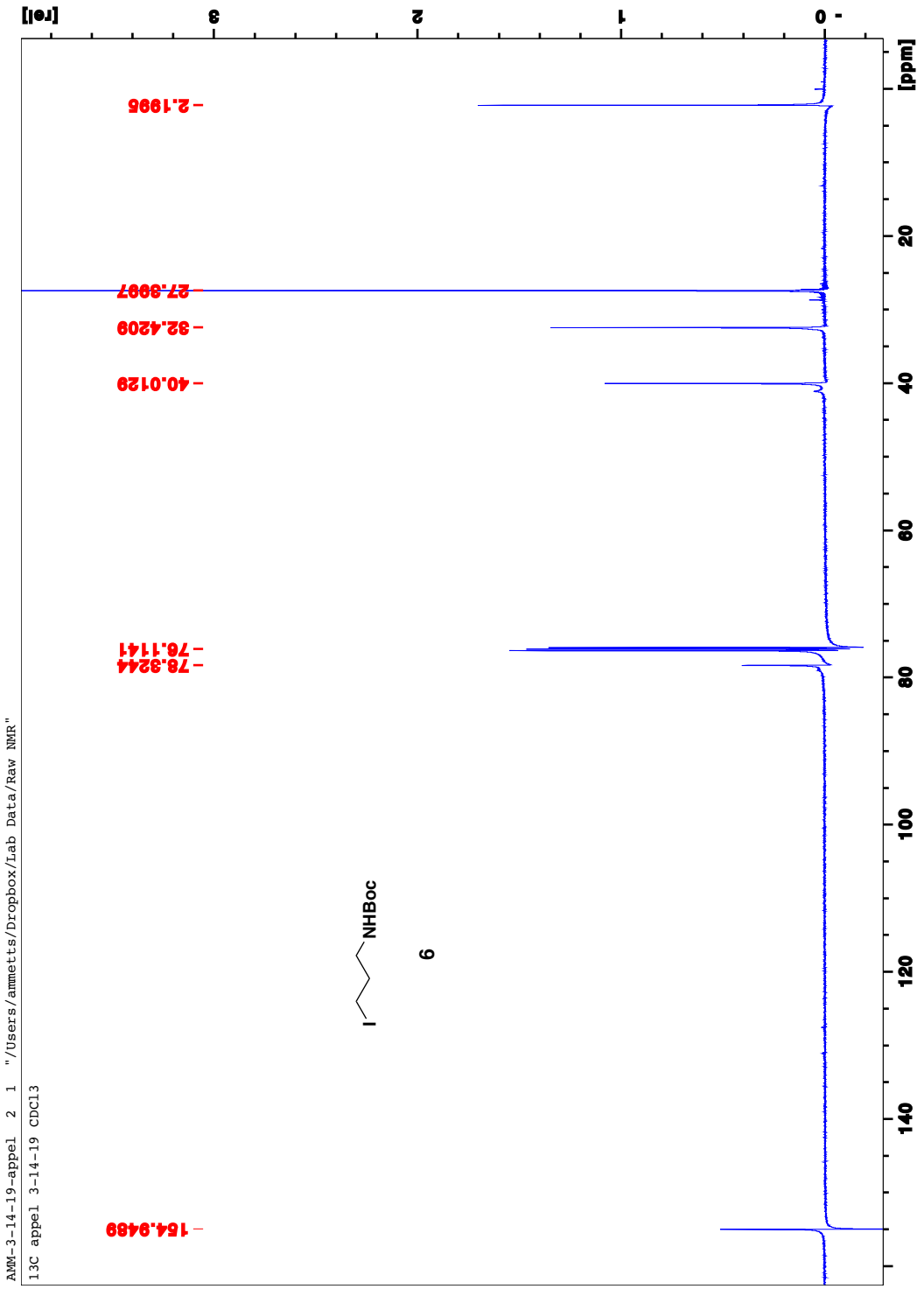

Supplemental Figure 7. LC/MS of tert-butyl(3-iodopropyl)carbamate **6.**

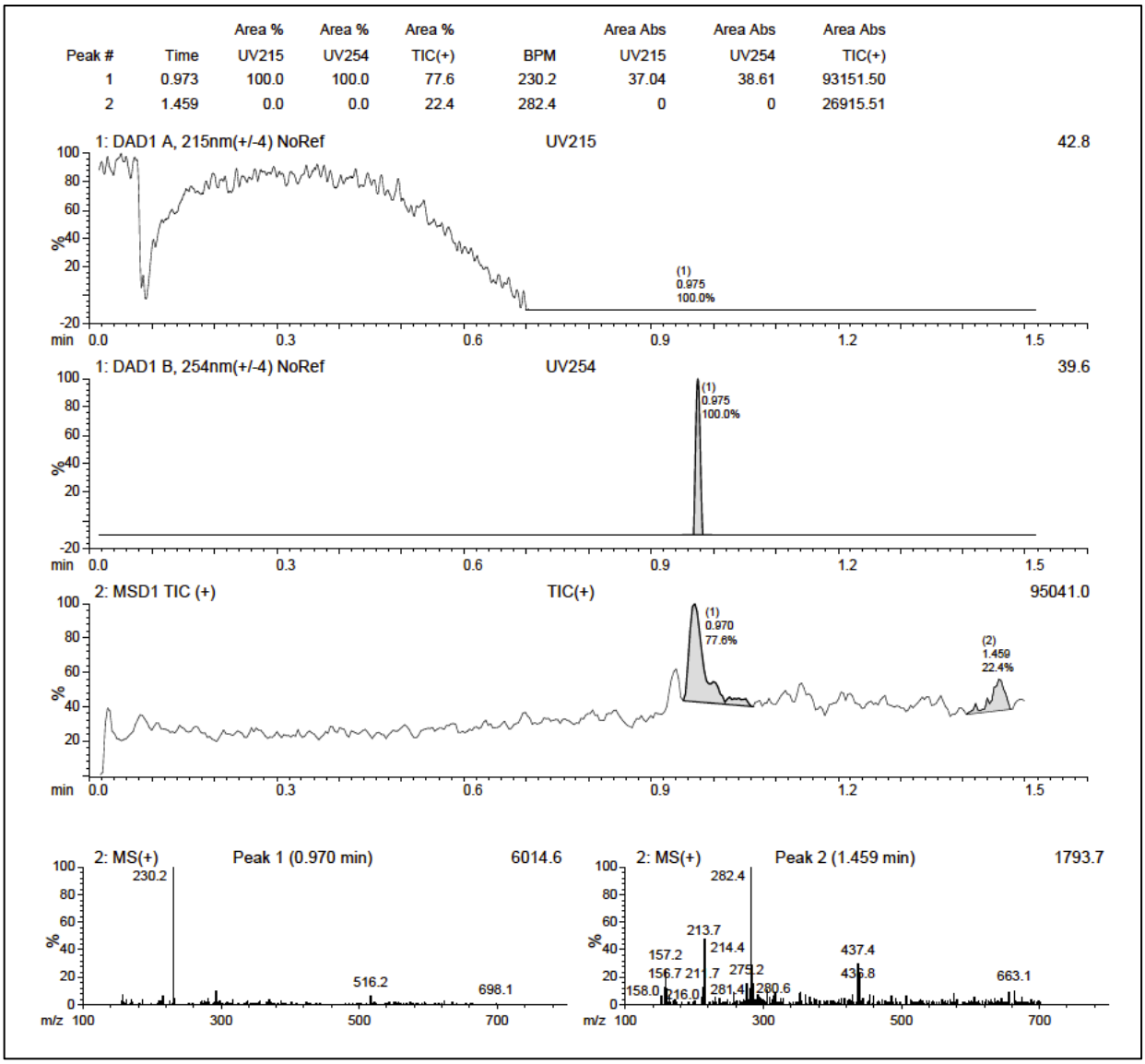

Supplemental Figure 8. ^{1}H-NMR (400 MHz) of TMP-C3-NHBoc **8** in $CHCl_3$.

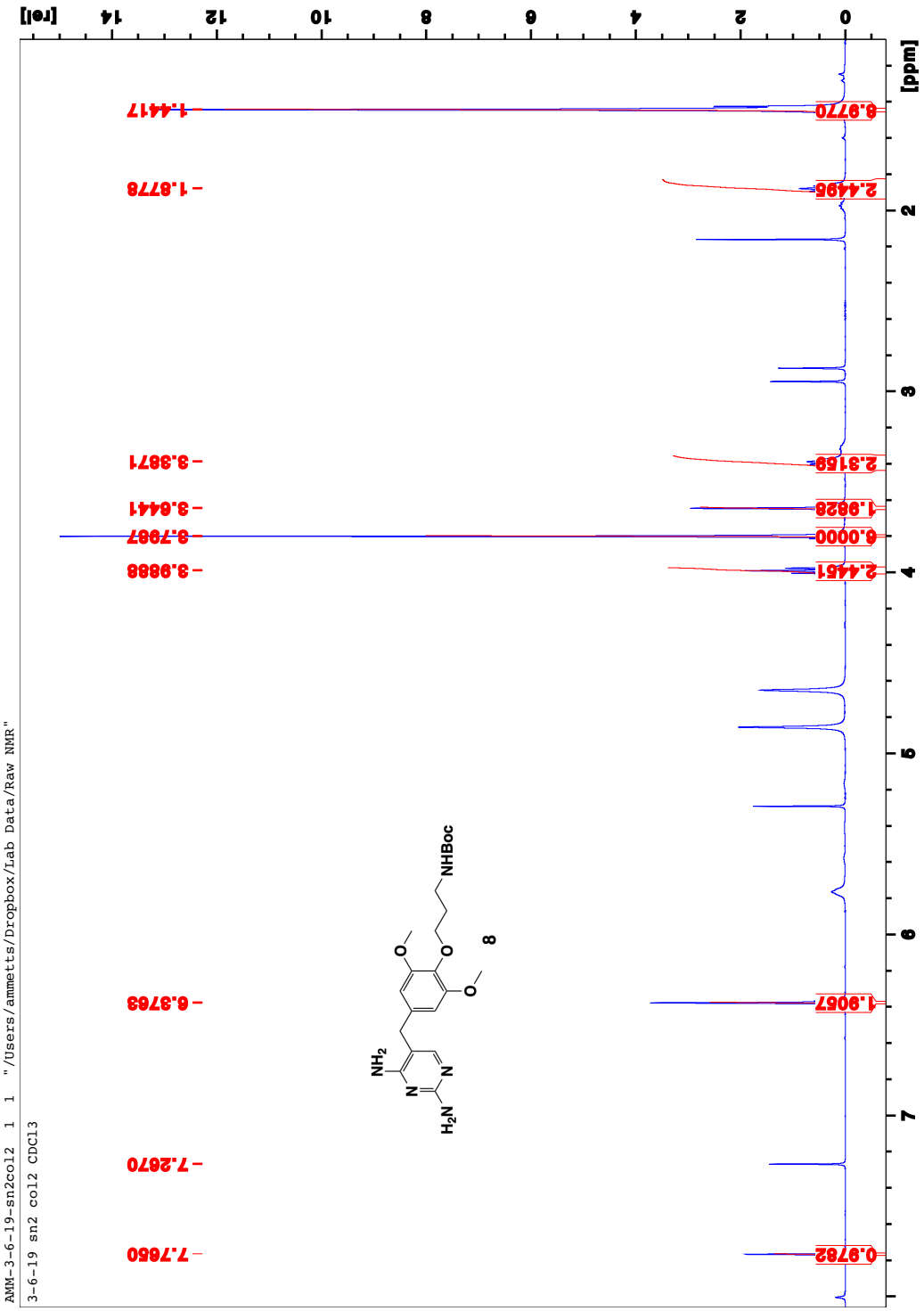

Supplemental Figure 9. ^{13}C-NMR (400 MHz) of TMP-C3-NHBoc **8** in $CDCl_3$.

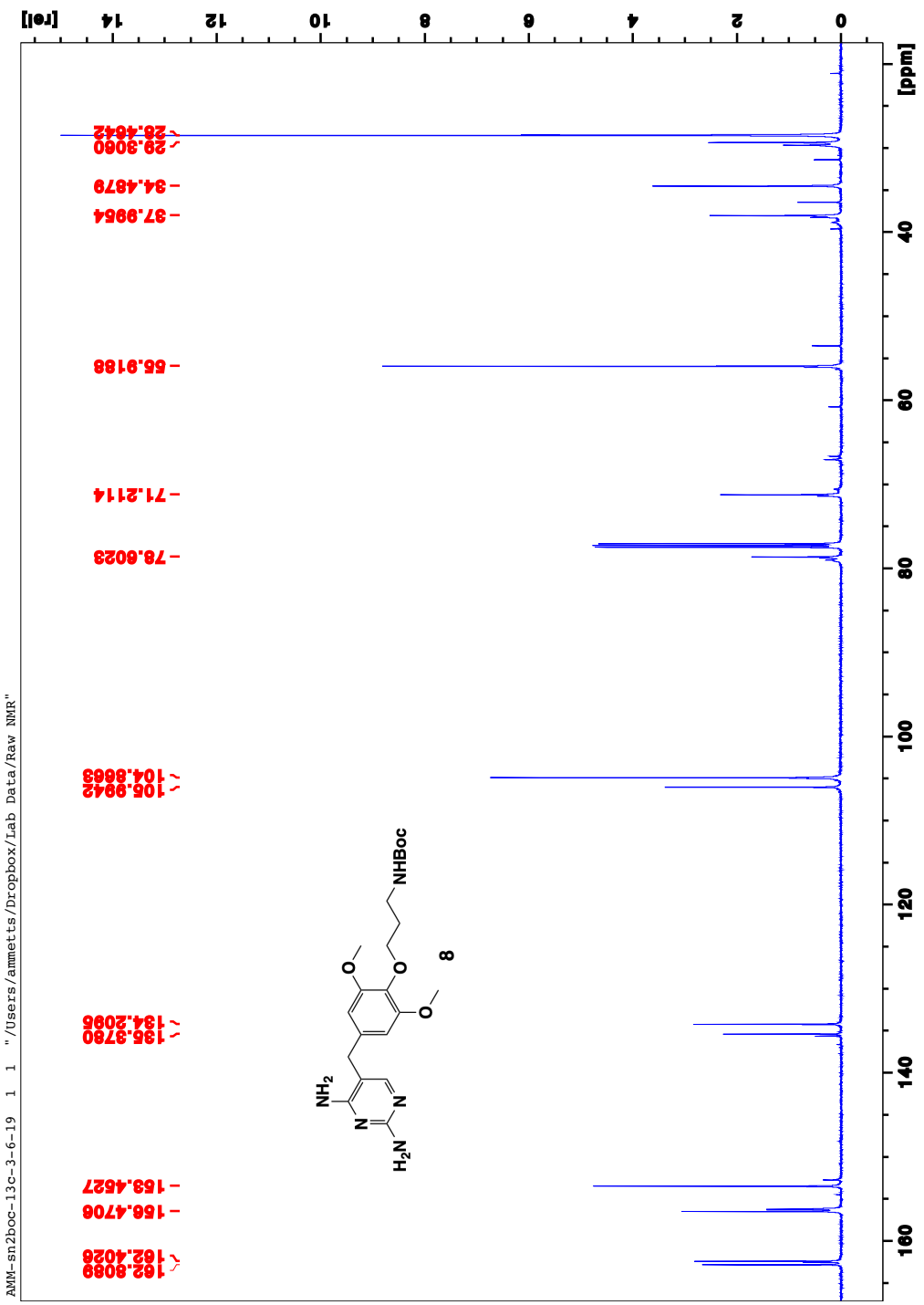

Supplemental Figure 10. LC/MS of TMP-C3-NHBoc **8.**

Peak #	Time	Area % UV215	Area % UV254	Area % TIC(+)	BPM	Area Abs UV215	Area Abs UV254	Area Abs TIC(+)
1	0.087	1.8	8.1	0.6	215.3	69.96	64.71	32112.71
2	0.825	82.0	80.8	62.8	434.5	3200.25	646.70	3144296.75
3	0.951	0.3	0.0	36.5	577.5	10.51	0	1828053.00
4	0.972	16.0	11.1	0.0	577.5	622.61	88.69	0

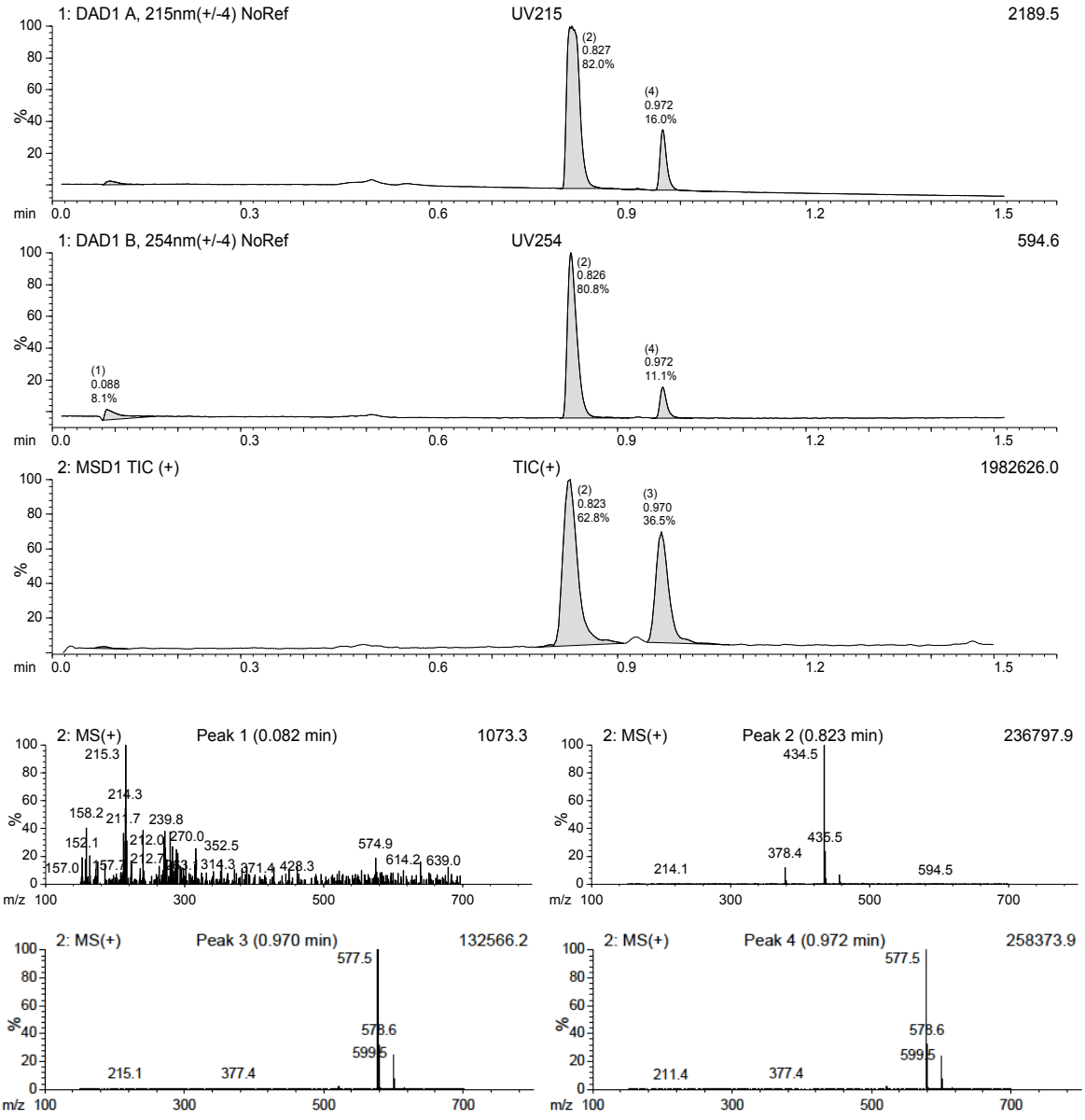

Supplemental Figure 11. ^{1}H-NMR (400 MHz) of TMP-C3-NH_2 **3** in MeOD.

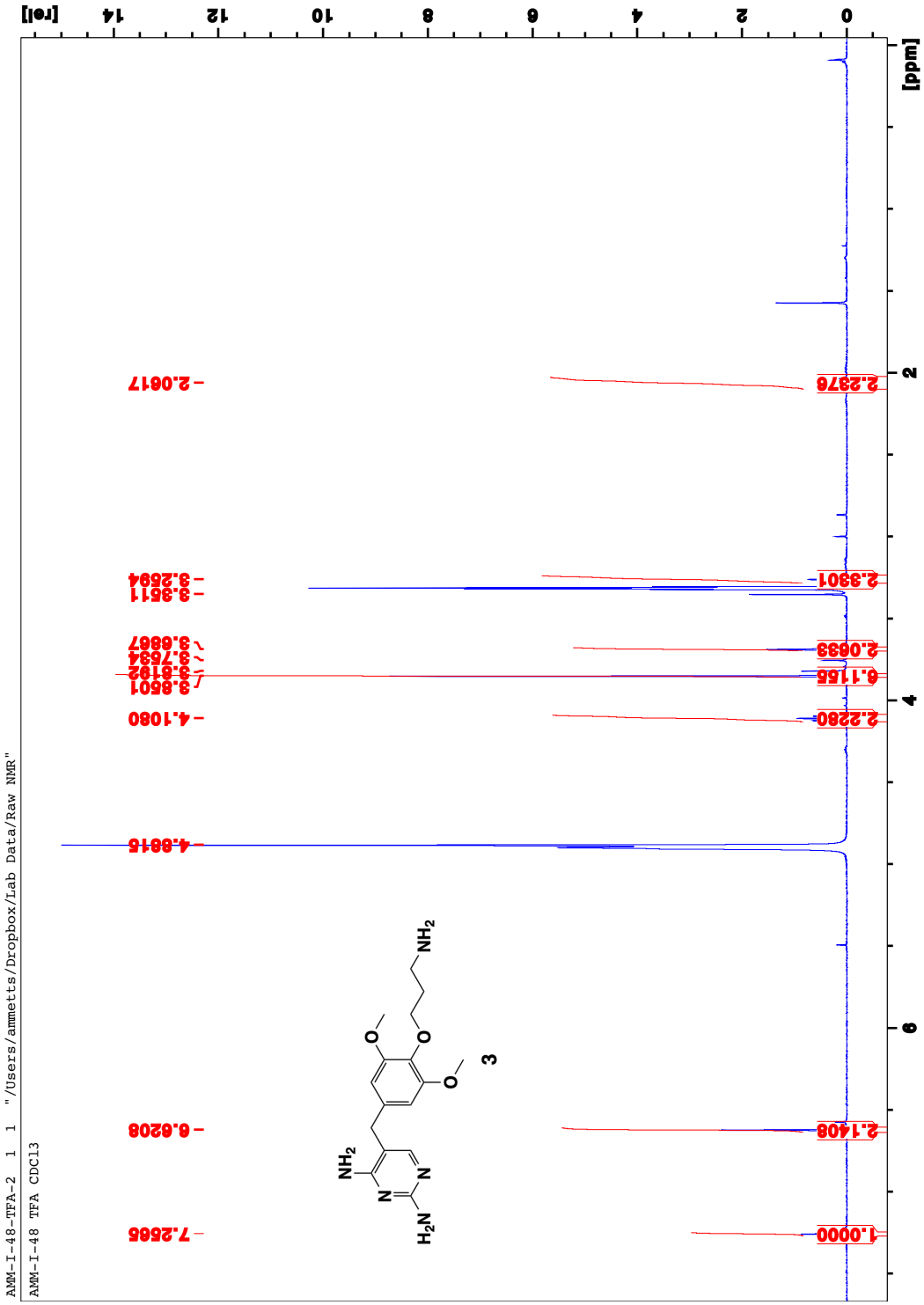

Supplemental Figure 12. ^{13}C-NMR (600 MHz) of TMP-C3-NH_2 **3** in MeOD.

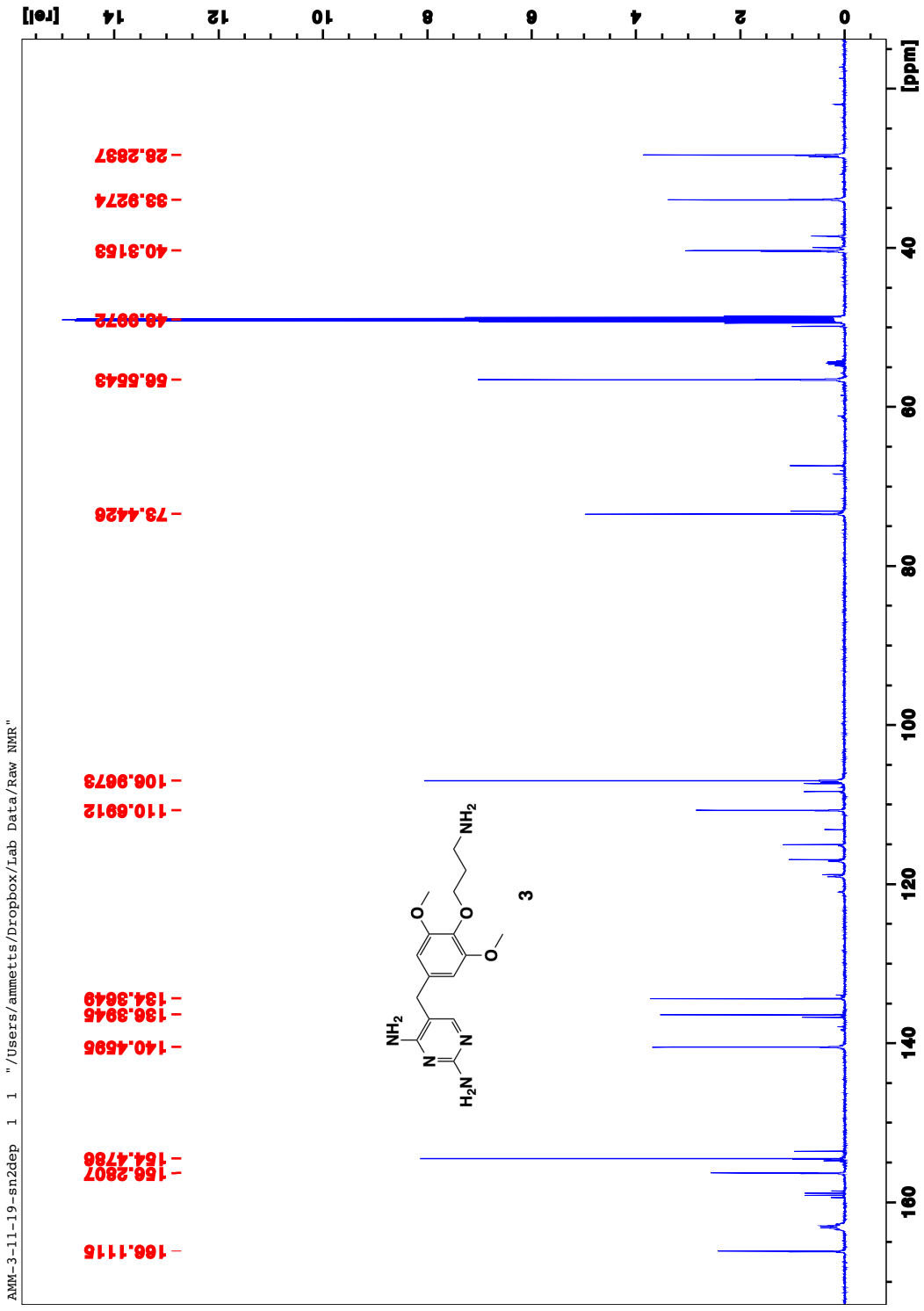

Supplemental Figure 13. LC/MS of TMP-C3-NH_2 **3.**

Peak #	Time	Area % UV215	Area % UV254	Area % TIC(+)	BPM	Area Abs UV215	Area Abs UV254	Area Abs TIC(+)
1	0.085	65.8	100.0	74.6	334.3	190.13	19.78	167996.08
2	0.291	34.2	0.0	0.0	214.3	98.97	0	0
3	1.066	0.0	0.0	16.2	215.3	0	0	36519.75
4	1.454	0.0	0.0	9.2	282.4	0	0	20617.54

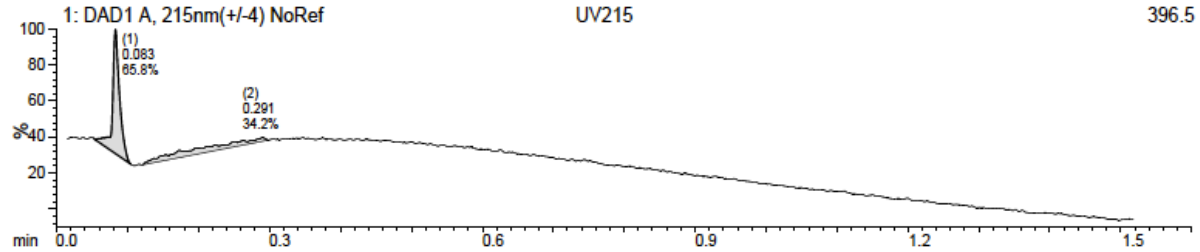

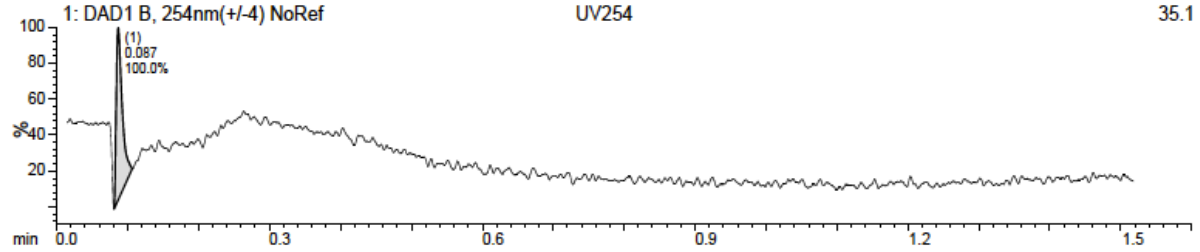

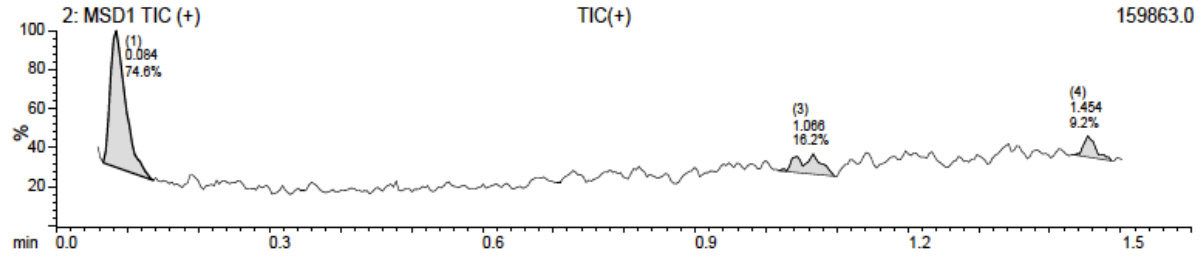

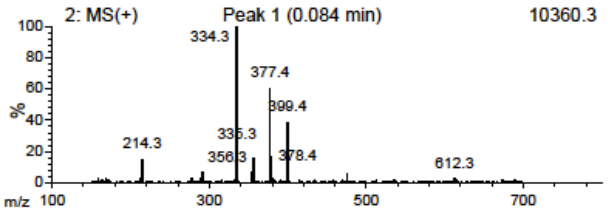

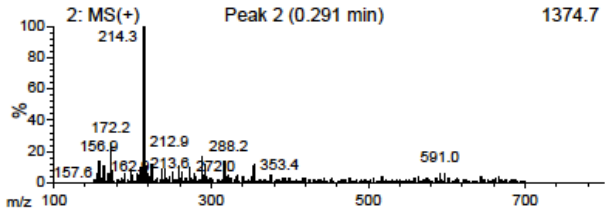

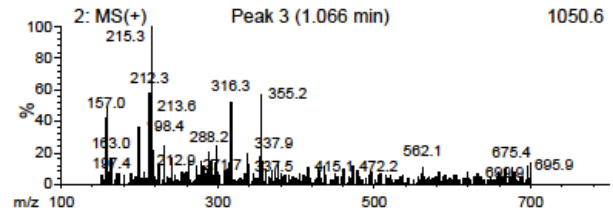

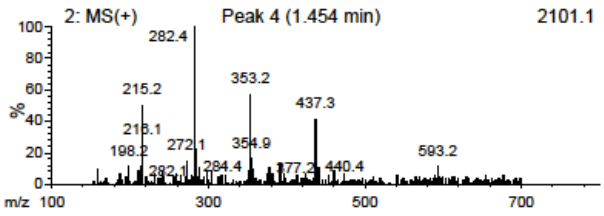

Supplemental Figure 14. ^{1}H-NMR (400 MHz) of TMP-alkyne-NHBoc **9** in $CDCl_3$.

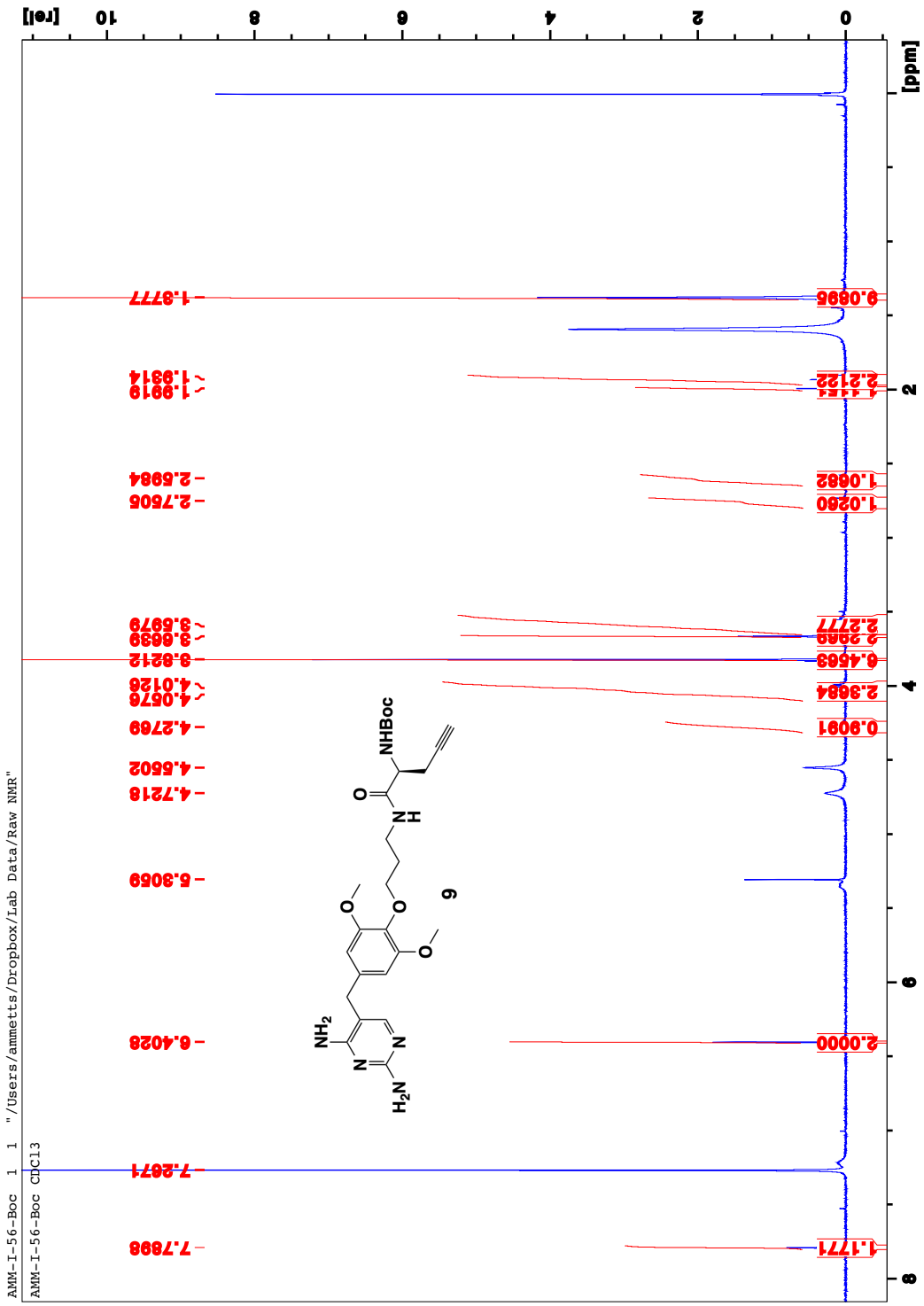

Supplemental Figure 15. LC/MS of TMP-alkyne-NHBoc **9**.

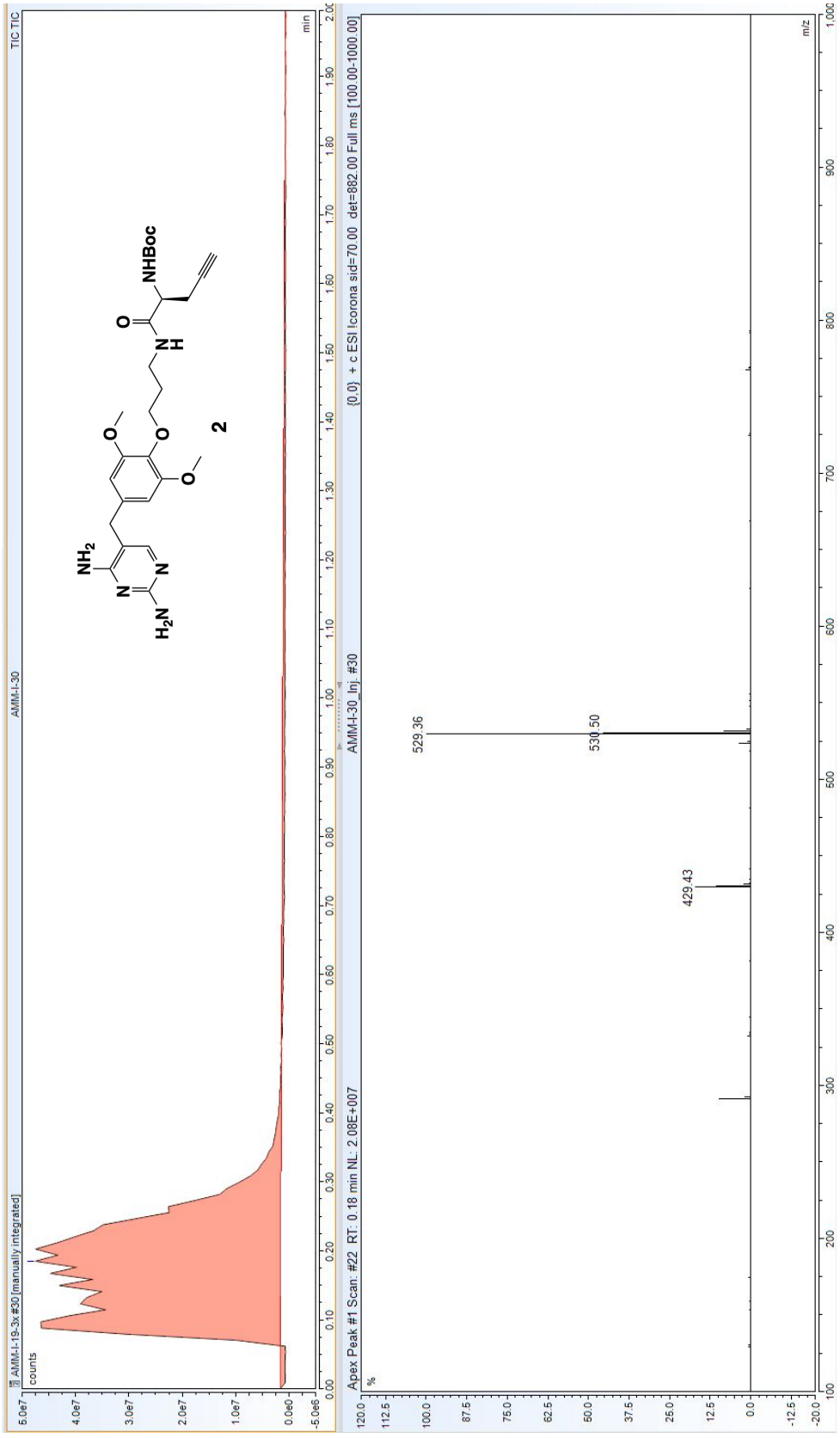

Supplemental Figure 16. ^{1}H-NMR (400 MHz) of TMP-alkyne-NH_2 **2** in $CDCl_3$.

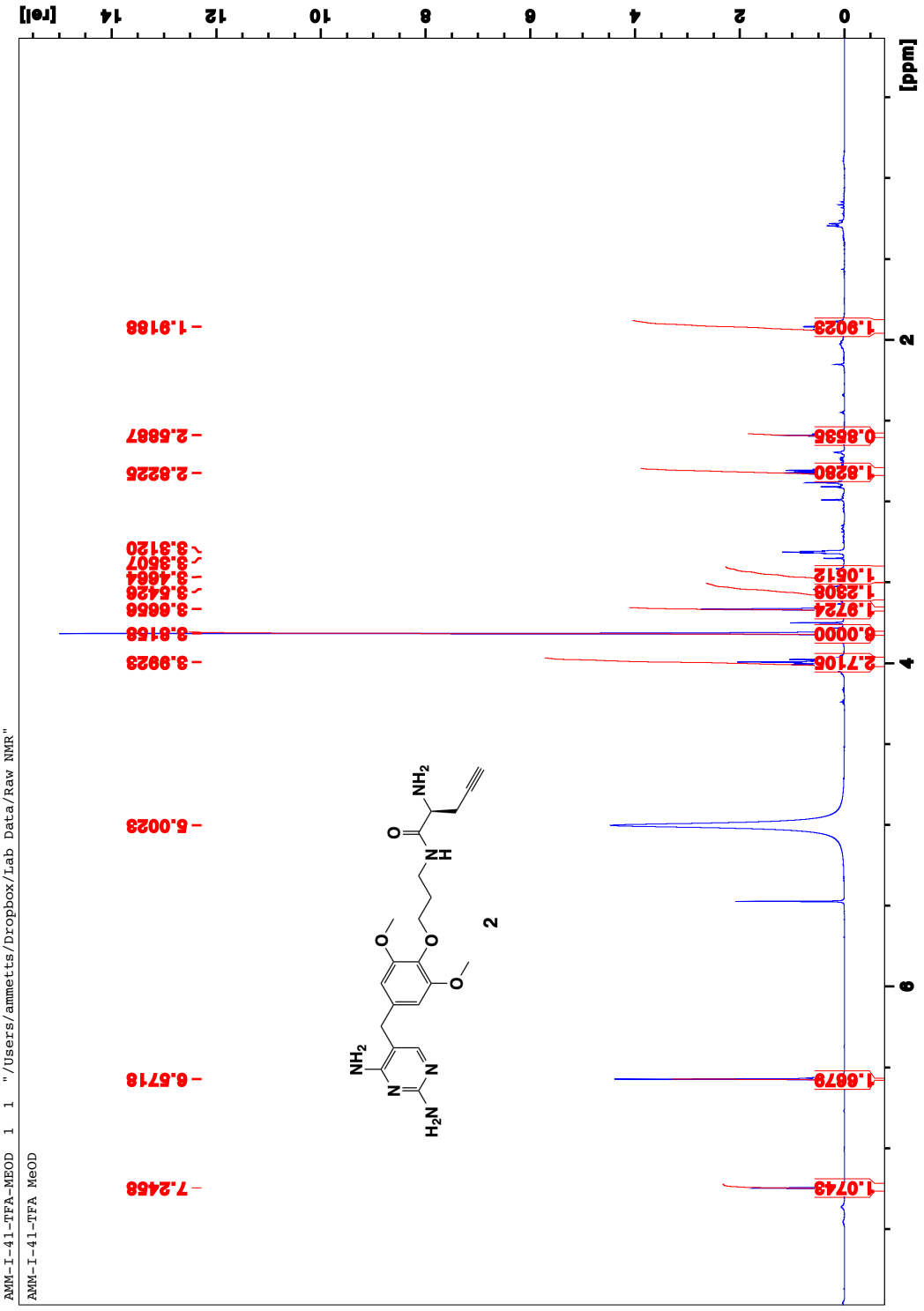

Supplemental Figure 17. ^{13}C-NMR (600 MHz) of TMP-alkyne-NH_2 **2** in $CDCl_3$.

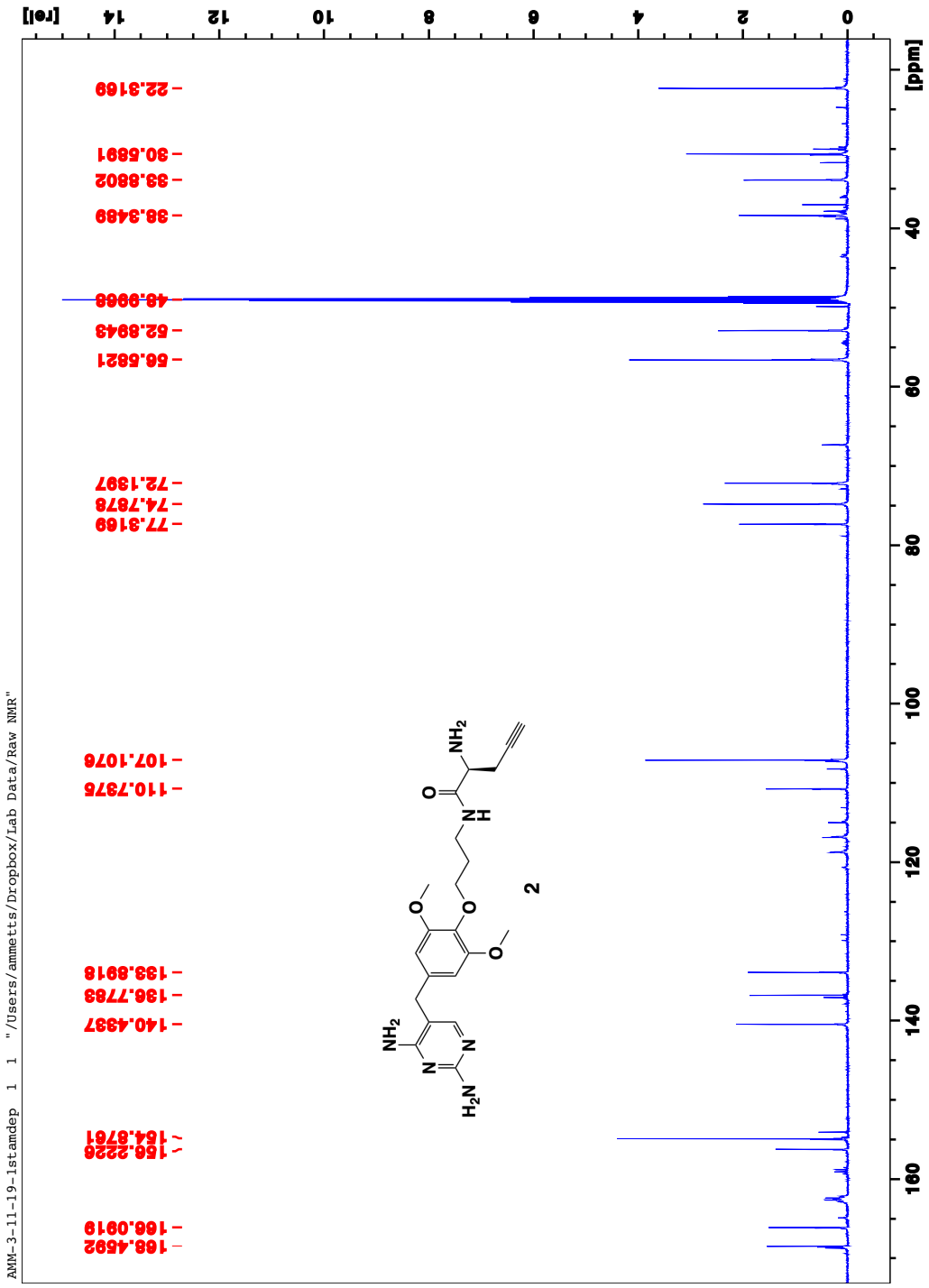

Supplemental Figure 18. ^{1}H-NMR (400 MHz) of 3-maleimidopropanoic acid **7a** in $CDCl_3$.

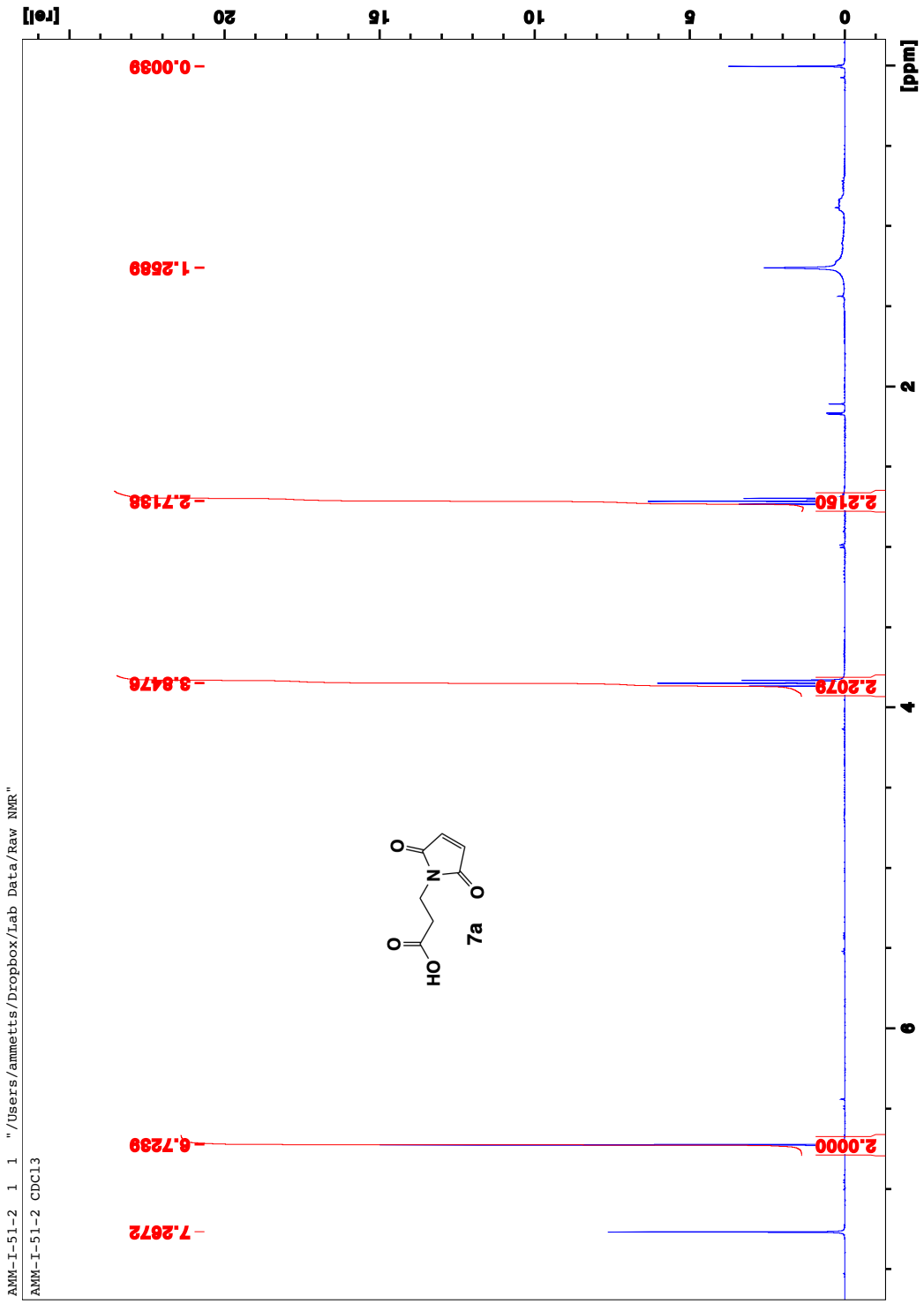

Supplemental Figure 19. ^{13}C-NMR (600 MHz) of 3-maleimidopropanoic acid **7a** in $CDCl_3$.

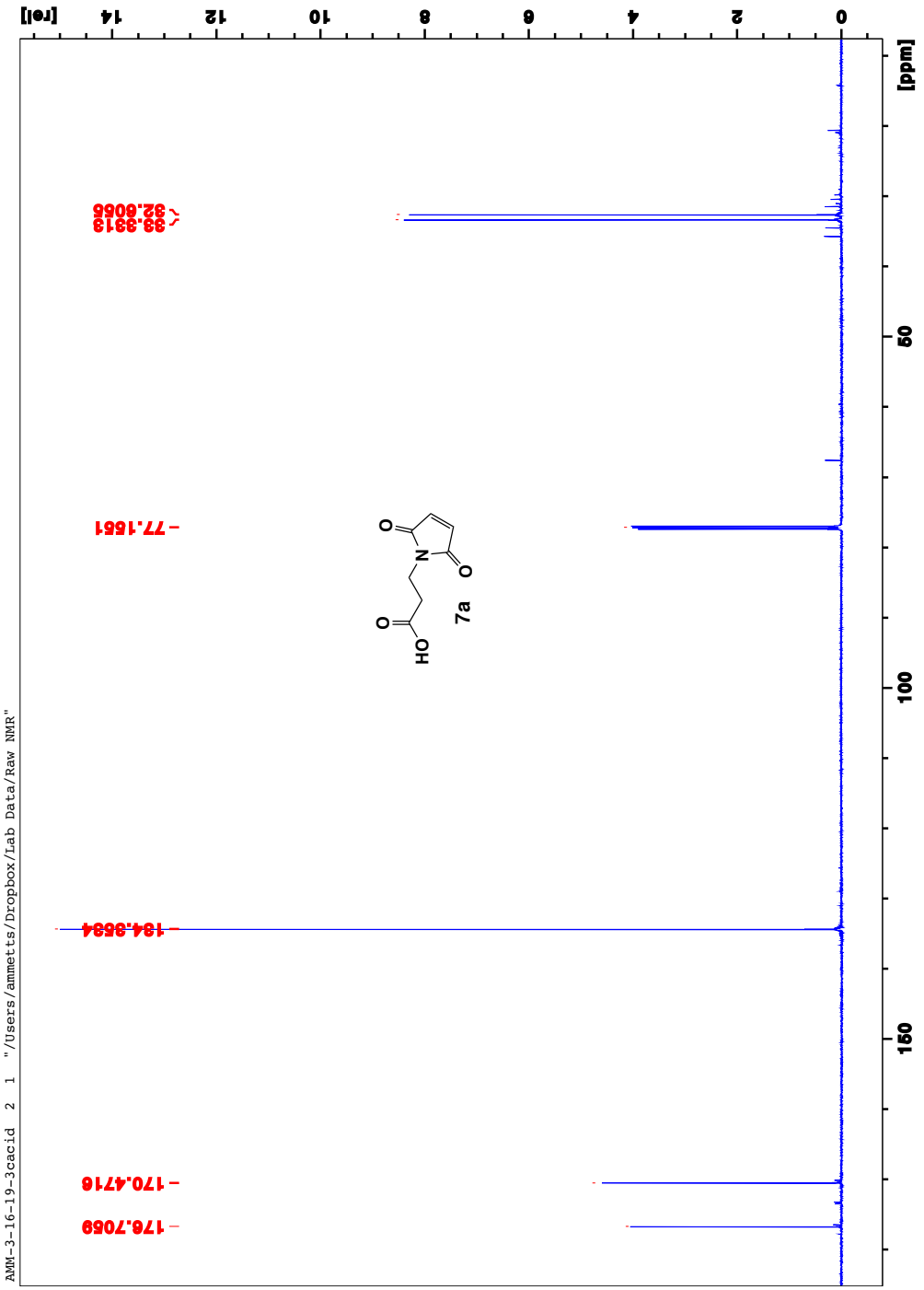

Supplemental Figure 20. ^{1}H-NMR (400 MHz) of 4-maleimidopropanoic acid **7b** in $CDCl_3$.

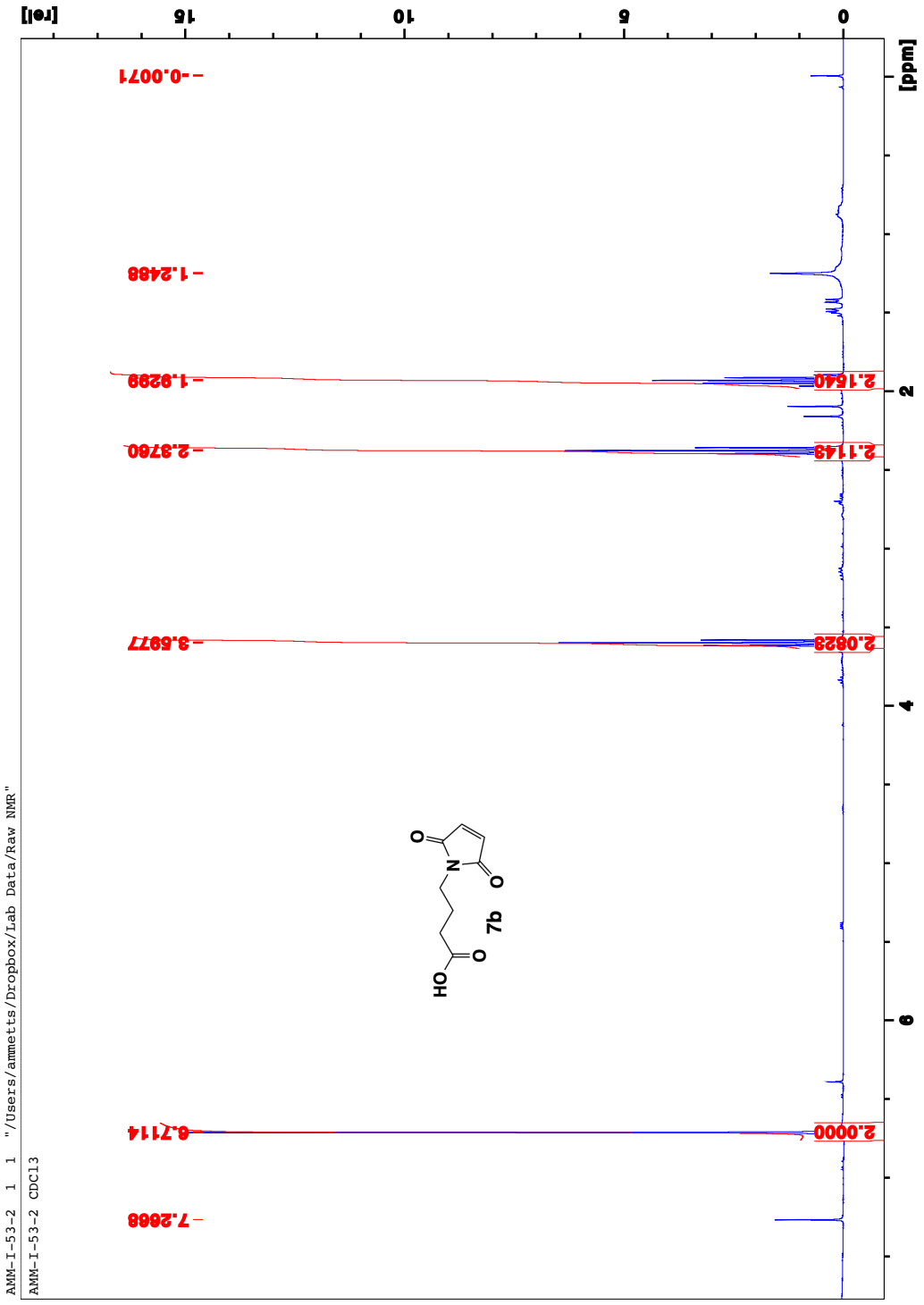

Supplemental Figure 21. ^{13}C-NMR (600 MHz) of 4-maleimidopropanoic acid **7b** in $CDCl_3$.

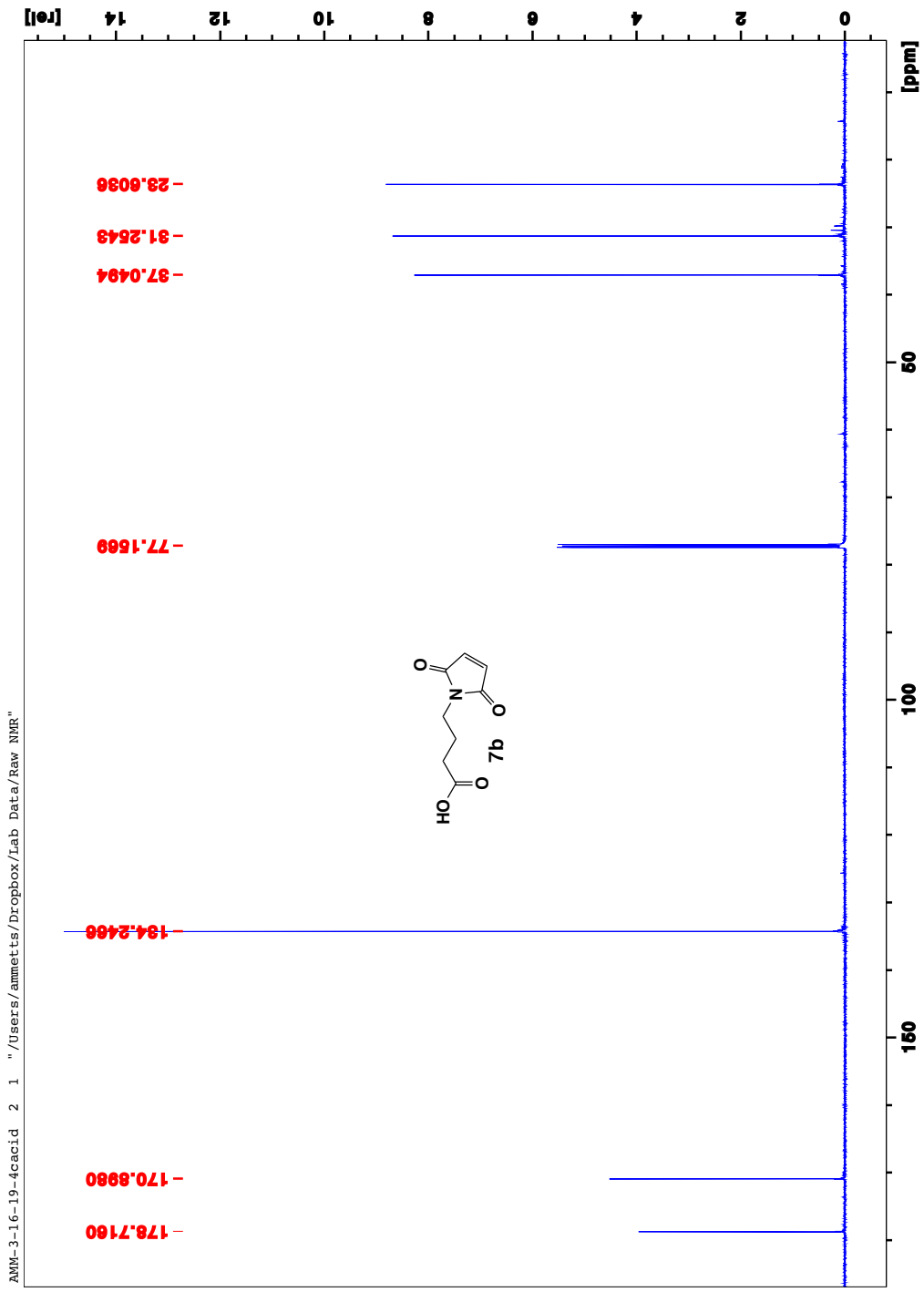

Supplemental Figure 22. ^{1}H-NMR (400 MHz) of 3CMal **1a** in $CDCl_3$.

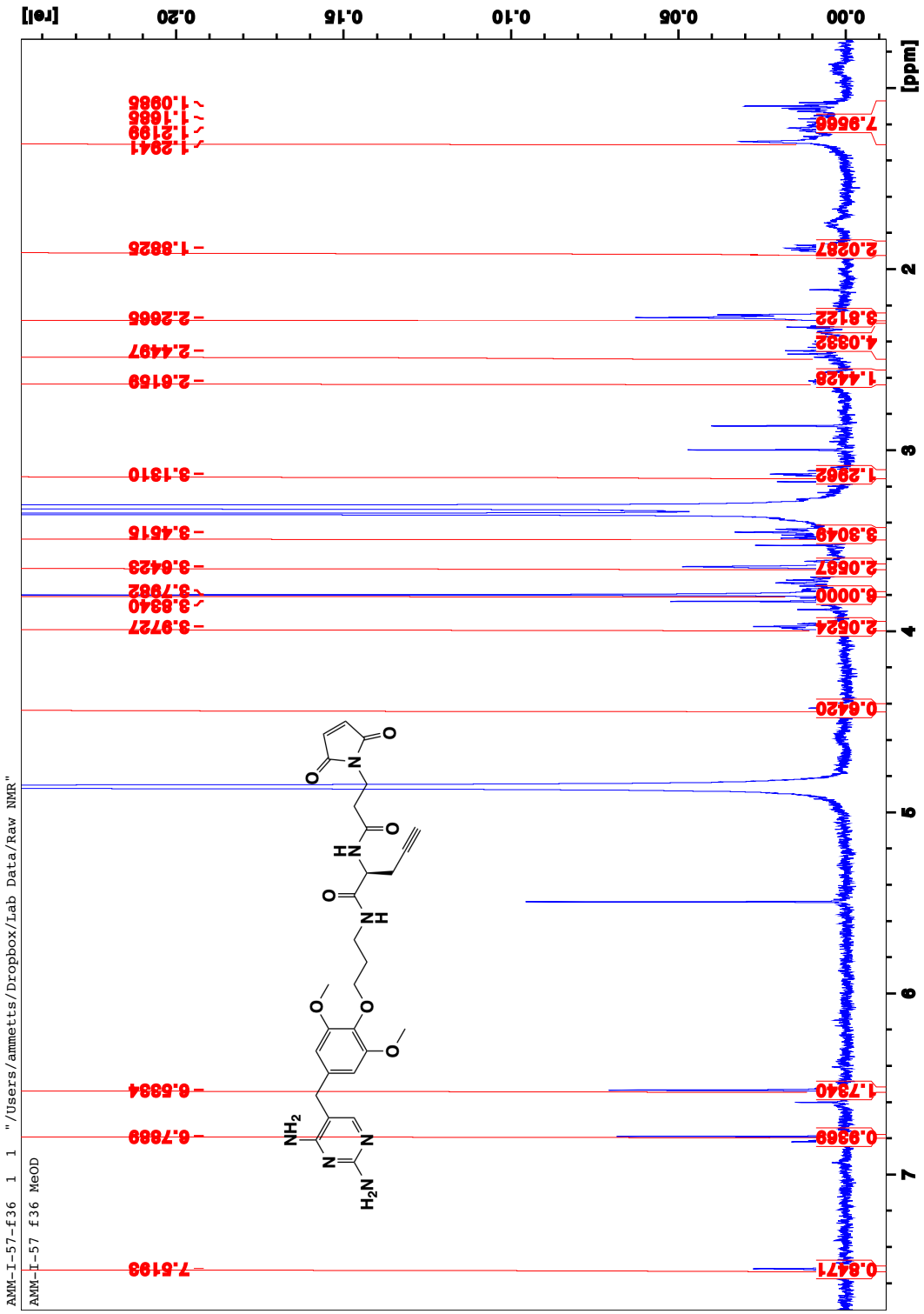

Supplemental Figure 23. ^{1}H-NMR (400 MHz) of 4CMal **1b** in $CDCl_3$.

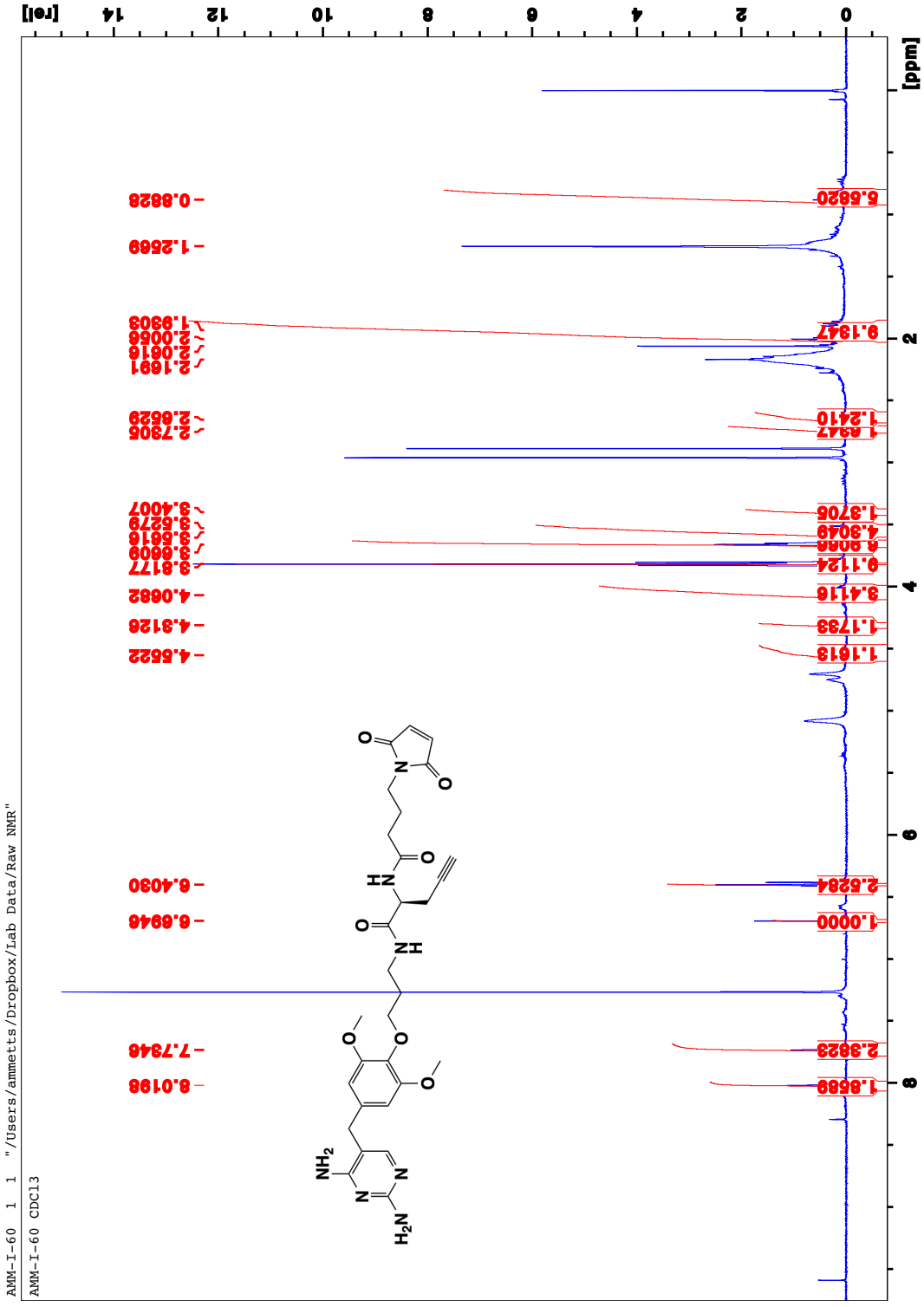

Supplemental Figure 24. ^{1}H-NMR (400 MHz) of 6CMal **1c** in $CDCl_3$.

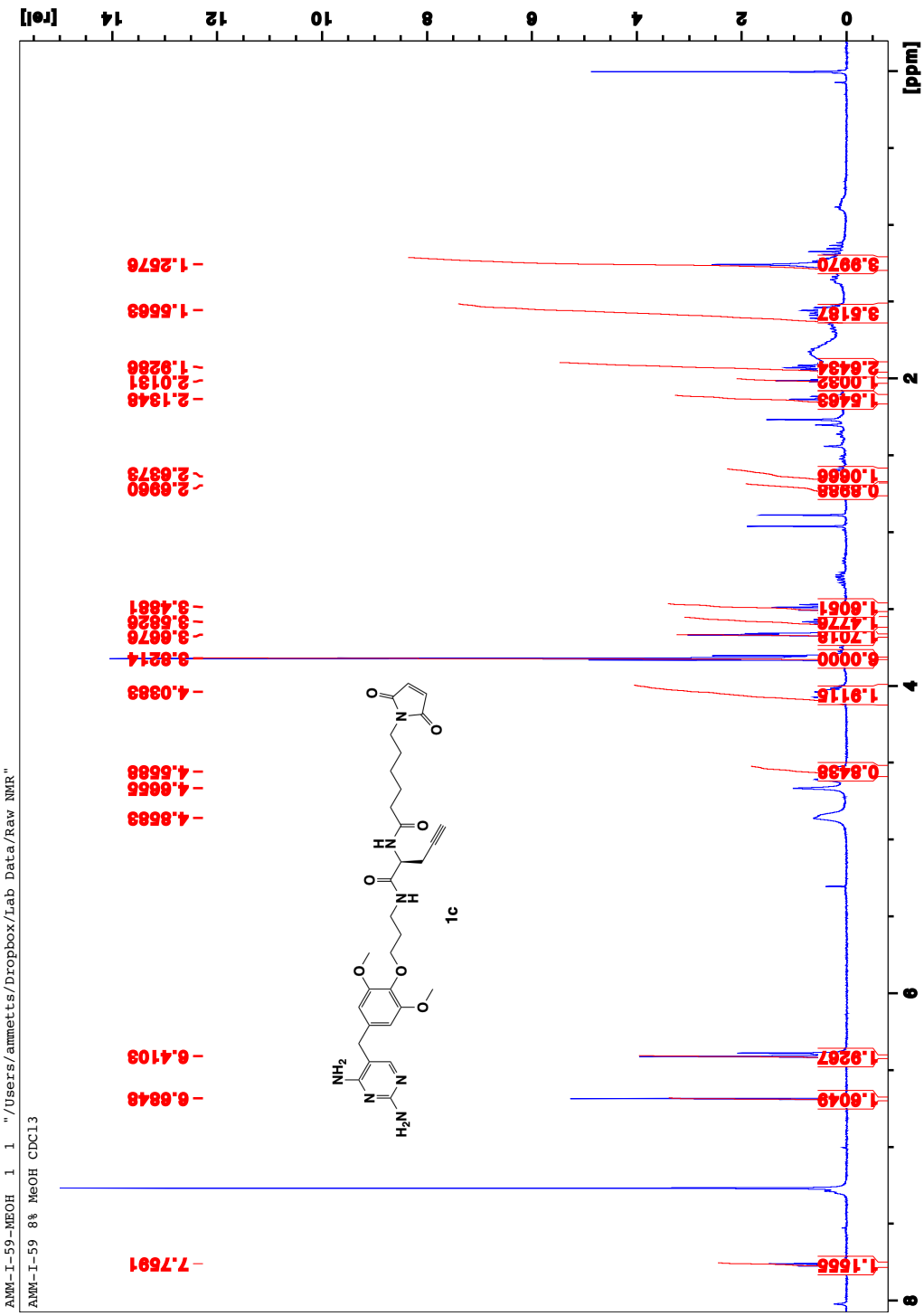

Supplemental Figure 25. LC/MS of 6CMal **1c**.

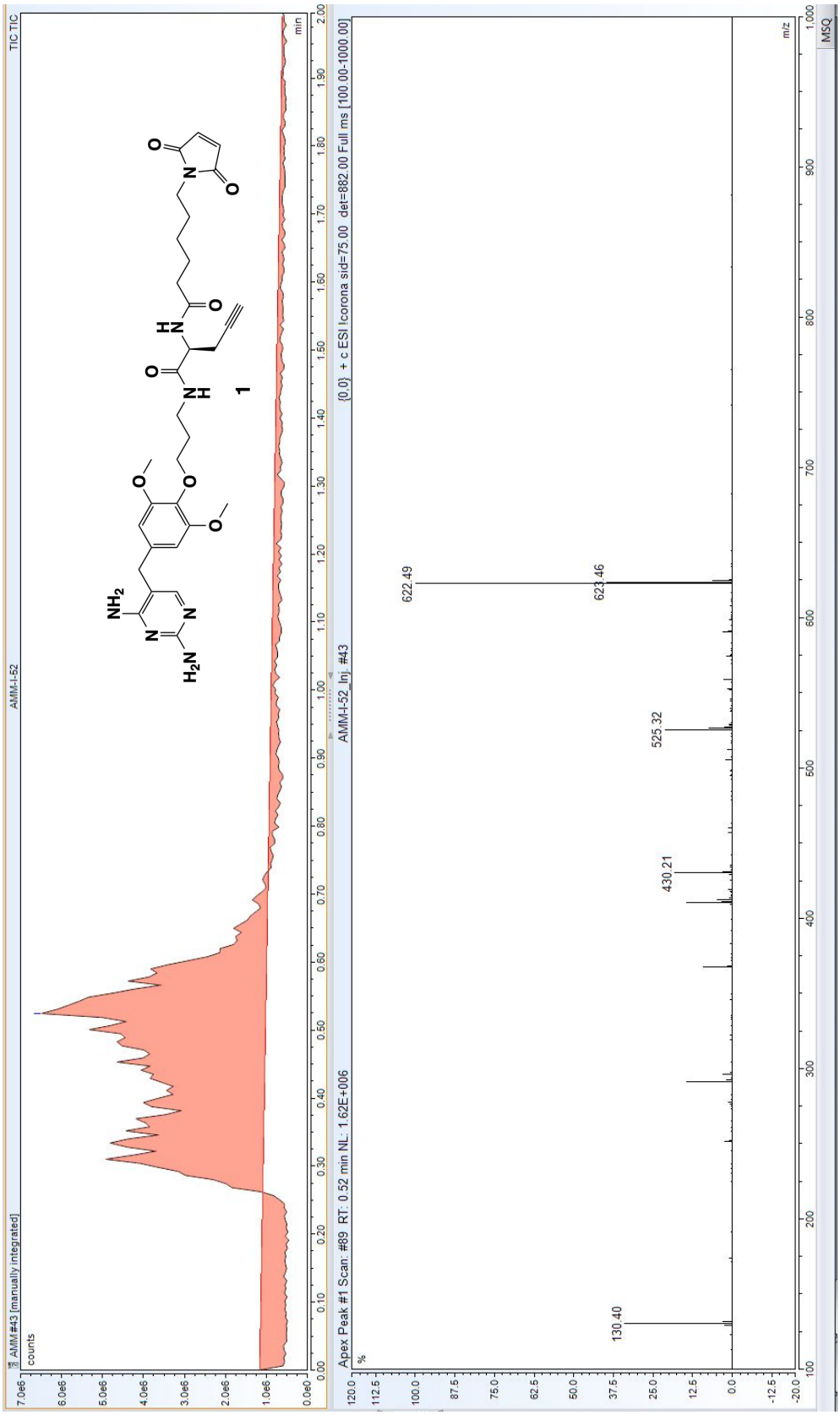

Blot Appendix

Supplemental Figure 1. Western blot of DHFR^{N23C}-YFP and DHFR^{P25C}-YFP expressed in HEK293DAX cells that were reacted with 50 µM of TMP or with the indicated compound at the indicated concentration (3CMal at 10 µM, 4CMal at 10 µM, etc) for 3 hours. These were compared with control lanes of whole cell lysates with or without proteome-wide incorporation of homo-propargyl glycine (HPG). Blot imaged for Cy3 after Click reaction with probe labeled lysates with pycolyl-Cy3 to visualize extent of covalent labeling. Lanes showing red refer to over-exposed labeling.

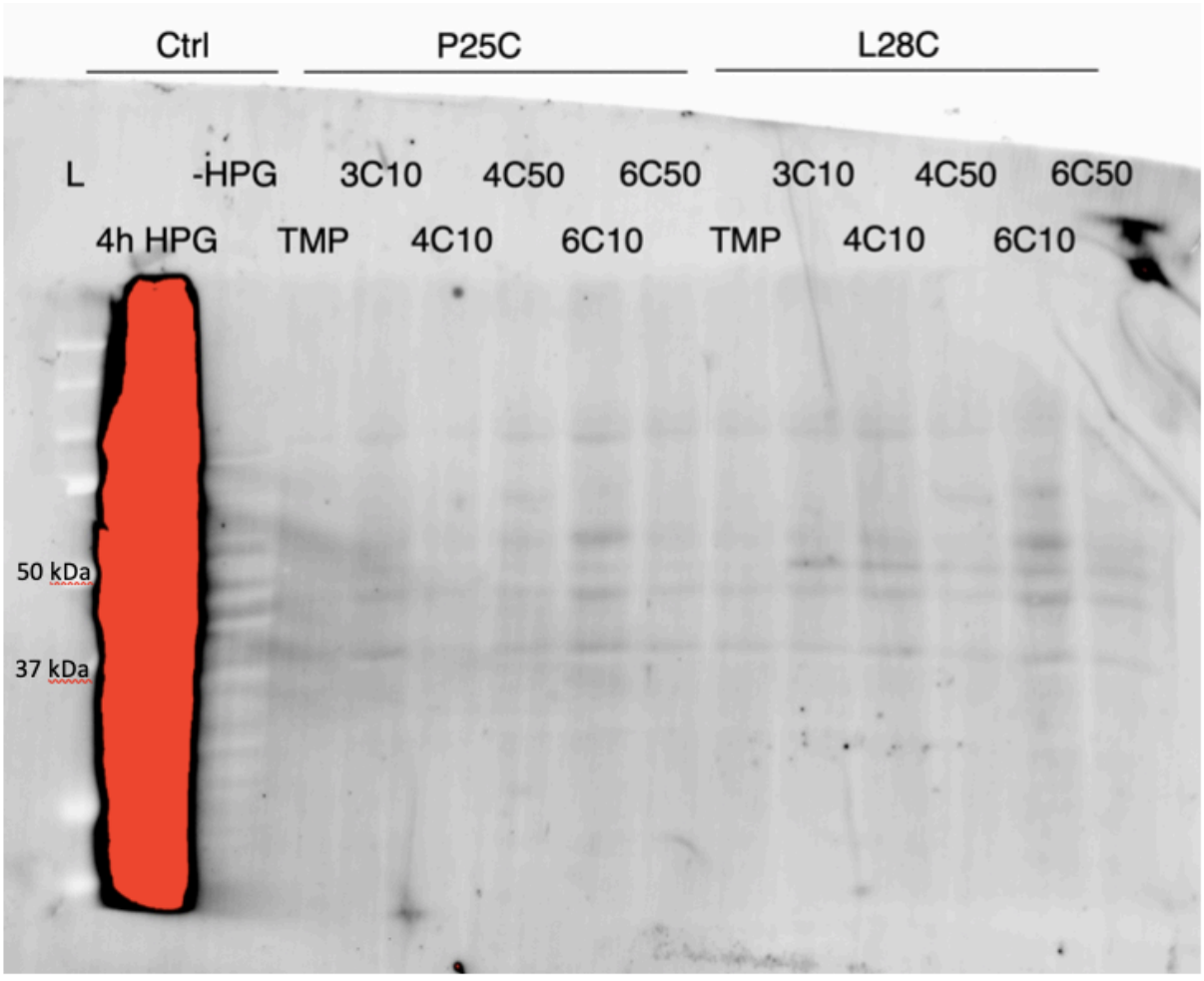

Supplemental Figure 2. Western blot of DHFR^{N23C}-YFP and DHFR^{P25C}-YFP expressed in HEK293DAX cells that were reacted with 50 μM of TMP or with the indicated compound at the indicated concentration (3CMal at 10 μM, 4CMal at 10 μM, etc) for 3 hours. These were compared with control lanes of whole cell lysates with or without proteome-wide incorporation of homo-propargyl glycine (HPG). Western blot using anti-GFP antibody to visualize total expressed DHRF-YFP.

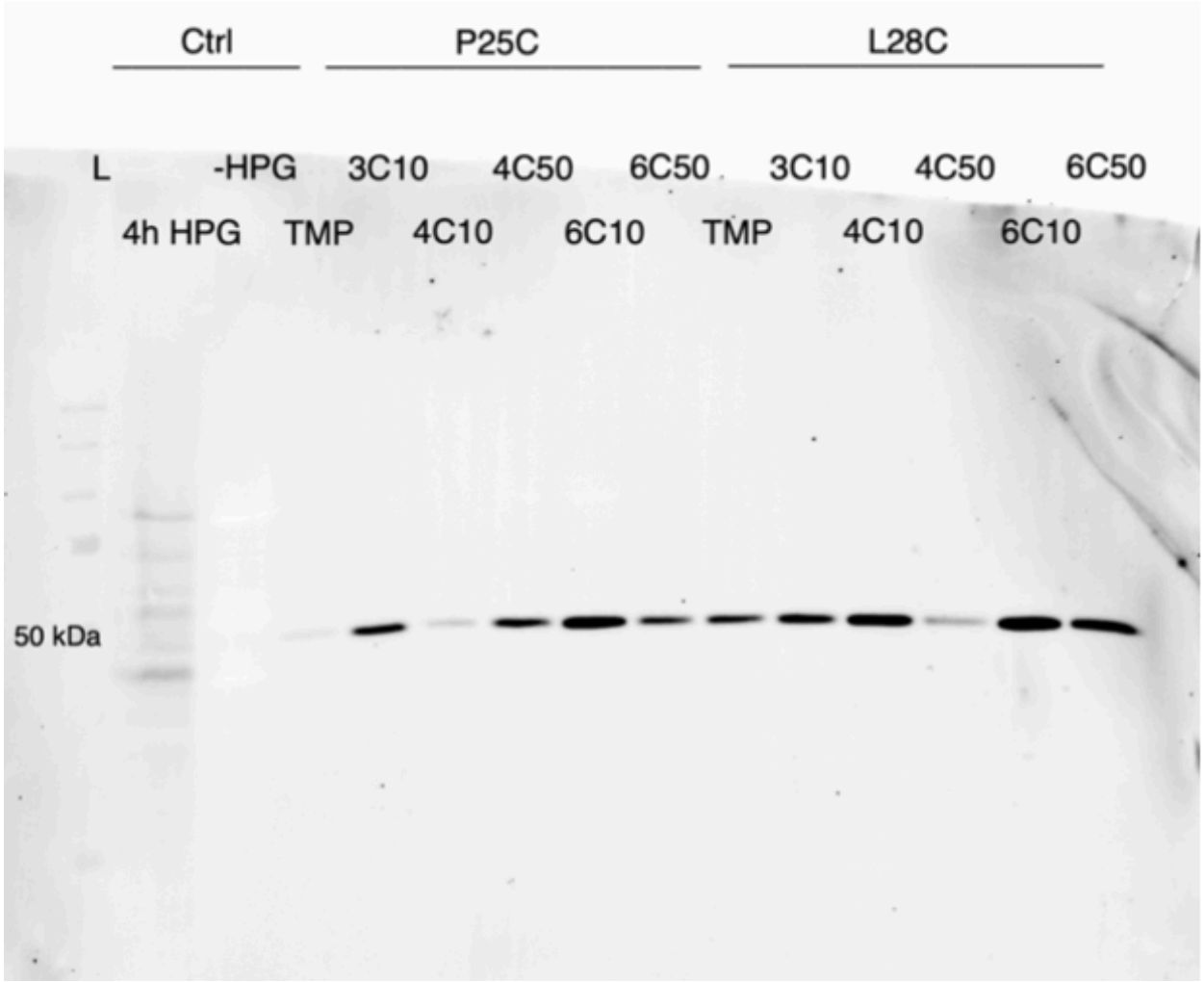

Supplemental Figure 3. Western blot of DHFR-YFP cysteine mutant variants expressed in HEK293DAX cells and cell lysates reacted with the indicated probe compounds (50μM) for 4h to test labeling efficiency for combination of Cys mutants and linker lengths (1a: 6-carbon, 1b, 4-carbon, etc, TMP control). Blot imaged for Cy3 after Click reaction with probe labeled lysates with pycolyl-Cy3 to visualize extent of covalent labeling. Lanes showing red refer to over-exposed labeling.

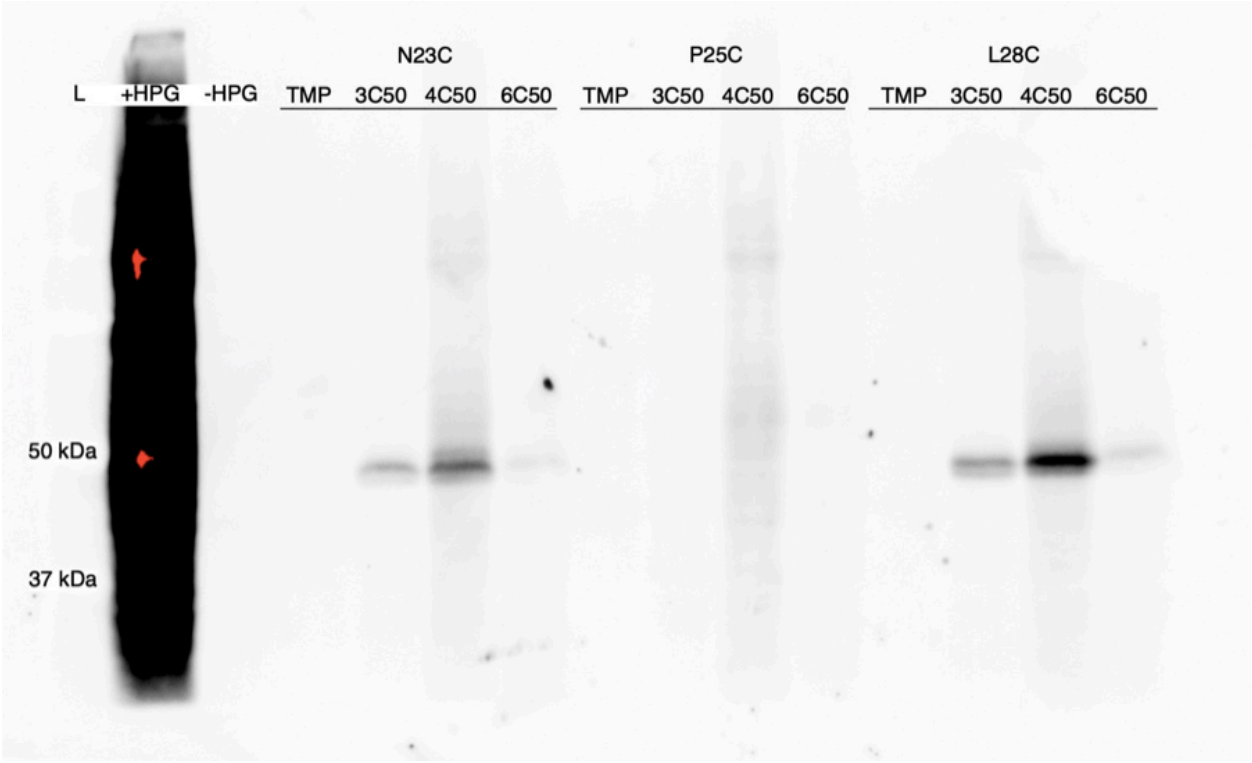

Supplemental Figure 4. Western blot of DHFR-YFP cysteine mutant variants expressed in HEK293DAX cells and cell lysates reacted with the indicated probe compounds (50μM) for 4h to test labeling efficiency for combination of Cys mutants and linker lengths (1a: 6-carbon, 1b, 4-carbon, etc, TMP control). Western blot using anti-GFP antibody to visualize total expressed DHRF-YFP.

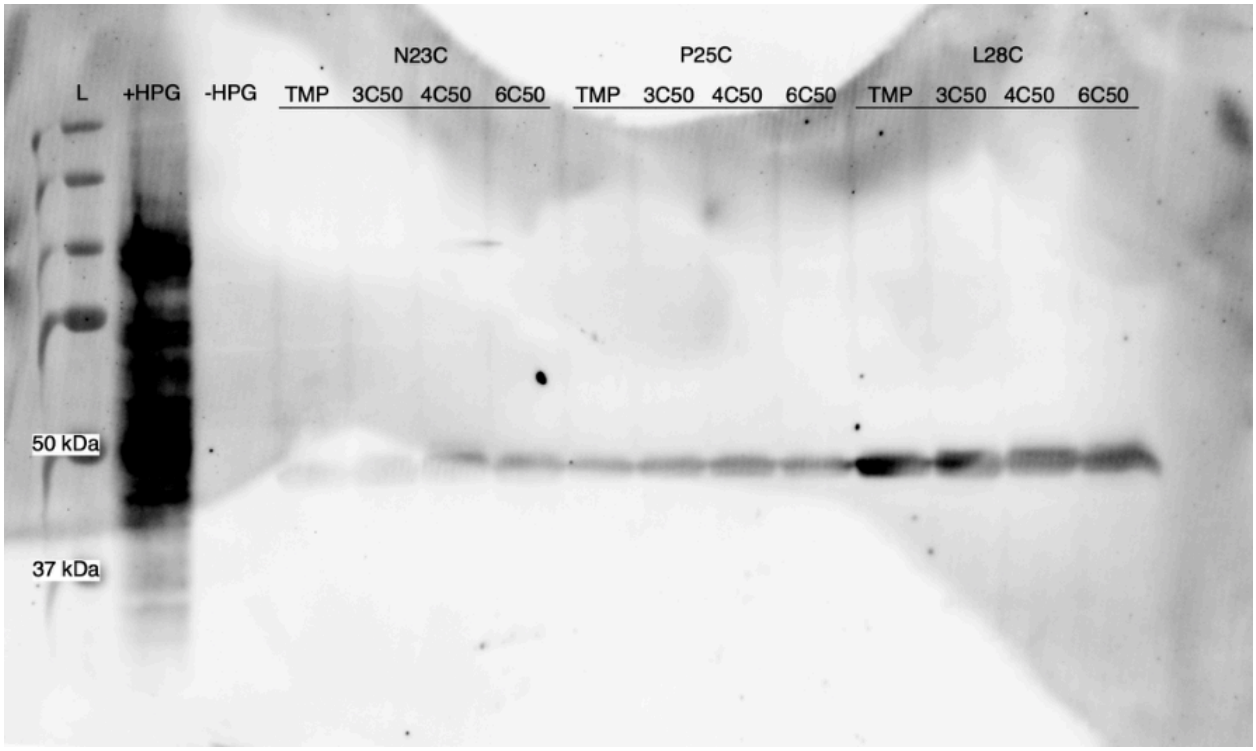

Supplemental Figure 5. Western blot of DHFR-YFP cysteine mutant variants expressed in HEK293DAX cells and cell lysates reacted with the indicated probe compounds (50µM) for 4h to test labeling efficiency for combination of Cys mutants and linker lengths (1a: 6-carbon, 1b, 4-carbon, etc, TMP control). Overlay of both image channels (green: anti-GFP, red: Cy3).

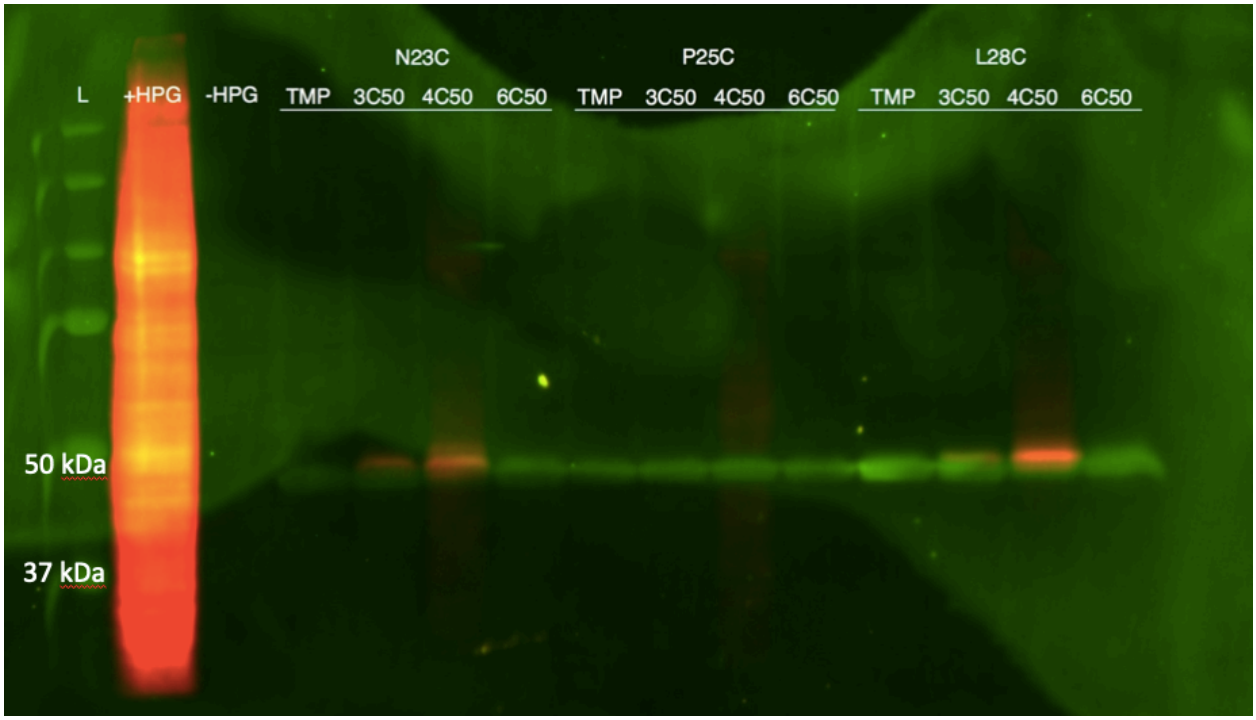

Supplemental Figure 6. Western blot of DHFR-YFP cysteine mutant variants expressed in HEK293DAX cells and cell lysates reacted with the indicated probe compounds (50μM) for 4h to test labeling efficiency for combination of Cys mutants and linker lengths (**1a**: 6-carbon, **1b**, 4-carbon, etc, TMP control). Blot imaged for Cy3 after Click reaction with probe labeled lysates with pycolyl-Cy3 to visualize extent of covalent labeling. Lanes showing red refer to over-exposed labeling.

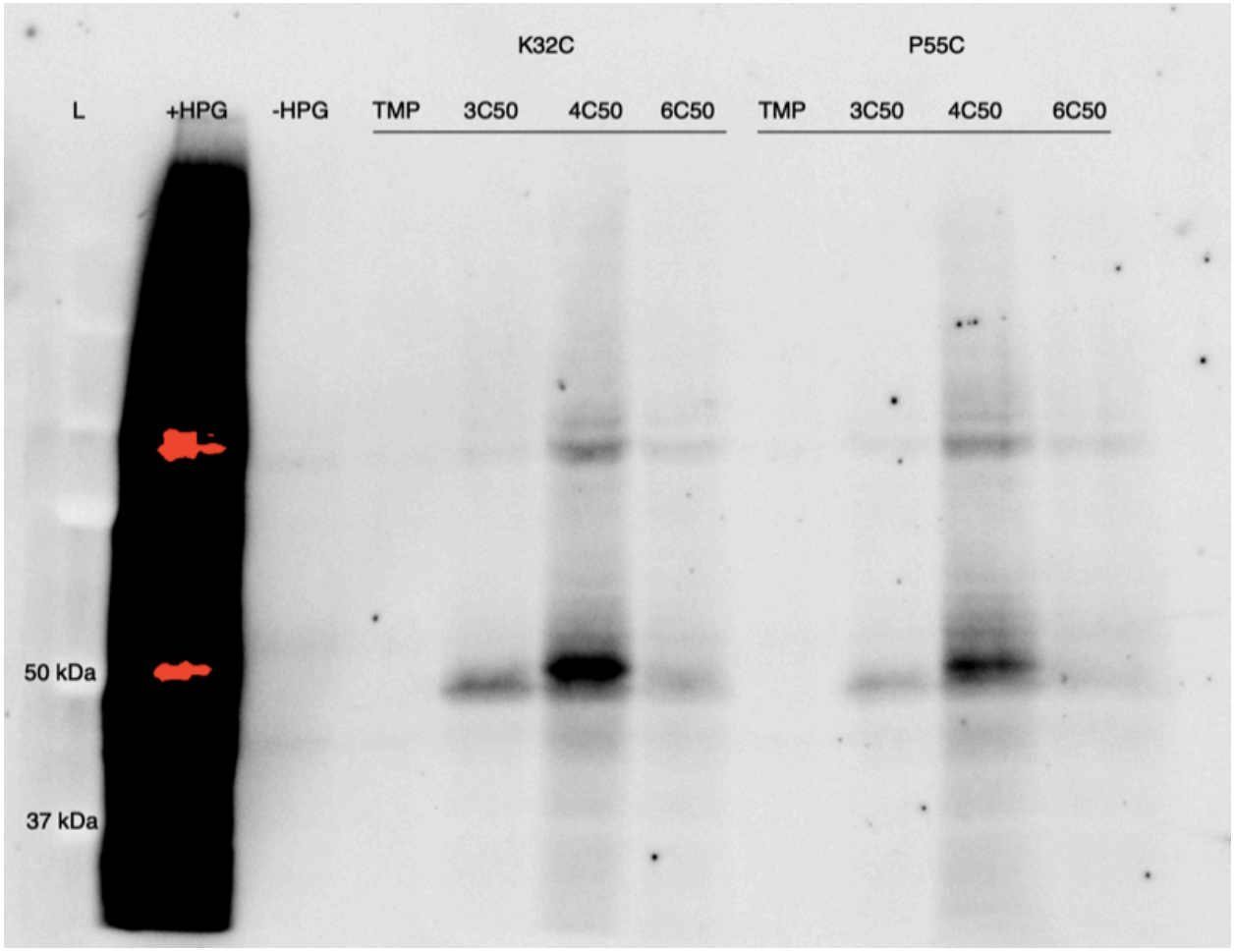

Supplemental Figure 7. Western blot of DHFR-YFP cysteine mutant variants expressed in HEK293DAX cells and cell lysates reacted with the indicated probe compounds (50μM) for 4h to test labeling efficiency for combination of Cys mutants and linker lengths (**1a**: 6-carbon, **1b**, 4-carbon, etc, TMP control). Western blot using anti-GFP antibody to visualize total expressed DHRF-YFP.

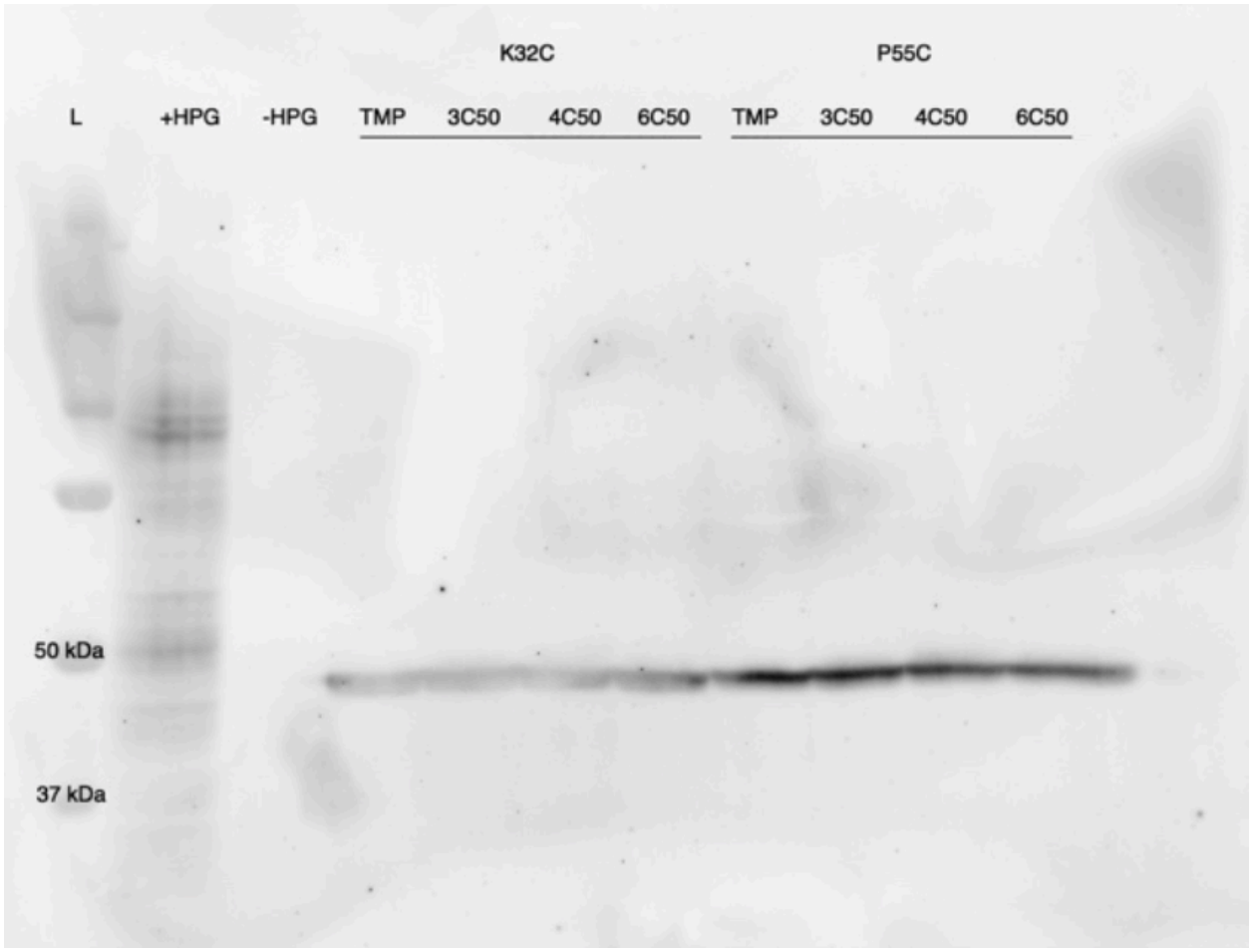

Supplemental Figure 8. Western blot of DHFR-YFP cysteine mutant variants expressed in HEK293DAX cells and cell lysates reacted with the indicated probe compounds (50μM) for 4h to test labeling efficiency for combination of Cys mutants and linker lengths (**1a**: 6-carbon, **1b**, 4-carbon, etc, TMP control). Overlay of both image channels (green: anti-GFP, red: Cy3).

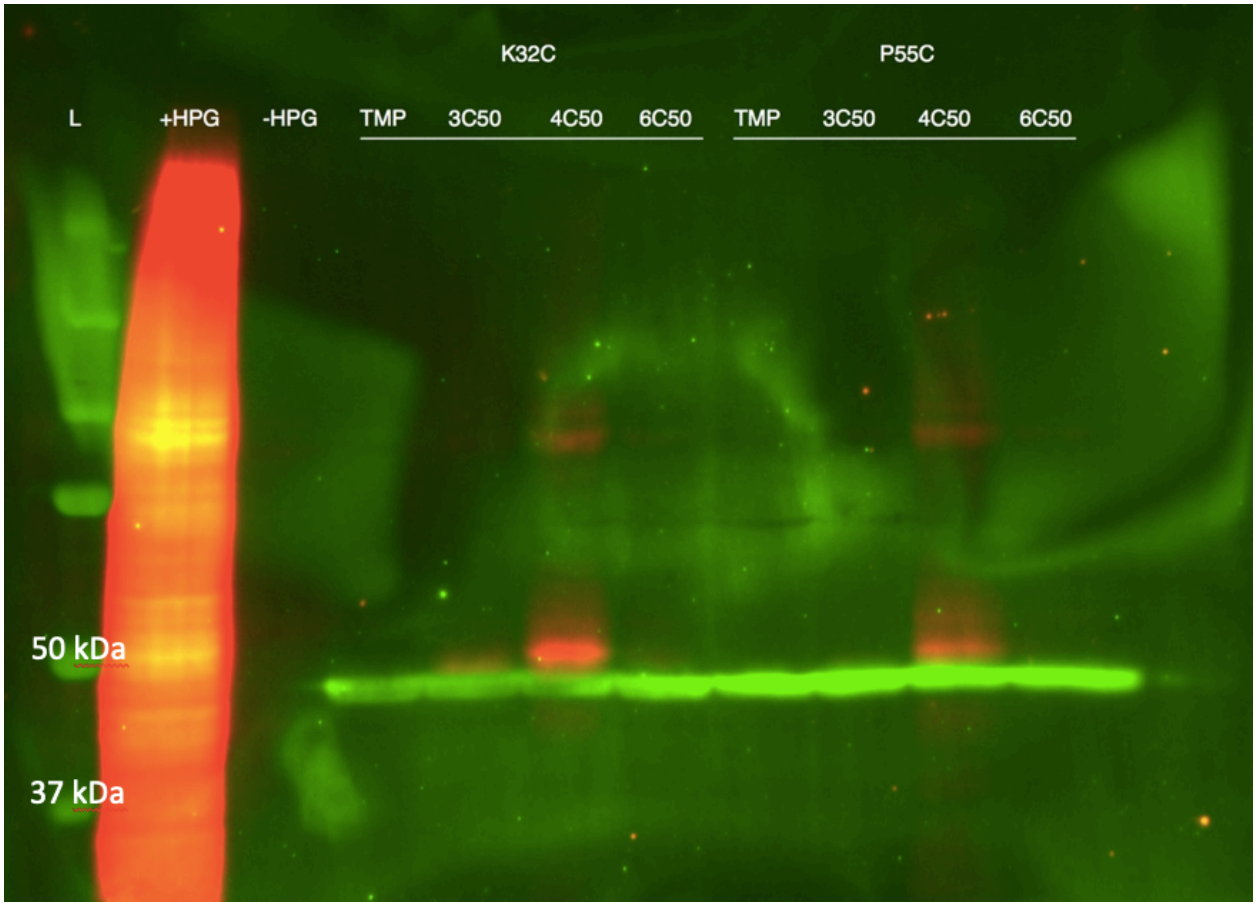

Supplemental Figure 9. Western blot of DHFR^{L28C}-YFP cysteine mutant expressed in HEK293DAX cells and cell lysates reacted with the 4CMal probe compound (**1b**) for 4 hours to test labeling efficiency at various concentrations using the probe and Cys-mutant combination showing the most efficient labeling. Blot imaged for Cy3 after Click reaction with probe labeled lysates with pycolyl-Cy3 to visualize extent of covalent labeling. Lanes showing red refer to over-exposed labeling.

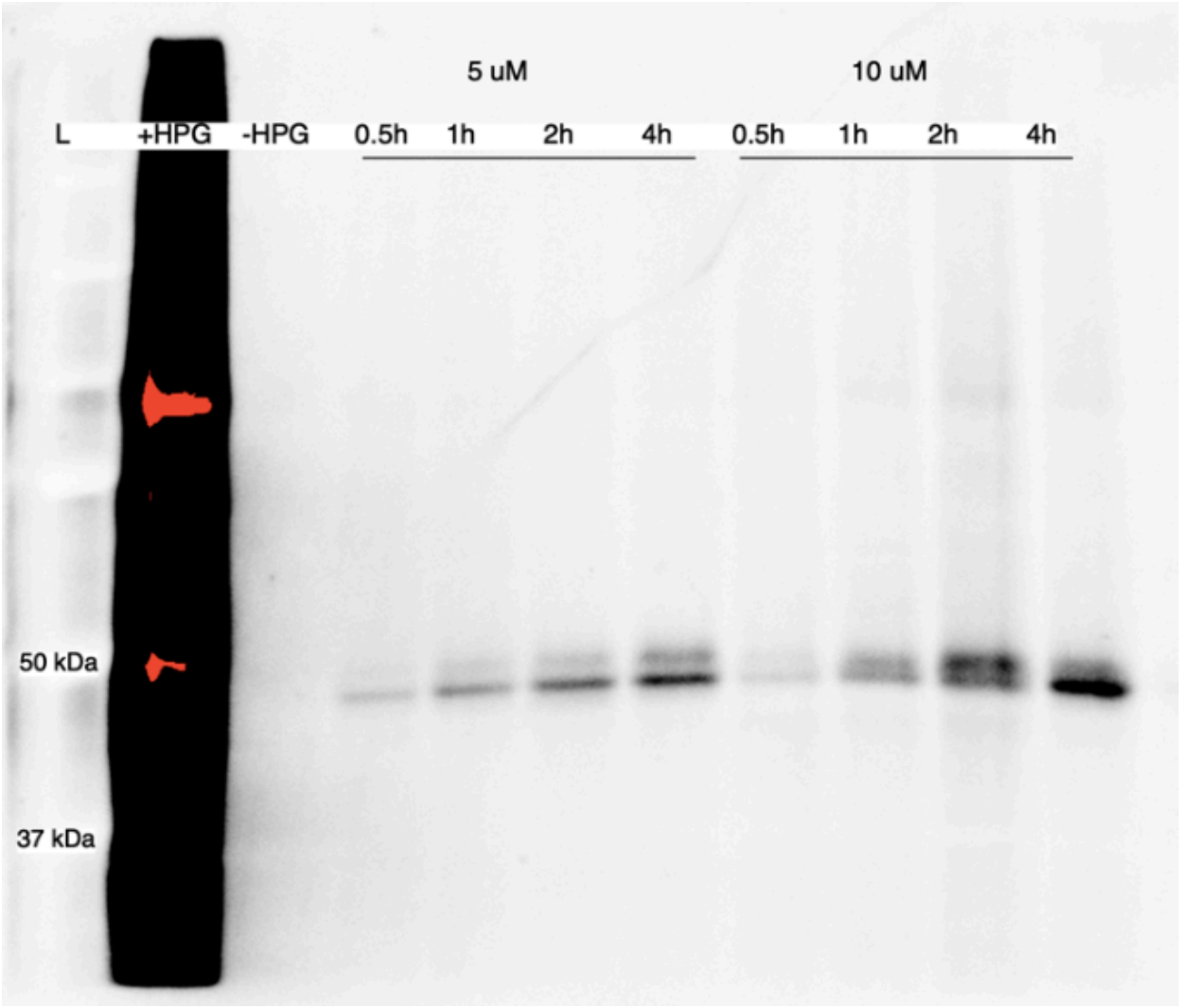

Supplemental Figure 10. Western blot of DHFR^{L28C}-YFP cysteine mutant expressed in HEK293DAX cells and cell lysates reacted with the 4CMal probe compound (**1b**) for 4 hours to test labeling efficiency at various concentrations using the probe and Cys-mutant combination showing the most efficient labeling. Western blot using anti-GFP antibody to visualize total expressed DHRF-YFP. Lanes showing red refer to over-exposed labeling.

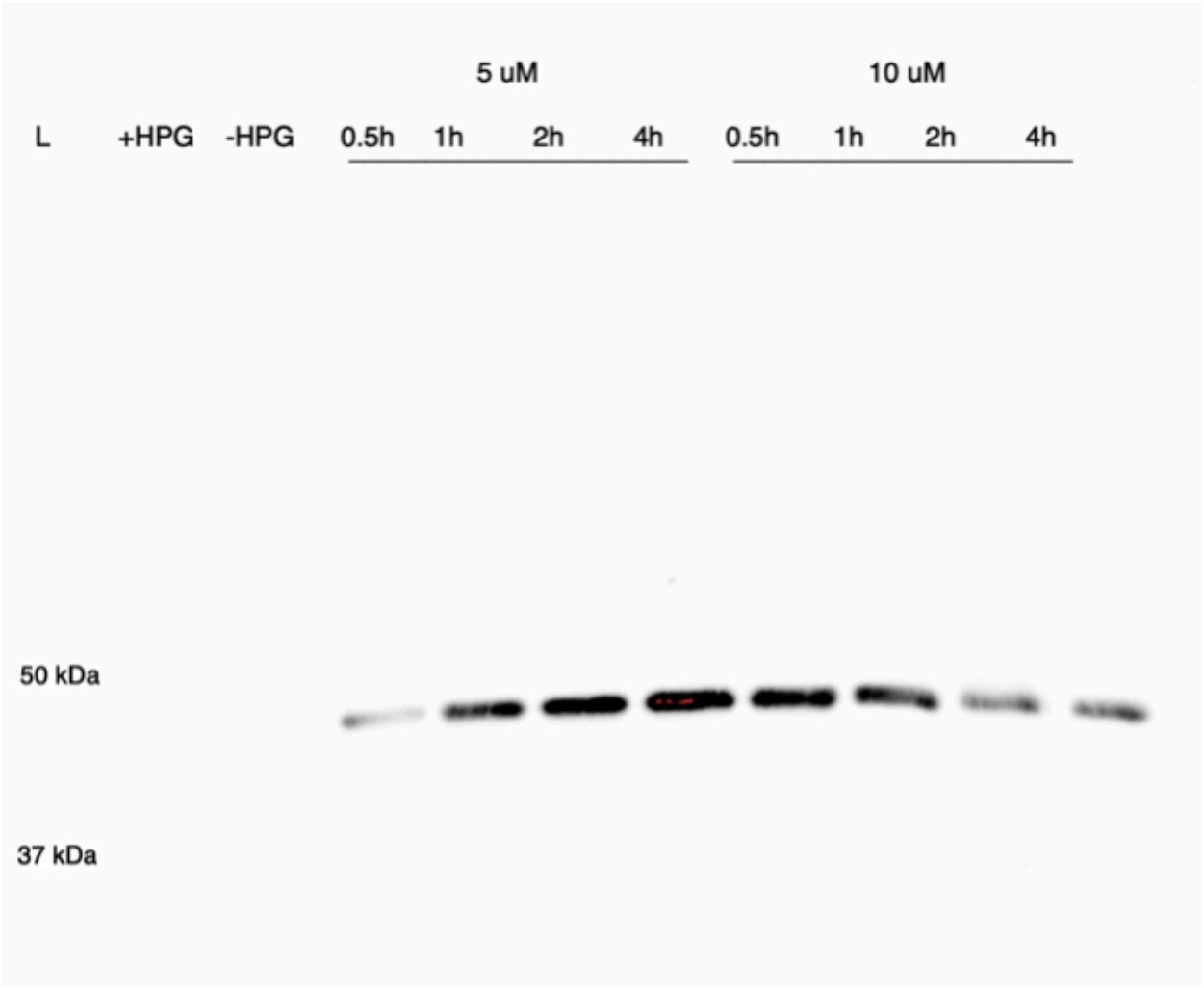

Supplemental Figure 11. Western blot of DHFR^{L28C}-YFP cysteine mutant expressed in HEK293DAX cells and cell lysates reacted with the 4CMal probe compound (**1b**) for 4 hours to test labeling efficiency at various concentrations using the probe and Cys-mutant combination showing the most efficient labeling. Overlay of both image channels (green: anti-GFP, red: Cy3).

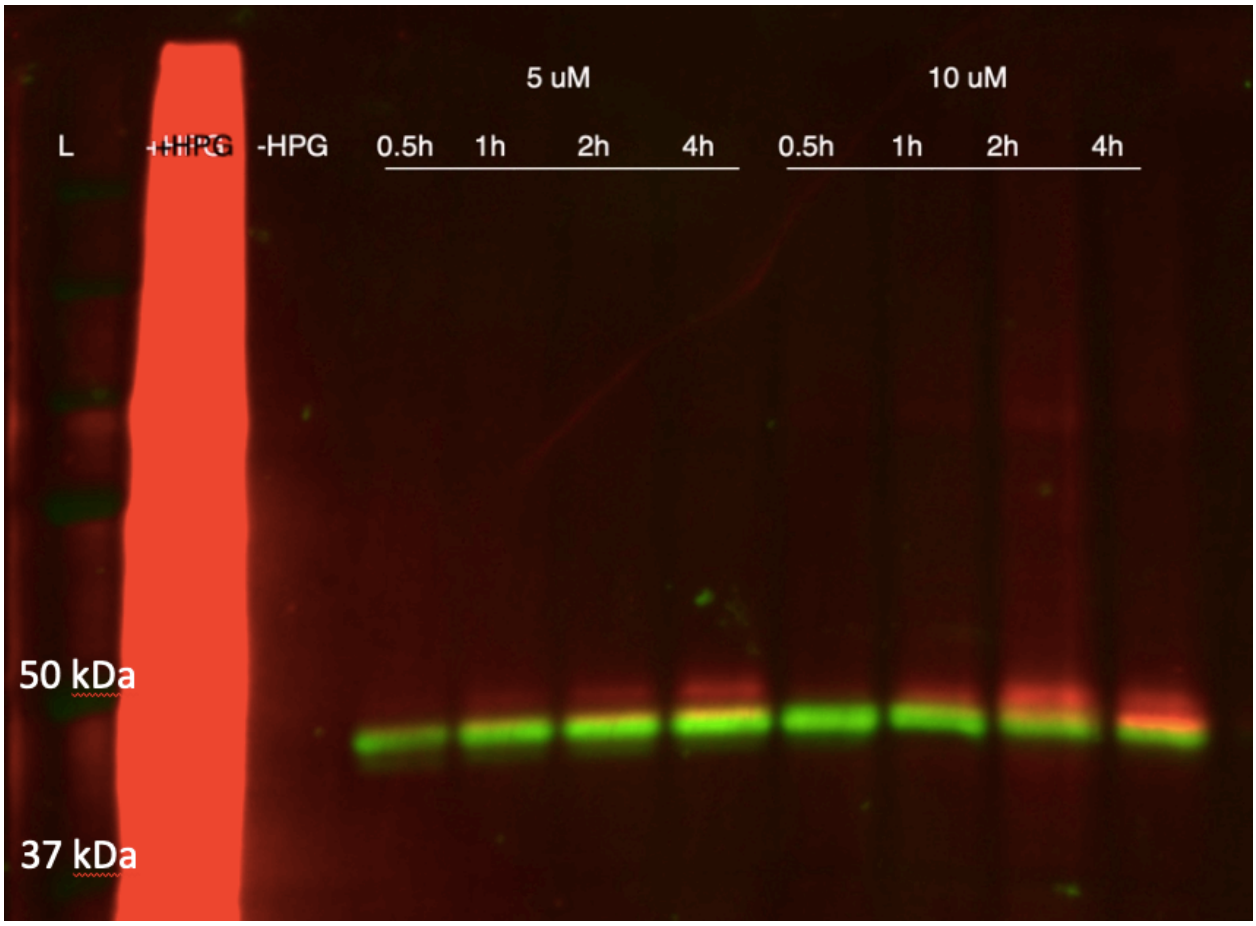

Supplemental Figure 12. Western blot of DHFR^{L28C}-YFP cysteine mutant expressed in HEK293DAX cells and cell lysates reacted with the 4CMal probe compound (**1b**) for 4 hours to test labeling efficiency at various concentrations using the probe and Cys-mutant combination showing the most efficient labeling. Blot imaged for Cy3 after Click reaction with probe labeled lysates with pycolyl-Cy3 to visualize extent of covalent labeling. Lanes showing red refer to over-exposed labeling.

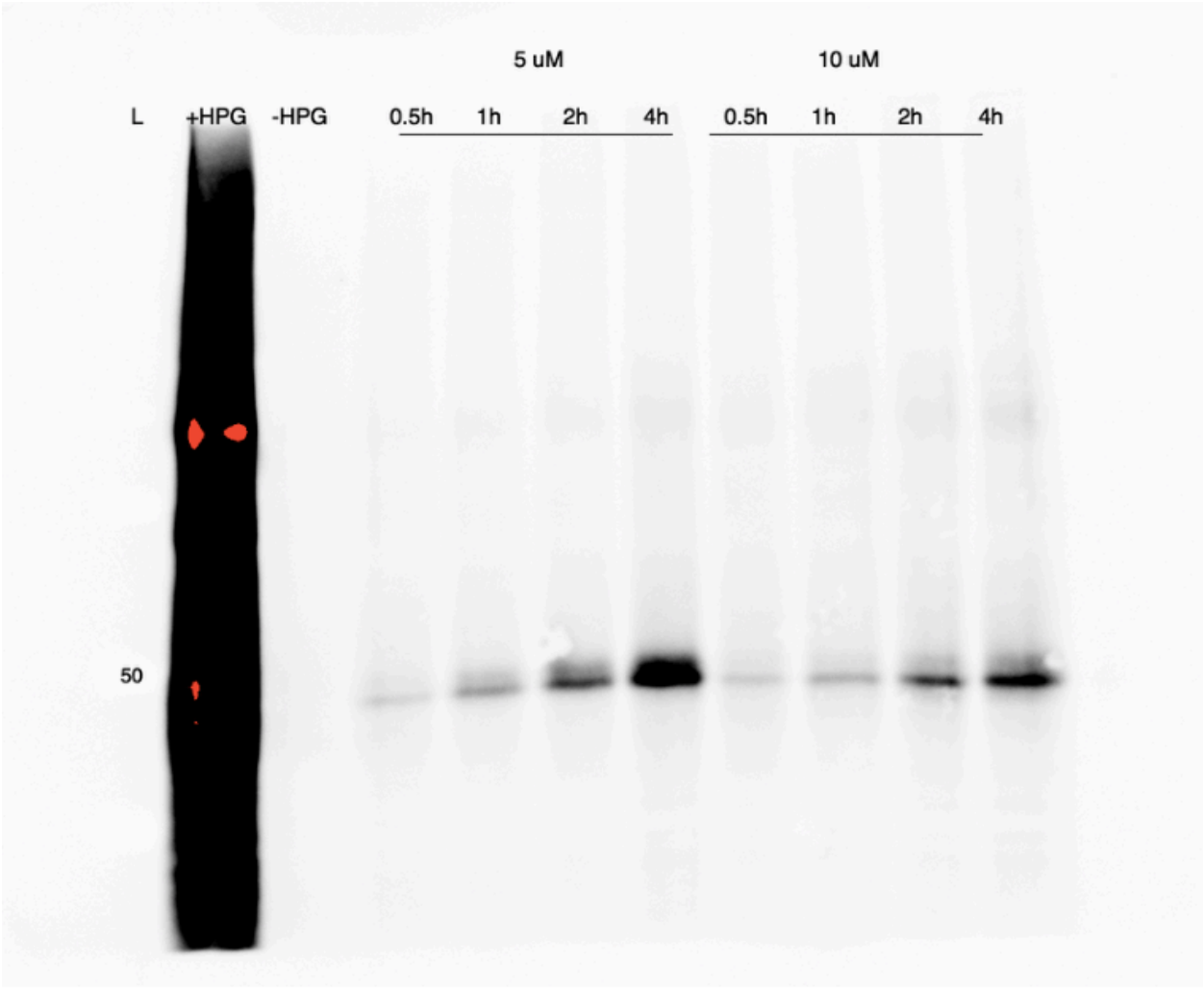

Supplemental Figure 13. Western blot of DHFR^{L28C}-YFP cysteine mutant expressed in HEK293DAX cells and cell lysates reacted with the 4CMal probe compound (**1b**) for 4 hours to test labeling efficiency at various concentrations using the probe and Cys-mutant combination showing the most efficient labeling. Western blot using anti-GFP antibody to visualize total expressed DHRF-YFP. Lanes showing red refer to over-exposed labeling.

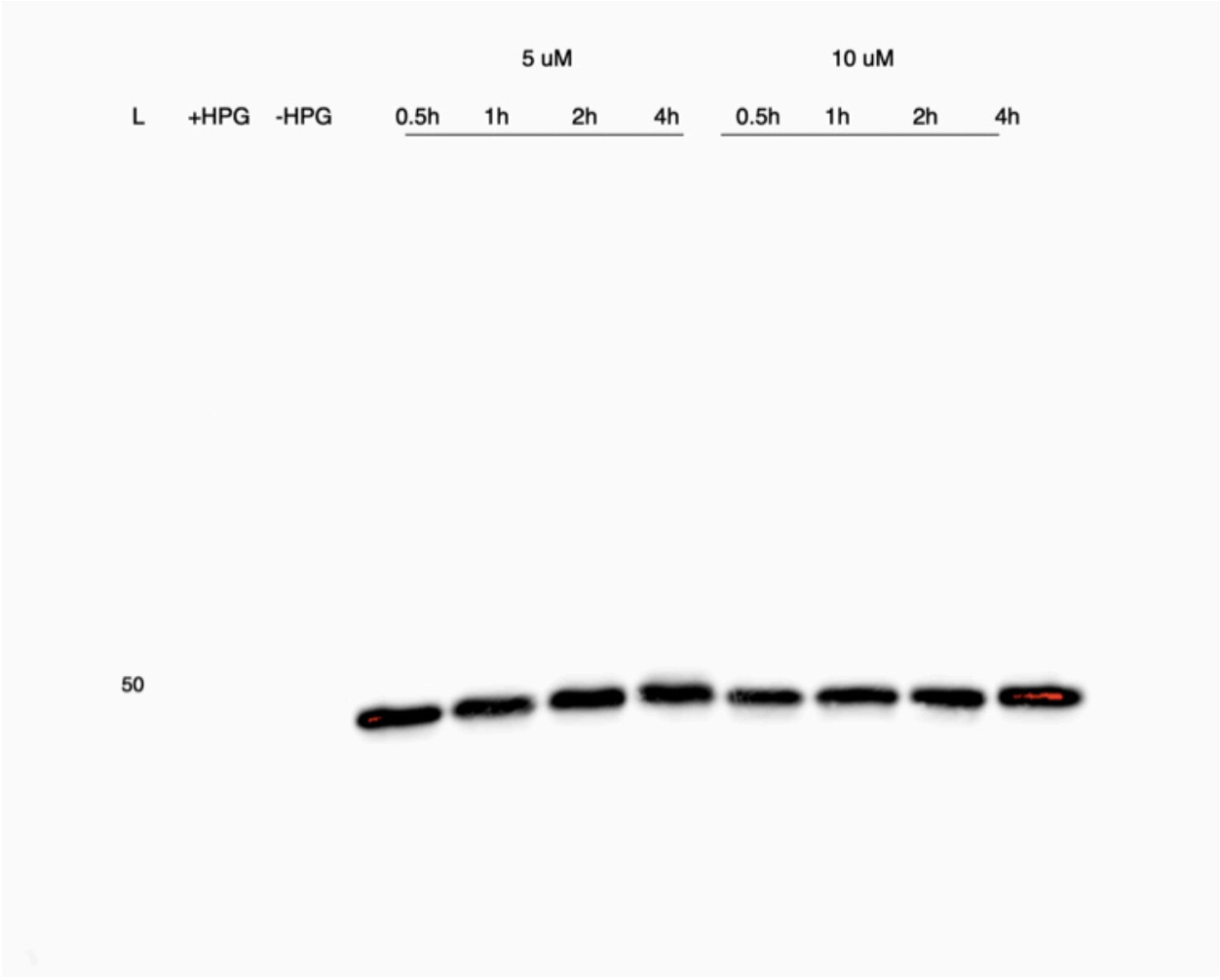

Supplemental Figure 14. Western blot of DHFR^{L28C}-YFP cysteine mutant expressed in HEK293DAX cells and cell lysates reacted with the 4CMal probe compound (**1b**) for 4 hours to test labeling efficiency at various concentrations using the probe and Cys-mutant combination showing the most efficient labeling. Overlay of both image channels (green: anti-GFP, red: Cy3).

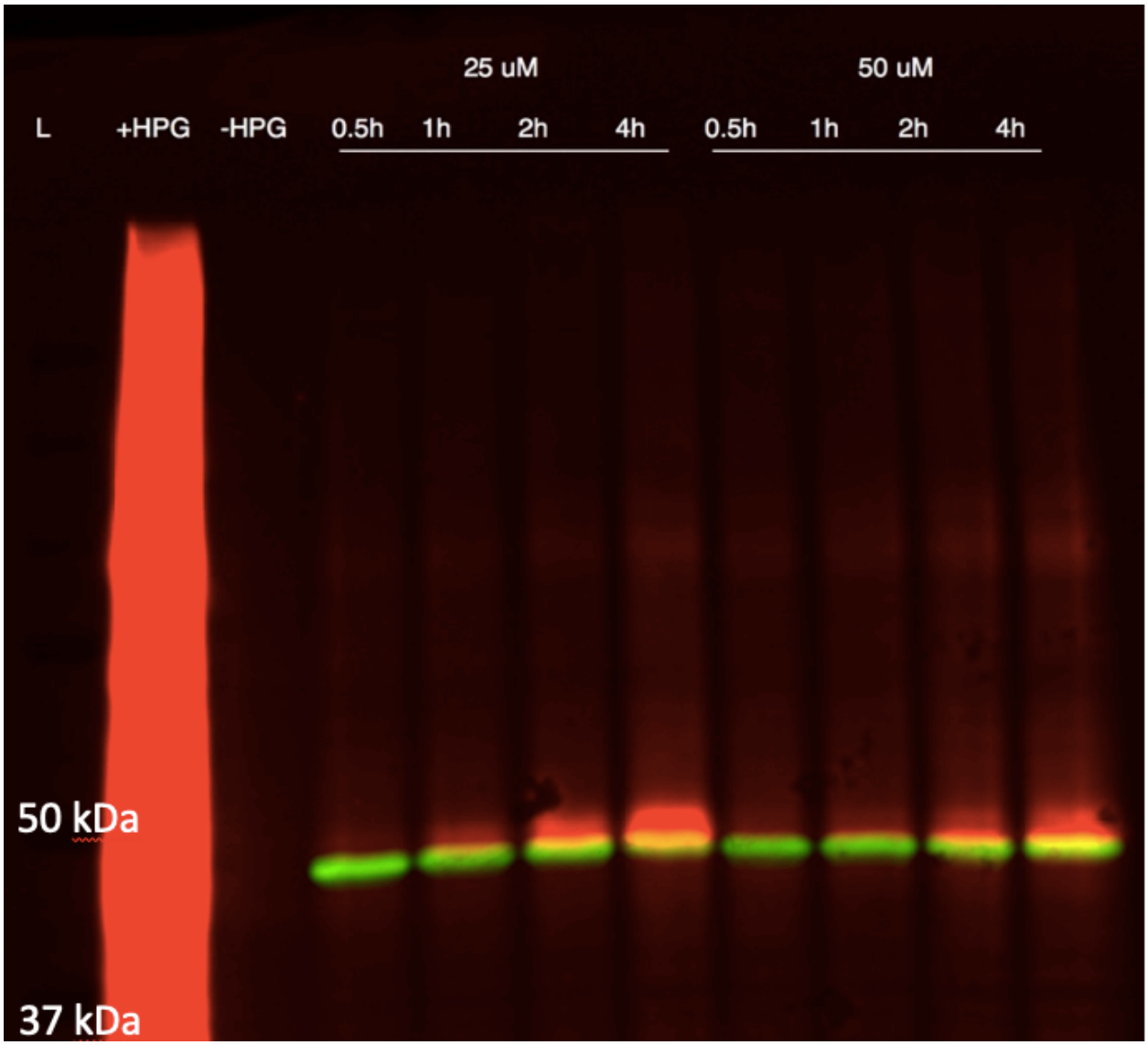

Supplemental Figure 15. Western blot of DHFR^{L28C}-YFP cysteine mutant expressed in HEK293DAX cells and cell lysates reacted with the 4CMal probe compound (**1b**) to test labeling efficiency at various concentrations and time points using the probe and Cys-mutant combination showing the most efficient labeling. Blot imaged for Cy3 after Click reaction with probe labeled lysates with pycolyl-Cy3 to visualize extent of covalent labeling. Lanes showing red refer to over-exposed labeling.

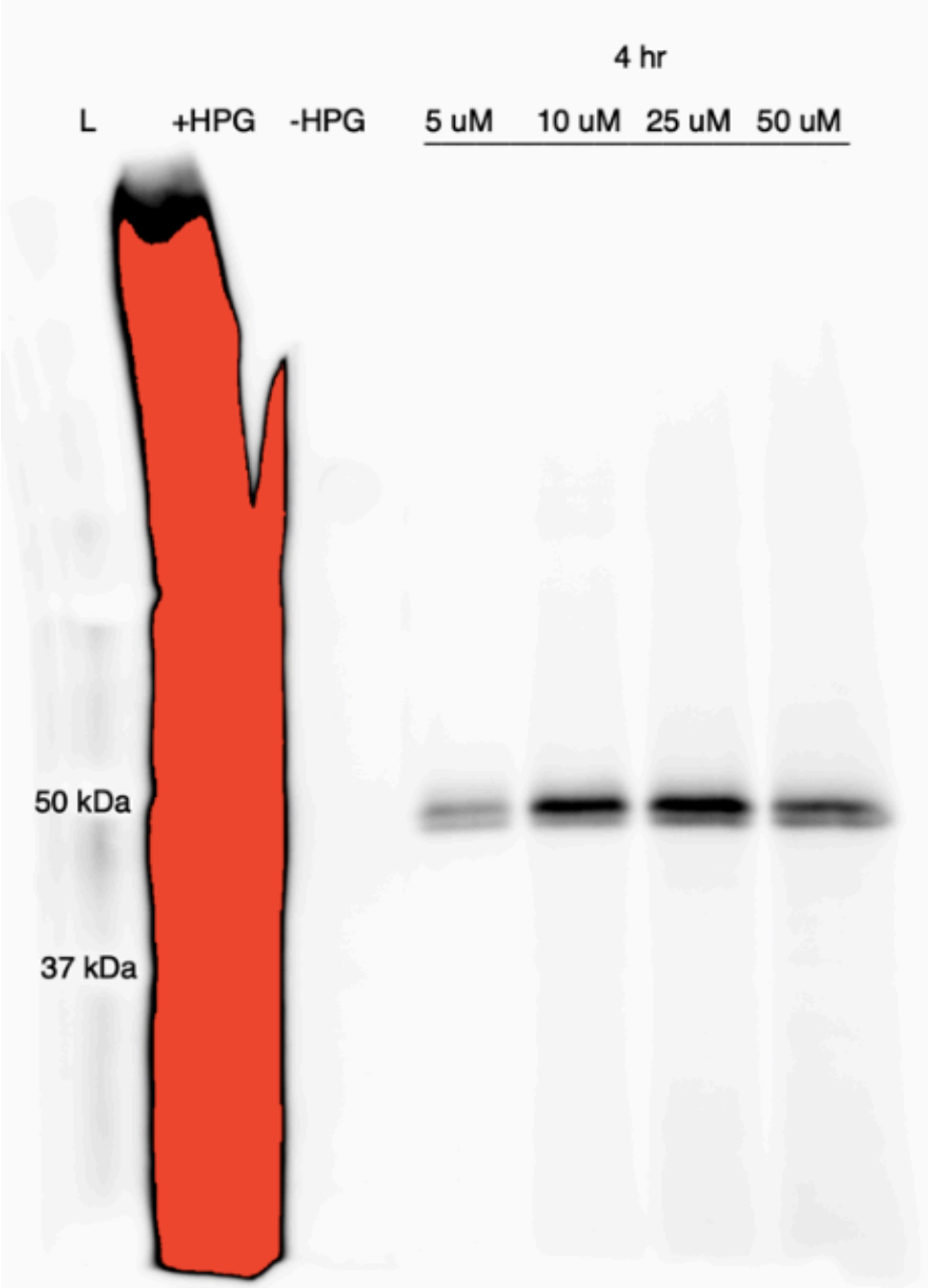

Supplemental Figure 16. Western blot of $DHFR^{L28C}$-YFP cysteine mutant expressed in HEK293DAX cells and cell lysates reacted with the 4CMal probe compound (**1b**) to test labeling efficiency at various concentrations and time points using the probe and Cys-mutant combination showing the most efficient labeling. Western blot using anti-GFP antibody to visualize total expressed DHRF-YFP.

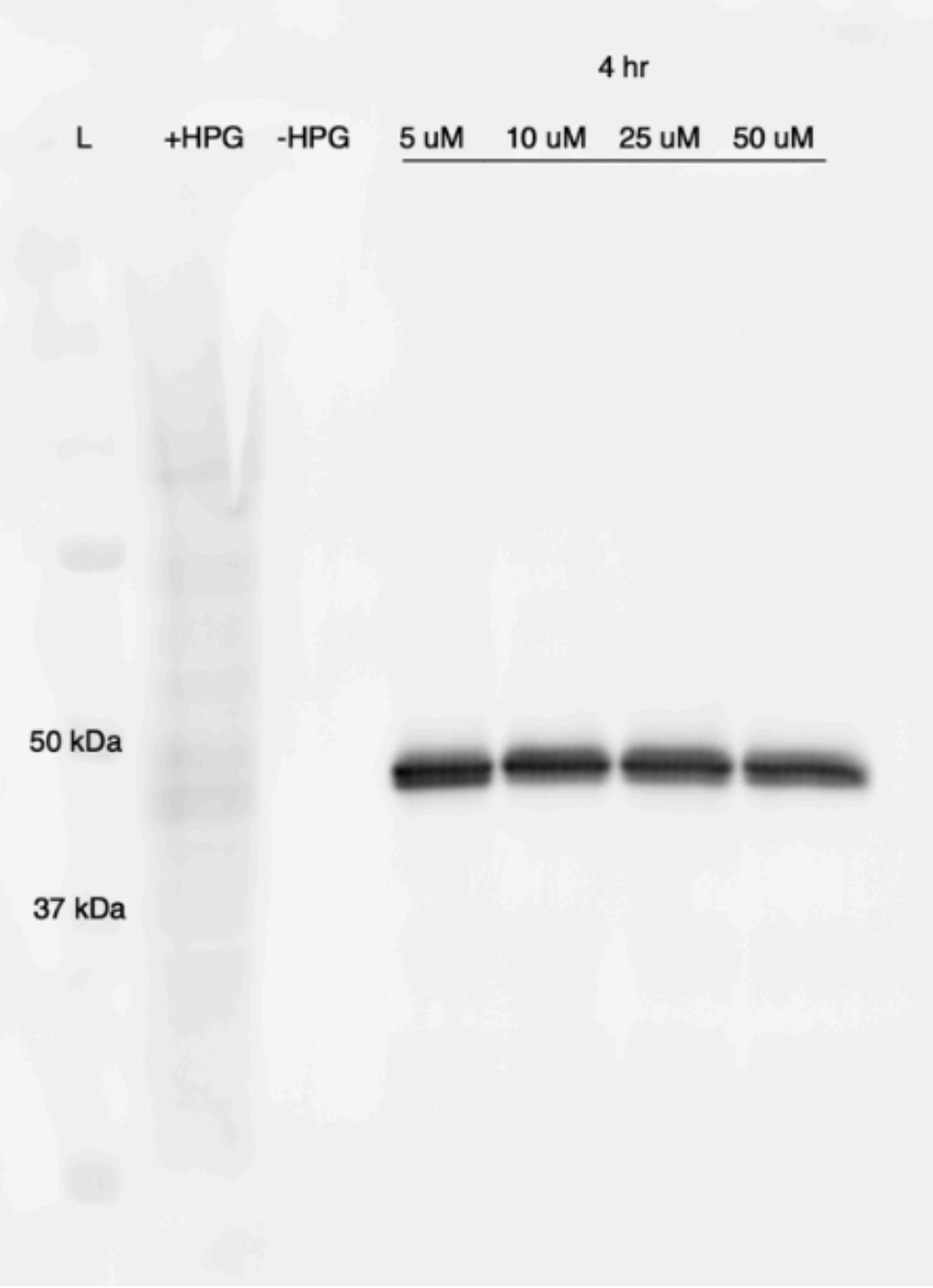

Supplemental Figure 17. Western blot of DHFR^{L28C}-YFP cysteine mutant expressed in HEK293DAX cells and cell lysates reacted with the 4CMal probe compound (**1b**) to test labeling efficiency at various concentrations and time points using the probe and Cys-mutant combination showing the most efficient labeling. Overlay of both image channels (green: anti-GFP, red: Cy3). Lanes showing red refer to over-exposed labeling.

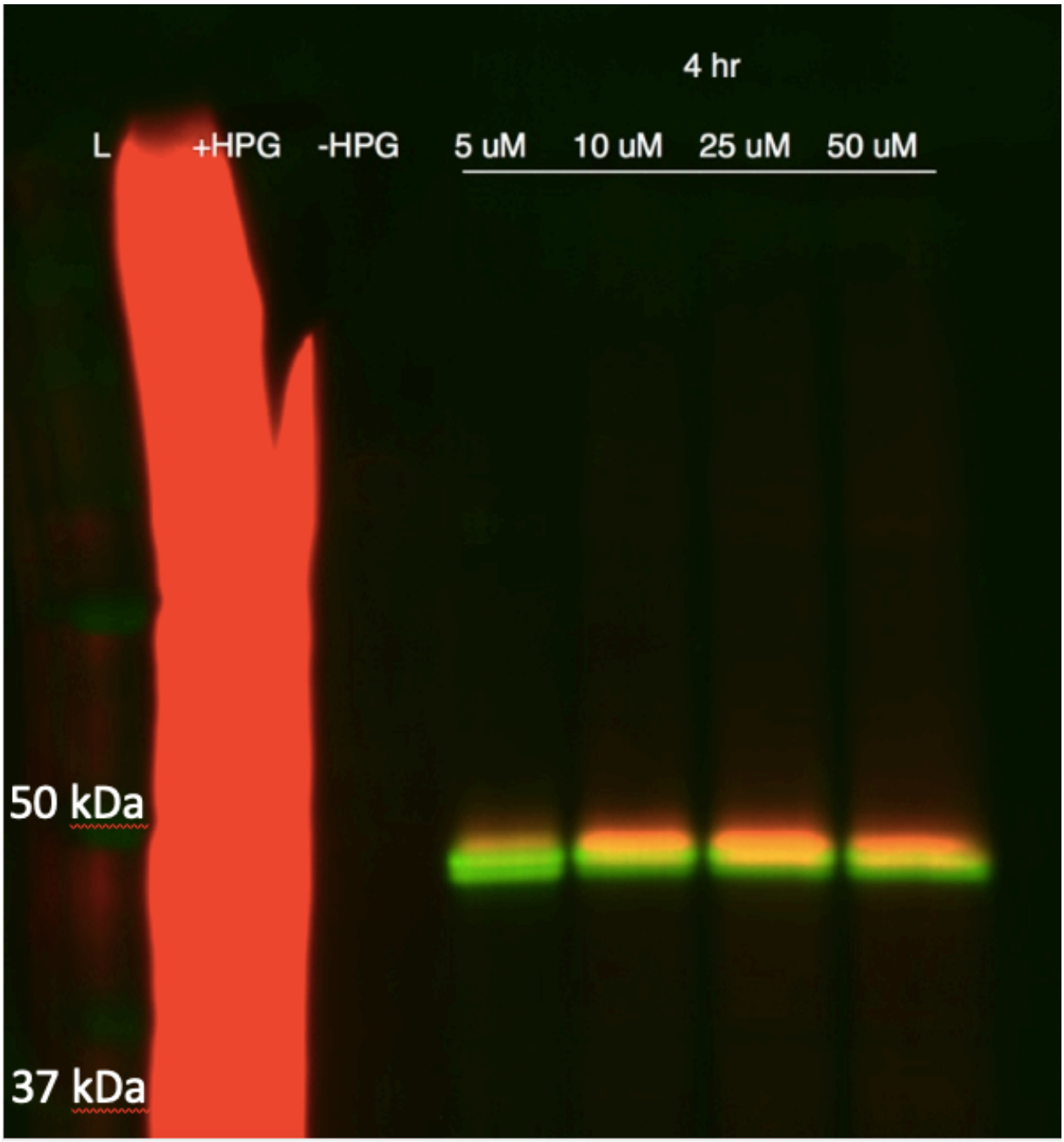

Supplemental Figure 18. Western blot using anti-GFP antibody to visualize total expressed DHRF-YFP. Western blot of dd-DHFR-YFP expressed in HEK293DAX cells that were reacted with DMSO control, 50 μM of TMP, or 50 μM of 6CMal (**1c**) at various time points. Lanes showing red refer to over-exposed labeling.

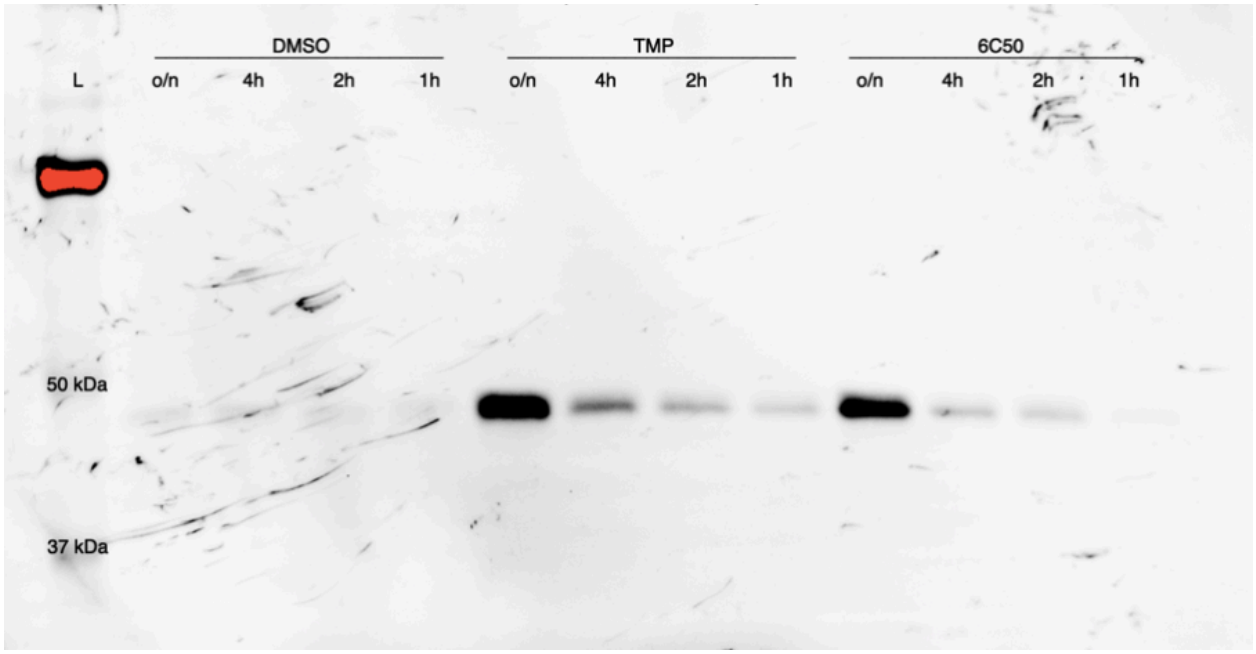

Supplemental Figure 19. Western blot using anti-GFP antibody to visualize total expressed DHRF-YFP. Western blot of dd-DHFR^{L28C}-YFP cysteine mutant expressed in HEK293DAX cells that were reacted with DMSO control, 50 μM of TMP, or 50 μM of 6CMal (**1c**) at various time points. Lanes showing red refer to over-exposed labeling.

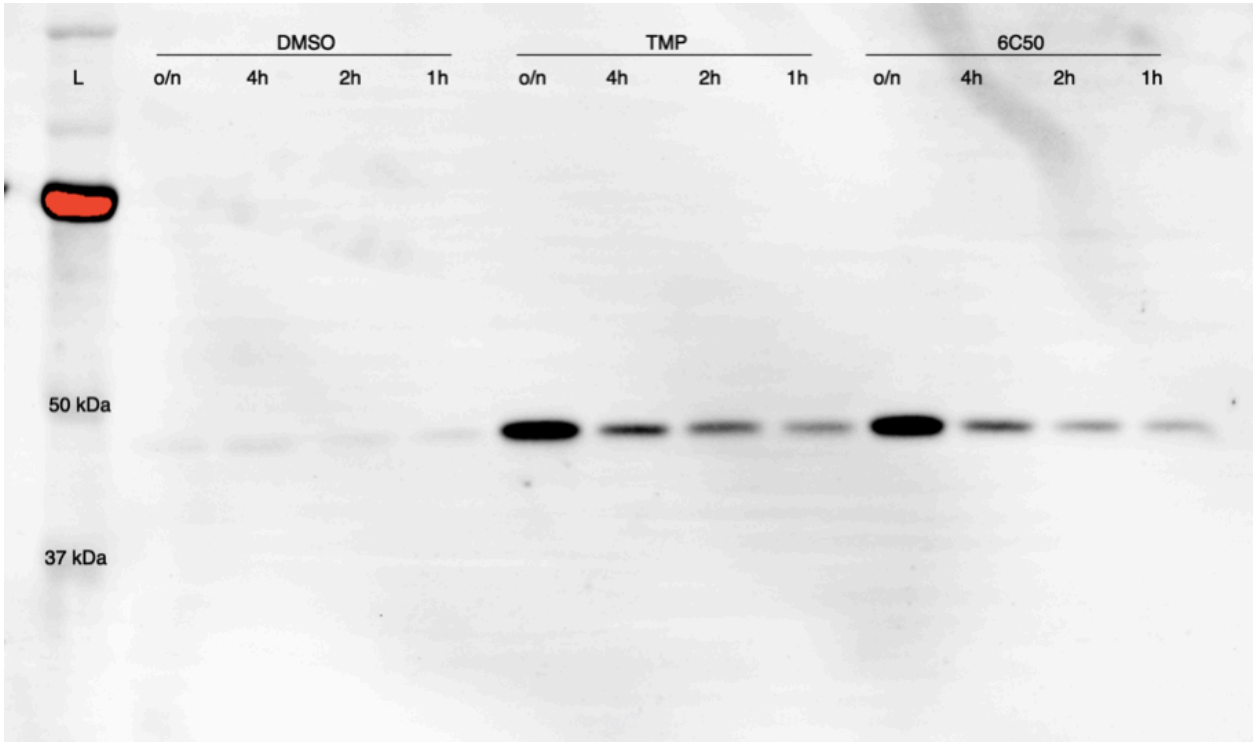

Supplemental Figure 20. Western blot of DHFR^{L28C}-YFP, dd-DHFR-YFP, or ddDHFR^{L28C}-YFP expressed in HEK293DAX cells that were reacted with DMSO control, 50 µM of TMP, or 50 µM of 6CMal (**1c**) overnight. Blot imaged for Cy3 after Click reaction with probe labeled lysates with pycolyl-Cy3 to visualize extent of covalent labeling. Lanes showing red refer to over-exposed labeling.

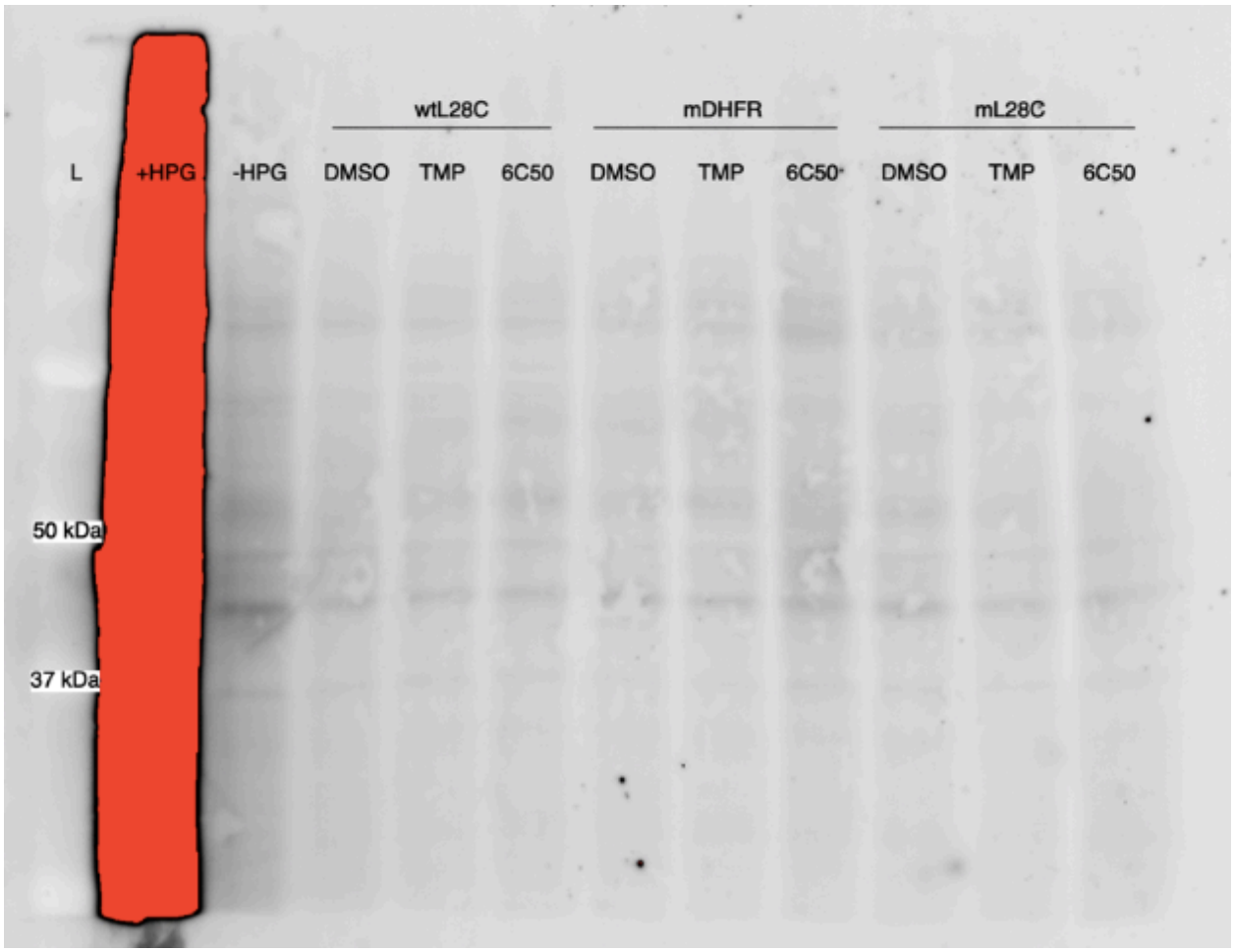

Supplemental Figure 21. Western blot of $DHFR^{L28C}$-YFP, dd-DHFR-YFP, or $ddDHFR^{L28C}$-YFP expressed in HEK293DAX cells that were reacted with DMSO control, 50 μM of TMP, or 50 μM of 6CMal (1c) overnight. Western blot using anti-GFP antibody to visualize total expressed DHRF-YFP.

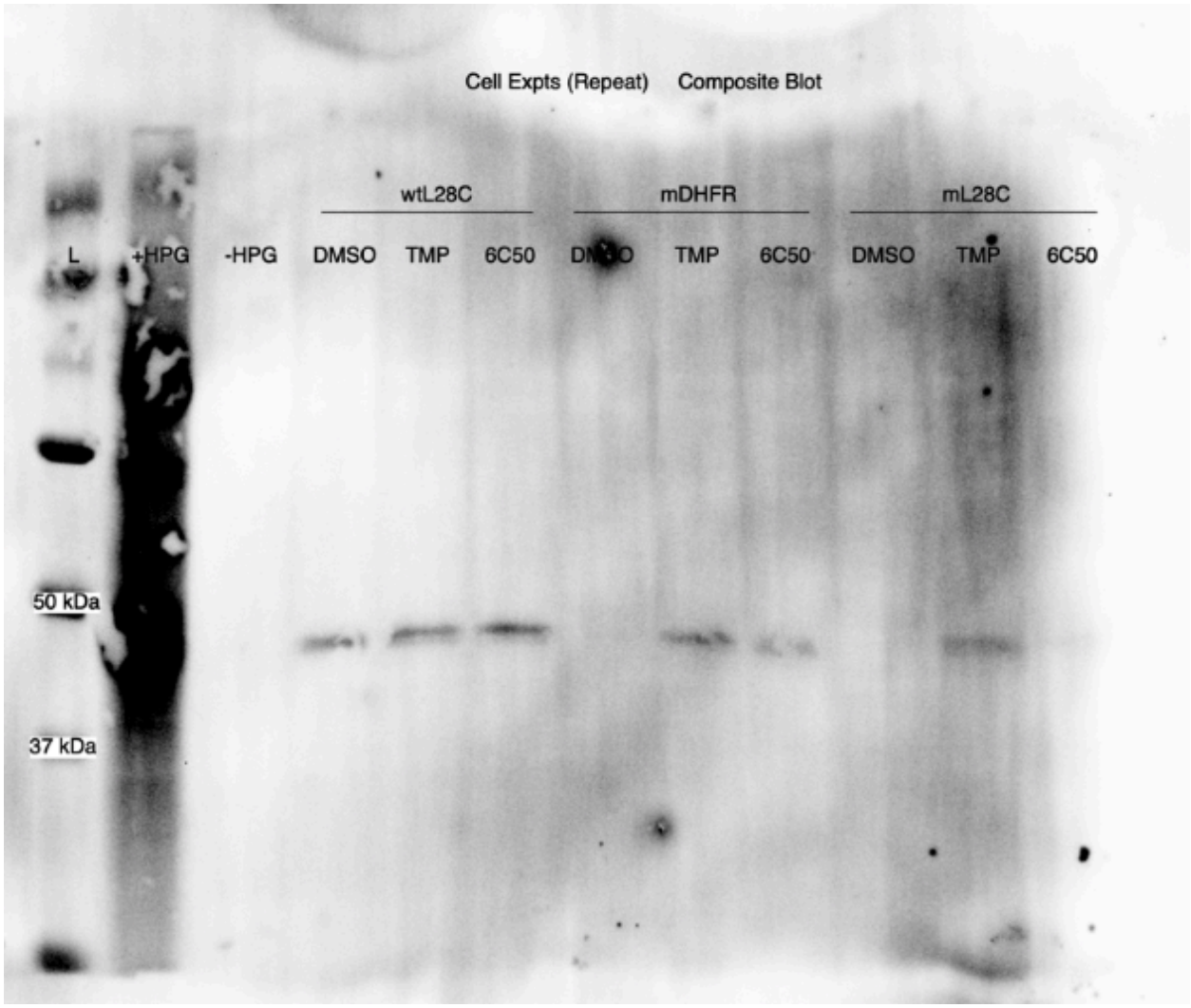

Supplemental Figure 22. Western blot of DHFR^{L28C}-YFP, dd-DHFR-YFP, or ddDHFR^{L28C}-YFP expressed in HEK293DAX cells that were reacted with DMSO control, 50 µM of TMP, or 50 µM of 6CMal (1c) overnight. Western blot using anti-GFP antibody to visualize total expressed DHRF-YFP. Overlay of both image channels (green: anti-GFP, blue: Cy3).

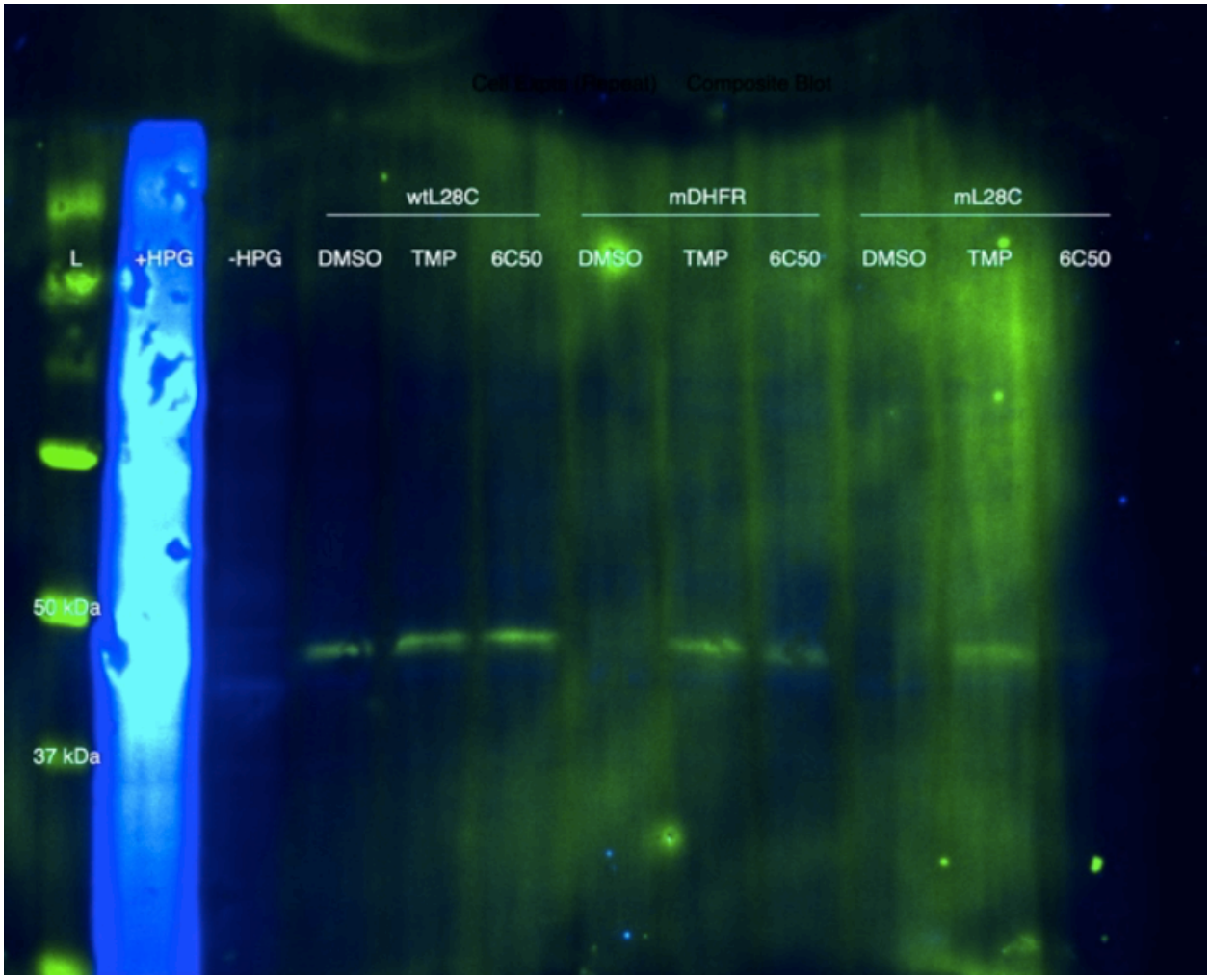

Supplemental Figure 23. Western blot of DHFR-YFP cysteine mutant variants expressed in HEK293DAX cells that were reacted with 50 μM of 4CMal (**1b**) for 4 hours, with control lanes of whole cell lysates with or without proteome-wide incorporation of homo-propargyl glycine (HPG). A. Blot imaged for IR680 after Click reaction with probe labeled lysates with diazo-PEG-biotin azide and treated with streptavidin attached to an IR680 dye to visualize extent of covalent labeling. Lanes showing red refer to over-exposed labeling.

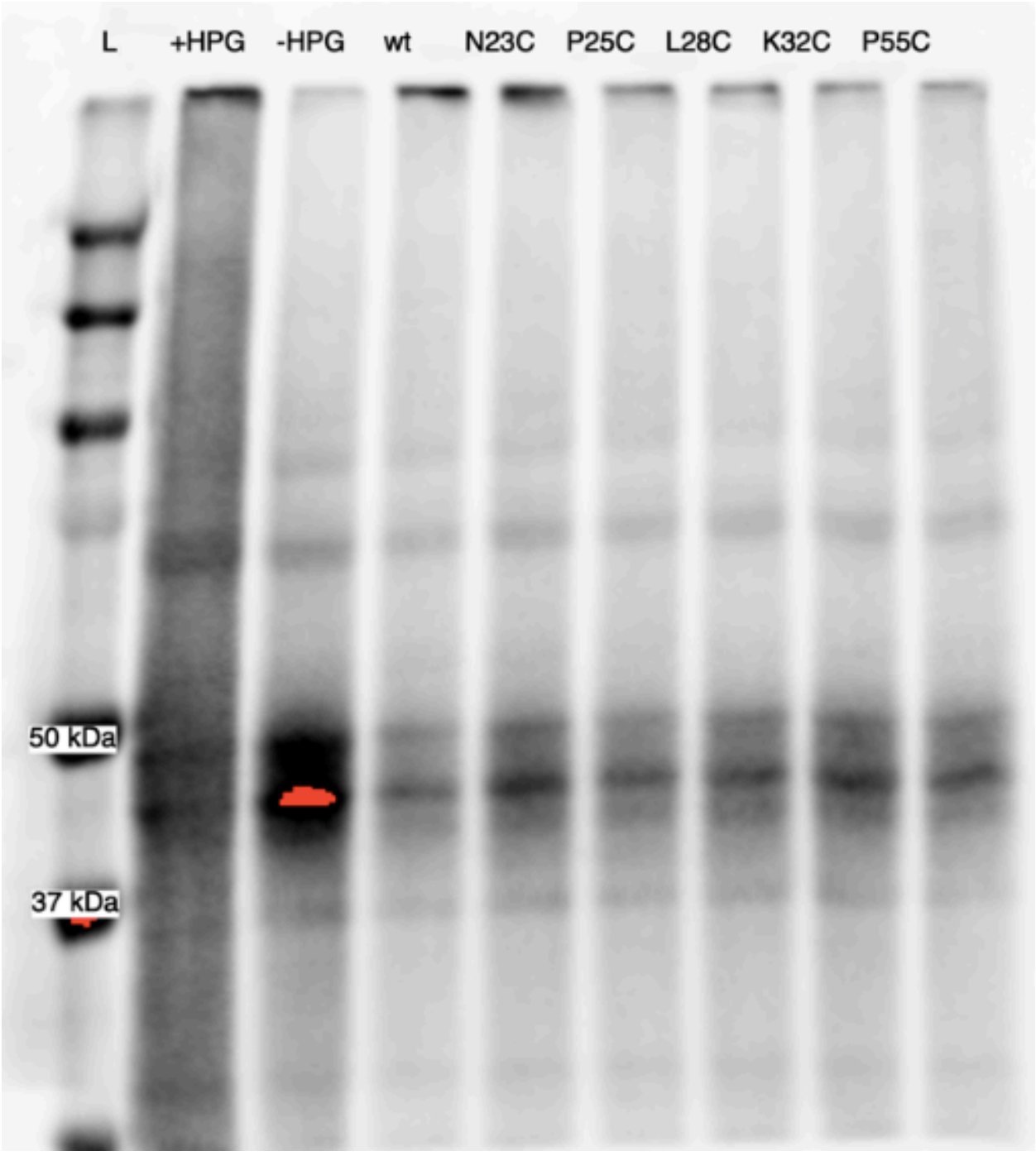

REFERENCES

Chapter 1

(1) Agrawal, N.; Dasaradhi, P. V. N.; Mohmmed, A.; Malhotra, P.; Bhatnagar, R. K.; Mukherjee, S. K. *Microbiol. Mol. Biol. Rev.* **2003**, *67* (4), 657–685.

(2) Doudna, J. A.; Charpentier, E. *Science* **2014**, *346* (6213), 1258096–1258096.

(3) Prelich, G. *Genetics* **2012**, *190* (3), 841–854.

(4) Andrianantoandro, E.; Basu, S.; Karig, D. K.; Weiss, R. *Mol Syst Biol* **2006**, *2* (1), 1866.

(5) Khera, N.; Rajput, S. *J. Cell. Biochem.* **2017**, *118* (5), 959–961.

(6) Hopkins, A. L.; Groom, C. R. *Nat Rev Drug Discov* **2002**, *1* (9), 727–730.

(7) Berg, T. *Angew. Chem. Int. Ed.* **2003**, *42* (22), 2462–2481.

(8) Balani, S.; Miwa, G.; Gan, L.-S.; Wu, J.-T.; Lee, F. *Curr Top Med Chem* **2005**, *5* (11), 1033–1038.

(9) Pickart, C. M.; Eddins, M. J. *Biochimica et Biophysica Acta (BBA) - Molecular Cell Research* **2004**, *1695* (1-3), 55–72.

(10) Wilkinson, K. D. *Proceedings of the National Academy of Sciences of the United States of America* **2005**, *102* (43), 15280–15282.

(11) Ardley, H. C.; Robinson, P. A. *Essays Biochem.* **2005**, *41*, 15–30.

(12) Burslem, G. M.; Crews, C. M. *Chemical reviews* **2017**, *117* (17), 11269–11301.

(13) Sakamoto, K. M.; Kim, K. B.; Verma, R.; Ransick, A.; Stein, B.; Crews, C. M.; Deshaies, R. J. *Mol. Cell Proteomics* **2003**, *2* (12), 1350–1358.

(14) Sakamoto, K. M.; Kim, K. B.; Kumagai, A.; Mercurio, F.; Crews, C. M.; Deshaies, R. J. *Proceedings of the National Academy of Sciences of the United States of America* **2001**, *98* (15), 8554–8559.

(15) Schneekloth, J. S.; Fonseca, F. N.; Koldobskiy, M.; Mandal, A.; Deshaies, R.; Sakamoto, K.; Crews, C. M. *J. Am. Chem. Soc.* **2004**, *126* (12), 3748–3754.

(16) Schneekloth, A. R.; Pucheault, M.; Tae, H. S.; Crews, C. M. *Bioorg. Med. Chem. Lett.* **2008**, *18* (22), 5904–5908.

(17) Ivan, M.; Kondo, K.; Yang, H.; Kim, W.; Valiando, J.; Ohh, M.; Salic, A.; Asara, J. M.; Lane, W. S.; Kaelin, W. G. *Science* **2001**, *292* (5516), 464–468.

(18) Lu, J.; Qian, Y.; Altieri, M.; Dong, H.; Wang, J.; Raina, K.; Hines, J.; Winkler, J. D.; Crew, A. P.; Coleman, K.; Crews, C. M. *Chem. Biol.* **2015**, *22* (6), 755–763.

(19) Chu, T.-T.; Gao, N.; Li, Q.-Q.; Chen, P.-G.; Yang, X.-F.; Chen, Y.-X.; Zhao, Y.-F.; Li, Y.-M. *Cell Chemical Biology* **2016**, *23* (4), 453–461.

(20) Montrose, K.; Krissansen, G. W. *Biochemical and Biophysical Research Communications* **2014**, *453* (4), 735–740.

(21) Winter, G. E.; Buckley, D. L.; Paulk, J.; Roberts, J. M.; Souza, A.; Dhe-Paganon, S.; Bradner, J. E. *Science* **2015**, *348* (6241), 1376–1381.

(22) Maynard-Smith, L. A.; Chen, L.-C.; Banaszynski, L. A.; Ooi, A. G. L.; Wandless, T. J. *J. Biol. Chem.* **2007**, *282* (34), 24866–24872.

(23) Egeler, E. L.; Urner, L. M.; Rakhit, R.; Liu, C. W.; Wandless, T. J. *J. Biol. Chem.* **2011**, *286* (36), 31328–31336.

(24) Rodriguez, S.; Wolfgang, M. J. *Chemistry & Biology* **2012**, *19* (3), 391–398.

(25) Park, E. C.; Finley, D.; Szostak, J. W. *Proceedings of the National Academy of Sciences of the United States of America* **1992**, *89* (4), 1249–1252.

(26) Dohmen, R. J.; Wu, P.; Varshavsky, A. *Science* **1994**, *263* (5151), 1273–1276.

(27) Bachmair, A.; Finley, D.; Varshavsky, A. *Science* **1986**, *234* (4773), 179–186.

(28) Bachmair, A.; Varshavsky, A. *Cell* **1989**, *56* (6), 1019–1032.

(29) Banaszynski, L. A.; Chen, L.-C.; Maynard-Smith, L. A.; Ooi, A. G. L.; Wandless, T. J. *Cell* **2006**, *126* (5), 995–1004.

(30) Edwards, S. R.; Wandless, T. J. *J. Biol. Chem.* **2007**, *282* (18), 13395–13401.

(31) Iwamoto, M.; Björklund, T.; Lundberg, C.; Kirik, D.; Wandless, T. J. *Chem. Biol.* **2010**, *17* (9), 981–988.

(32) Matthews, D. A.; Bolin, J. T.; Burridge, J. M.; Filman, D. J.; Volz, K. W.; Kraut, J. *J. Biol. Chem.* **1985**, *260* (1), 392–399.

(33) Harrison, H.; Pegg, H. J.; Thompson, J.; Bates, C.; Shore, P. *BMC Cancer* **2018**, *18* (1), R92.

(34) Shoulders, M. D.; Ryno, L. M.; Cooley, C. B.; Kelly, J. W.; Wiseman, R. L. *J. Am. Chem. Soc.* **2013**, *135* (22), 8129–8132.

(35) Moore, C. L.; Dewal, M. B.; Nekongo, E. E.; Santiago, S.; Lu, N. B.; Levine, S. S.; Shoulders, M. D. *ACS Chem. Biol.* **2015**, *11* (1), 200–210.

(36) Quintino, L.; Namislo, A.; Davidsson, M.; Breger, L. S.; Kavanagh, P.; Avallone, M.; Elgstrand-Wettergren, E.; Isaksson, C.; Lundberg, C. *Molecular Therapy - Methods & Clinical Development* **2018**, *11*, 29–39.

(37) Wagner, T. E.; Becraft, J. R.; Bodner, K.; Teague, B.; Zhang, X.; Woo, A.; Porter, E.; Alburquerque, B.; Dobosh, B.; Andries, O.; Sanders, N. N.; Beal, J.; Densmore, D.; Kitada, T.; Weiss, R. *Nat. Chem. Biol.* **2018**, *14* (11), 1043–1050.

(38) Tarassov, K.; Messier, V.; Landry, C. R.; Radinovic, S.; Molina, M. M. S.; Shames, I.; Malitskaya, Y.; Vogel, J.; Bussey, H.; Michnick, S. W. *Science* **2008**, *320* (5882), 1465–1470.

(39) Stelzl, U.; Worm, U.; Lalowski, M.; Haenig, C.; Brembeck, F. H.; Goehler, H.; Stroedicke, M.; Zenkner, M.; Schoenherr, A.; Koeppen, S.; Timm, J.; Mintzlaff, S.; Abraham, C.; Bock, N.; Kietzmann, S.; Goedde, A.; Toksöz, E.; Droege, A.; Krobitsch, S.; Korn, B.; Birchmeier, W.; Lehrach, H.; Wanker, E. E. *Cell* **2005**, *122* (6), 957–968.

(40) Butland, G.; Peregrín-Alvarez, J. M.; Li, J.; Yang, W.; Yang, X.; Canadien, V.; Starostine, A.; Richards, D.; Beattie, B.; Krogan, N.; Davey, M.; Parkinson, J.; Greenblatt, J.; Emili, A. *Nature* **2005**, *433* (7025), 531–537.

(41) Gavin, A.-C.; Aloy, P.; Grandi, P.; Krause, R.; Boesche, M.; Marzioch, M.; Rau, C.; Jensen, L. J.; Bastuck, S.; Dümpelfeld, B.; Edelmann, A.; Heurtier, M.-A.; Hoffman, V.; Hoefert, C.; Klein, K.; Hudak, M.; Michon, A.-M.; Schelder, M.; Schirle, M.; Remor, M.; Rudi, T.; Hooper, S.; Bauer, A.; Bouwmeester, T.; Casari, G.; Drewes, G.; Neubauer, G.; Rick, J. M.; Kuster, B.; Bork, P.; Russell, R. B.; Superti-Furga, G. *Nature* **2006**, *440* (7084), 631–636.

(42) Barrios-Rodiles, M. *Science* **2005**, *307* (5715), 1621–1625.

(43) Bisson, N.; James, D. A.; Ivosev, G.; Tate, S. A.; Bonner, R.; Taylor, L.; Pawson, T. *Nat Biotechnol* **2011**, *29* (7), 653–658.

(44) Lobingier, B. T.; Hüttenhain, R.; Eichel, K.; Miller, K. B.; Ting, A. Y.; Zastrow, von, M.; Krogan, N. J. *Cell* **2017**, *169* (2), 350–360.e12.

(45) Choi, H.; Larsen, B.; Lin, Z.-Y.; Breitkreutz, A.; Mellacheruvu, D.; Fermin, D.; Qin, Z. S.; Tyers, M.; Gingras, A.-C.; Nesvizhskii, A. I. *Nat Methods* **2010**, *8* (1), 70–73.

(46) Jing, C.; Cornish, V. W. *ACS Chem. Biol.* **2013**, *8* (8), 1704–1712.

Chapter 2

(1) Jing, C.; Cornish, V. W. *ACS Chem. Biol.* **2013**, *8* (8), 1704–1712.

(2) Ando, T.; Tsukiji, S.; Tanaka, T.; Nagamune, T. *Chem. Commun.* **2007**, *16* (47), 4995–4997.

(3) Liu, W.; Li, F.; Chen, X.; Hou, J.; Yi, L.; Wu, Y.-W. *J. Am. Chem. Soc.* **2014**, *136* (12), 4468–4471.

(4) Rashid, U.; Ahmad, W.; Hassan, S. F.; Qureshi, N. A.; Niaz, B.; Muhammad, B.; Imdad, S.; Sajid, M. *Bioorg. Med. Chem. Lett.* **2016**, *26* (23), 5749–5753.

(5) Ensch, C.; Hesse, M. *Helvetica Chimica Acta* **2002**, *85* (6), 1659–1673.

(6) Han, J.; Sun, L.; Chu, Y.; Li, Z.; Huang, D.; Zhu, X.; Qian, H.; Huang, W. *J. Med. Chem.* **2013**, *56* (24), 9955–9968.

Chapter 3

(1) Jing, C.; Cornish, V. W. *ACS Chem. Biol.* **2013**, *8* (8), 1704–1712.

(2) Shoulders, M. D.; Ryno, L. M.; Genereux, J. C.; Moresco, J. J.; Tu, P. G.; Wu, C.; Yates, J. R.; Su, A. I.; Kelly, J. W.; Wiseman, R. L. *Cell Rep* **2013**, *3* (4), 1279–1292.